

Master Thesis

The effect of wind and waves on the hydrodynamic and morphodynamic properties of sand waves

by:

Abhijeet Singh

(S2393964, Student M-CEM)

In fulfillment of requirements for the degree

Master of Science

in Civil Engineering and Management

Specialization: River and Coastal Engineering

Date: 27th August, 2021

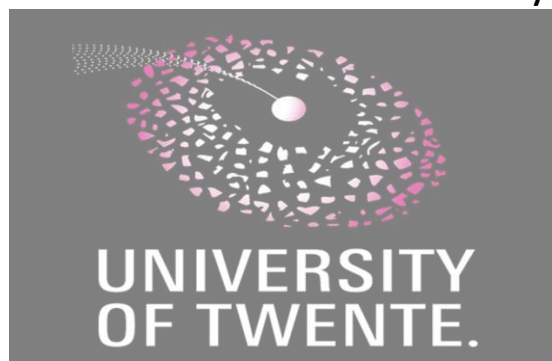
Graduation Committee:

dr. ir. B.W. Borsje

University of Twente

dr. ir. J.H. Damveld

University of Twente



Preface

This research originally stemmed from my passion for studying water under varying circumstances using advanced numerical techniques to simulate its effect on surroundings. One of them is the marine environment, where water is subjected to external factors such as wind and short crested waves on the top, imbibed with long waves in the form of elliptical tides. These surrounding climatic conditions make bed forms dynamic. One of such evident bed forms covering the large part of the Netherlands Continental Shelf is sand waves. Their dynamic behaviour varies over the shelf. Besides their importance as an interesting morphological feature, sand waves play a role in managing activities concerning the sea floor. Especially the dynamic behaviour of sand waves interacts with engineering activities like maintenance dredging, construction and maintenance of wind farms, submarine cables, pipelines, sand mining locations and detection of objects on the sea floor. Thus, it embarks me on a journey to unravel the unknown processes related to the marine environment on sand waves seabed.

In truth, I could not have achieved my current progress without strong support and encouragement. First of all, my parents and friends supported me with love and understanding. Secondly, my committee members have provided patient advice, free guidance, personal motivation, and free coffee throughout the research process. I want to express my sincere gratitude to all for your unwavering support.

Summary

The seabed of shallow continental shelf consists of rhythmic bed patterns of varying spatial and temporal scales. It consists of as small as (mega)ripples to as large as tidal sand banks. Among them lies the intermediate dynamic bed forms, sand waves. They are formed when bottom perturbations are subjected to tidal flow. They may migrate up to several tens of meters per year and grow up to one-third of the local water depth. These physical features may severely influence offshore human activities, such as navigation, construction of wind farms, and dredging. Therefore, it is essential to understand the physical processes that affect sand wave morphology to ensure safety in shipping routes and optimize the strategies of expensive dredging work.

In general, the effect of several physical processes and factors have already been studied. For example, previous recorded observations and results of a simplified model by Campmans et al. (2018) demonstrated the significant effect of severe wind and waves on sand waves. However, few values of model results, such as migration rate or sand wave height, were overestimated compared to field observations. In particular, the model made certain physical processes simplified by using constant coefficient viscosity, linear wave-current interaction and excluding suspended load. Including these non-linear effects will add more insight and improve the previous findings related to the combined effect of wind and waves on sand wave properties.

Thus, this study presents a 2DV process-based model using Delft3D that investigates the effect of wind and waves on sand waves. The model includes advancements in physical processes such as variable eddy viscosity, non-linear wave-current interaction, and suspended load. The study examines both hydrodynamic and morphodynamic properties. All simulations related to hydrodynamic properties are performed on predefined four beds of the same wavelength (216 m), increasing amplitude (0-3 m), and varying asymmetry. These are short-term runs for two tidal cycles on a domain length of 45 km. The morphodynamic properties related simulations are performed on an initial bed: 0.25 m symmetrical sand wave of wavelength 216 m when wind and waves are present for the complete duration. At the same time, morphodynamic simulations for intermittent storms are performed on a randomly perturbed initial bed. These are long-term simulations for 100 years on a similar domain length.

The hydrodynamic results show an increase in average viscosity and turbulence with the addition of wind and waves. It distorts circulation cells formed due to symmetrical tide and leads to the asymmetrical distribution of bed shear stress over sand waves. In addition, it causes near-bed wind-driven residual in wind direction, including a small reverse drift above it opposite to the wind direction in tidally average horizontal flow. An increase in reverse drift with depth reverses near-bed mean velocity at 30 m or greater mean water depth. The effect of severe wind and waves is more significant than intermediate wind and waves on sand waves.

The morphodynamics results show that waves alone cause flattening of the crest but do not induce any significant migration. However, together with wind, waves intensify the migration, reduce sand wave height and increase wavelength. Our work also identifies that suspended load increases during storm conditions. This increase also intensifies the reduction

in sand wave height when compared to tide-only conditions. The change in hydrodynamic properties is reflected in morphodynamic properties as well. A steeply reducing migration rate is observed at 30 m or greater depth due to reverse drift observed in tidally average flow. The above results concern steady-state complete duration storm conditions. In actuality, storms are intermittent, and this study considered short-duration storm conditions of frequency three months per year. In their presence, sand wave fields show a migration rate of 0.5 – 1 m/year. The storm conditions cause a height reduction of 33% when present for the complete duration and 5% – 8% when present intermittent, compared to no storm conditions.

The results of this research study related to the sand wave properties are comparable to field data. Additionally, it shows that the effect of intermittent storms depends on the wind speed, duration and the frequency between the calm and storm periods. Therefore, high speed and long duration wind conditions can add substantial value to migration. It will modify the safety factors while designing the foundation of offshore wind farms, the base layer of cables and pipelines. It will also help in refining the dredging work frequency required in navigation channels.

Further, it is recommended to include residual current with intermittent storms followed by the 2-D Fourier analysis of sand waves bed level as tides are not symmetrical in reality. Also, the calm period between intermittent storms is recovering the symmetrical behaviour of sand waves lost during storms due to symmetrical tide. Further, the suitability of the present lateral boundary conditions (Riemann boundary) should be checked with the periodic boundaries as few properties such as mean vertical velocity showed phase differences at the lateral boundaries. Unfortunately, this suitability could not be checked in this study as implementing periodic boundaries was not possible in the present version of Delft3D.

Contents

List of tables.....	6
List of figures	6
1. Introduction.....	9
1.1. Motivation and problem statement.....	9
1.2. Research gap.....	12
1.3. Research objective	12
1.4. Approach	13
1.5. Outline	16
2. Background.....	17
2.1. The physical mechanism behind sand wave formation.....	19
2.2. Physical processes affecting sand wave properties	19
2.3. Effect of wind and waves over various bathymetries.....	21
2.4. Sand wave model development overview	24
3. Sand wave model description.....	26
3.1. Hydrodynamics.....	27
3.2. Sediment transport and bed evolution	29
3.3. Model set up.....	30
4. Overview of model parameters for simulation runs.....	34
4.1. Reference situation: Hydrodynamic properties for sand waves in symmetrical tide-only forcing.....	34
4.2. Hydrodynamic properties for sand waves in the presence of symmetrical tide, wind and waves	34
4.3. Sand wave morphology in the presence of wind and waves	35
5. Results.....	37
5.1. Reference situation: Hydrodynamic properties for sand waves in a symmetrical tide	37
5.2. Hydrodynamic properties for sand waves in the presence of symmetrical tide, wind and waves	39
5.3. Morphodynamic properties of sand waves in the presence of severe wind and waves... 48	
5.3.1. Physical effects of wind and waves on sand wave growth and migration	48
5.3.2. Sand wave shape and migration at 25 m and 30 m depth	54
5.3.3. Effect of an intermittent storm on sand wave morphology	56
6. Discussion	59
6.1. Relevance of the study.....	59
6.2. Model limitations	60
6.3. Improvements in model.....	63
6.4. Calibration	63

7. Conclusion	64
8. Future recommendation	67
References	68
Appendices	72
Appendix-1: Model Sensitivity to vertical, horizontal, and temporal resolution	72
Appendix-2: Effect of adding background viscosity	73

List of tables

<i>Table 1: Comparison of implementation of several physical processes in a model by Campmans et al. (2018) with the possible implementation of the same physical processes in the Delft3D and its advantage in modelling sand wave.</i>	11
<i>Table 2: Comparison of Campmans et al. (2018) model results with field observations of sand wave properties in the North Sea. (Note that parameters used in the model by Campmans et al. (2018) were similar to the North Sea conditions. That is why model results are compared with sand waves field observations made in the North Sea.)</i>	11
<i>Table 3: The characteristic spacing, height, migration rate and evolution timescale of rhythmic bed patterns in the marine environment (Damveld et al., 2020; Dodd et al., 2003; Knaapen, 2005).</i>	17
<i>Table 4: Overview of common model parameters used in simulations.</i>	34
<i>Table 5: Overview of tidal and meteorological conditions used in different simulations.</i>	34
<i>Table 6: Comparison of hydrodynamic properties in tide-only, tide+wave, tide+wind and tide+wind+wave conditions over 0.25 m symmetric sand wave at a mean depth of 25 m. Only severe wind and wave conditions are shown here. The shades of colour weigh the property impact, where blue shows the low impact, yellow shows medium impact and red shows the highest value.</i>	44
<i>Table 7: Variation of Stokes number with water depth</i>	45
<i>Table 8: Comparison of morphodynamic properties in tide-only, tide+wave, tide+wind and tide+wind+wave conditions over 0.25 m symmetric sand wave at a mean depth of 25 m. Only severe wind and wave conditions are shown here. The shades of colour weigh the property impact, where blue shows the low impact, yellow shows medium impact and red shows the highest impact.</i>	54

List of figures

<i>Figure 1: High-resolution digital rendering of sand waves at the mouth of San Francisco Bay near the Golden Gate bridge. Credit: US Geological Survey. This massive bed form field covers an area of approximately four square kilometers in water depths ranging from 30 to 106 meters, featuring more than 40 distinct sand waves with crests aligned approximately perpendicular to the dominant tidally generated cross-shore currents, with wavelengths and heights that measure up to 220 meters and 10 meters, respectively. (Source: Barnard et al., 2006)</i>	9
<i>Figure 2: Morphodynamic loop</i>	12
<i>Figure 3: A schematic diagram for the approach used.</i>	15
<i>Figure 4: Interpolated survey images of 1 km² area, showing sand waves and megaripples near Egmond, Netherlands. Depths are given in decimeters to MSL. (Van Dijk et al., 2008)</i>	18
<i>Figure 5: Strong near-bed circulation which supports the growth of the bottom perturbation. The backward circulation in the upper flow part uses a larger part of the water column and is weaker (Refer to figure 12, Hulscher, 1996)</i>	19
<i>Figure 6: Schematic representation of (a) wavelength and height, (b) crest and trough length, crest and trough height, (c) lee and stoss asymmetry, (d) growth and migration of sand waves. Source: (Ijzer, 2010)</i>	20
<i>Figure 7: Eastward sand transport component and suspended load towards the Dutch coast using a model study (Van Der Molen, 2002) and ten years of wind data at the Texelhors meteorological station, due to (A) Tides, (B) Tides, wind and waves.</i>	22
<i>Figure 8: Definition sketch (top view) of the direction of tidal current (black), wind (orange) and wave vector (green).</i>	29
<i>Figure 9: The schematic view of a non-linear interaction of wave and current produced bed shear stresses (Soulsby et al., 1993).</i>	29
<i>Figure 10: (a) Horizontal grid distribution for the model runs, using a fine grid in the centre where the sand waves are calculated and a coarser grid towards the lateral boundaries and (b) the vertical distribution of the σ-layers over the water column, showing the spacing of 60 σ-layers down the water column. The spacing between the layers is small near the bed and surface, resulting in 8 σ-layers at the lower 1 m and top 1 m.</i>	31

Figure 11: (a) Types of initial bed used in this research study: a flat bed(solid black), 0.25 m finite-amplitude symmetrical bed (dotted red), 0.25 m finite-amplitude asymmetrical bed (dotted black), and 3 m developed bed (dashed black). Note that the wavelength of all the predefined wavy bed patterns is 216 m. (b) Symmetrical S2 Tidal cycle used in the model..... 32

Figure 12: Wind climate derived from the 10-year time series of wind observations from Texelhors (KNMI, Verkaik, pers.comm.). Contours denote the observed number of hourly occurrences. Winds are from the direction (in compass degrees from north) indicated in the figure..... 33

Figure 13: Distribution of intermittent storms, having frequency of 3 months in a year, within one tidal cycle. It shows the distribution of three storms in three morphological years present in one tidal cycle based on Morfac value of 2000. Left axis shows the surfce tidal velocity and right axis shows the velocity of wind. The grey shaded area shows the storm. 36

Figure 14: Tidally average velocity (in m/s) for 0.25 m symmetrical sand wave (a), for 3 m amplitude asymmetrical sand wave (b). Blue arrow shows the direction of mean velocity and red dots shows the centre of circulation cells. Note that wavelength of both the bed is 216 m. 37

Figure 15: (a) Variation of vertical eddy viscosity (top) and turbulent energy (bottom) at crest position with tide duration. (b)Variation of tidally averaged bottom stress with sand wave evolution: a flat bed (black), 0.25m symmetrical sand wave (red), 0.25m asymmetrical sand wave (blue), real bed (cyan). The circle shows the stress at the crest position of sand waves ($x=0m$). It is in the presence of tide-only conditions..... 38

Figure 16: Variation of vertical eddy viscosity (left) and turbulent energy (right) at crest position over 0.25 m symmetrical sand wave in the presence of severe wind speed of 20 m/s. 40

Figure 17: Effect of intermediate wind (solid blue), severe wind (solid purple), combined intermediate wind and wave (dashed blue), combined severe wind and wave (dashed purple) in the presence of symmetrical tide at crest position of 0.25 m symmetrical sand wave in 25 m mean water depth. 42

Figure 18: Variation of vertical eddy viscosity (left) and turbulent energy (right) at crest position in the presence of severe wave height of 2.5m over 0.25m symmetrical sand wave. 42

Figure 19: Variation of vertical eddy viscosity (left) and turbulent energy (right) at crest position in the presence of severe wind of 20m/s and severe wave height of 2.5m over 0.25m symmetrical sand wave. 43

Figure 20: Vertical distribution of the amplitude (a, b, c) and phase (d, e, f) of zero frequency component (A_0 and ϕ_0), first harmonics (A_2 and ϕ_2) and second harmonics (A_4 and ϕ_4) of horizontal velocity in the presence of combined severe wind and severe wave at a mean depth of 25m. Respective amplitudes and phases are combined to get components S_0 , S_2 and S_4 (g, h, i). Horizontal velocity is reconstructed using S_0+S_2 (j), $S_0+S_2+S_4$ (k), S_0+S_4 (l). 44

Figure 21: Effect of severe wind on 0.25 m symmetrical sand wave crest at different water depth: 10 m (solid black), 25 m (solid red), 30 m (solid blue), 40 m (solid cyan); and effect of severe wind and wave at 25 m (dotted red) (left figure). Effect of several duration of severe wind on 0.25 m symmetrical sand wave crest at 30 m water depth: wind during the complete tidal cycle (solid blue), wind during ebb phase only (dashed cyan), wind during flood phase only (dashed black), wind during half tidal cycle (dashed magenta) (right figure). Note that the graph is plotted on normalized depth, and the bottom figure gives a zoomed view of velocity near 5% bottom depth..... 47

Figure 22: Mean horizontal velocity at the crest position of 0.25 m symmetrical sand wave (top) and 3 m asymmetrical sand wave (bottom) at mean water depth of 25 m depth (solid black line) and 30 m depth (solid red line). The graph is plotted for the bottom 5% normalized depth..... 47

Figure 23: Bed evolution in time (years) of 0.25 m symmetrical sand wave in the presence of symmetrical tide. The growth of the crest and trough is tracked with an asterisk and dot, respectively. 49

Figure 24: Bed evolution in time (years) of 0.25 m symmetrical sand wave in the presence of symmetrical tide and severe wave. The growth of the crest and trough is tracked with an asterisk and dot, respectively. 50

Figure 25: Bed evolution in time (years) of 0.25 m symmetrical sand wave in the presence of symmetrical tide and severe wind. The growth of the crest and trough is tracked with an asterisk and dot, respectively. 51

Figure 26: Bed evolution in time (years) of 0.25m symmetrical sand wave in the presence of symmetrical tide, severe wind and wave. The growth of the crest and trough is tracked with an asterisk and dot, respectively. .. 51

Figure 27: Sand wave profile development in the presence of tide (a), tide +wave (b), tide+ wind (c) and tide+ wind + wave (d) over 0.25 m symmetrical initial bed for 100 years. The vertical colour bar shows the bed level (m). 52

Figure 28: Position of crest and trough of sand wave profile in the presence of tide (blue), tide +wave (green), tide+ wind (cyan) and tide+ wind + wave (purple)..... 53

Figure 29: Sand wave profile in the presence of tide (blue), tide +wave (green), tide+ wind (cyan) and tide+ wind + wave (purple). The final sand wave profile is generated from 0.25 m initial amplitude sand wave (FGM=216 m) after the morphological development of 100 years. 53

Figure 30: The average migration rate, obtained through the average horizontal movement of crest and trough, in the presence of tide (blue), tide +wave (green), tide+ wind (cyan) and tide+ wind + wave (purple). 53

Figure 31: The sand wave field at 25m (cyan) and at 30m (red) water depth in tide and severe wind after t=100 years. 55

Figure 32: Sand wave evolution in the presence of tidal and severe wind conditions for 100 years at 30m mean depth. The vertical colour bar shows the bed level (m). 55

Figure 33: Migration of crest and trough at 25m (left) and 30m (right) water depth. The growth of the crest and trough is tracked with a blue asterisk and red dot, respectively. 55

Figure 34: Comparison of bedload transport (solid line) and suspended load transport (dashed line) at a mean depth of 25m (cyan) and 30m (red). 56

Figure 35: Sand wave evolution in the no storm (left) and intermittent storm conditions of 3 months/year (right) for 100 years at 25 m depth. The vertical colour bar shows the bed level (m). 57

Figure 36: Sand wave profile in the no storm (blue) and two random intermittent storm conditions of 3 months/year (cyan and green) after 100 years at 25 m mean depth. The same randomly perturbed bed is used at t=0 (grey) for the simulations presented here. 58

Figure 37: The tidal average vertical velocity (m/s) at the grid nodes near the lateral boundaries for wind conditions. 62

Figure 38: Mean Horizontal velocity at depth 60 for numerical settings- number of sigma layers (90 layers), horizontal distribution near the centre of the grid (1m) and hydrodynamic time step (0.1 minutes) (red) and - number of sigma layers (60 layers), horizontal distribution near the centre of the grid (2m) and hydrodynamic time step (0.2 minutes) (black) 72

Figure 39: The effect of adding background viscosity 0.005 m²/s to k-ε turbulence model on final vertical viscosity profile (left) and mean horizontal velocity (right). 73

1. Introduction

1.1. Motivation and problem statement

The bed of shallow shelf seas is rarely flat. Instead, dynamic wave-like sediment features of varying spatial scales may occur when sediment is in good supply, and tidal flows are sufficiently strong. The smallest among all the bed forms in the marine environment is classed as (mega)ripples and have heights of centimetres to decimetres and wavelengths up to tens of metres. The largest bed forms are tidal sand banks, their wavelengths span several kilometres, and their heights can be of the order of local water depth. The latter bed form migrates and changes its shape slowly. The time scale for these changes is in the order of years to decades (Ijzer, 2010).

In between these classes, the intermediate bed forms are sand waves. The wavelength of sand waves are up to hundreds of meters, the equilibrium heights may grow up to one-fourth of water depth, and migration rate up to several meters per year (Dorst et al., 2009; Knaapen, 2005; McCave, 1971; Van Dijk et al., 2005). Observations of the presence of sand waves in the marine environment date back to the early 20th century (McCave, 1971; Terwindt, 1971; Van Veen, 1935). The set of recorded and derived sand wave properties are discussed in chapter 2. These field observations show that sand waves are dynamic due to their considerable height and large migration rates. Figure 1 shows a field of giant sand waves mapped at the

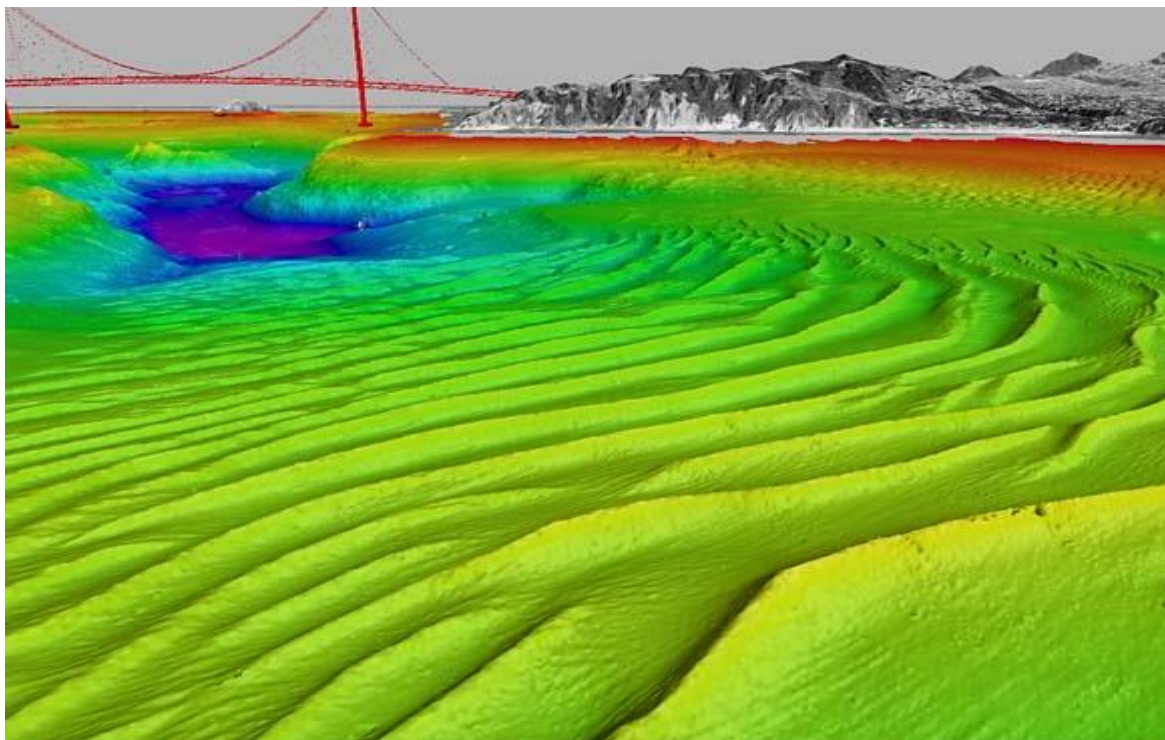


Figure 1: *High-resolution digital rendering of sand waves at the mouth of San Francisco Bay near the Golden Gate bridge.* Credit: US Geological Survey. This massive bed form field covers an area of approximately four square kilometers in water depths ranging from 30 to 106 meters, featuring more than 40 distinct sand waves with crests aligned approximately perpendicular to the dominant tidally generated cross-shore currents, with wavelengths and heights that measure up to 220 meters and 10 meters, respectively. (Source: Barnard et al., 2006)

mouth of San Francisco Bay in California (USA), with wavelengths, heights and migration rates that measure up to 220 m, 10 m and 7 m/year, respectively (Barnard et al., 2006). Such physical features have a significant influence on human activities. For example, this dynamic behaviour poses a hazard to offshore navigation channels, offshore wind farms, submarine pipelines, and telecommunication cables (Borsje et al., 2013). It also affects the maintenance dredging work in shipping routes through sand wave fields and sand mining in the North Sea (Terwindt, 1971). Thus, it is essential to account for the major processes that affect the behaviour of sand waves. The prior research studies have already analysed the effect of several factors and processes on sand wave dynamics. These processes and factors include the residual current, flow depth, tidal velocity (Németh et al., 2002; 2007), tidal asymmetry (Giovanni Besio et al., 2004), bed roughness variation (due to variable grain size), time-(in)variant eddy viscosity (Borsje et al., 2013), flow effect and slope effect of the bed transport (Borsje et al., 2014; Campmans et al., 2017) and suspended load transport (Borsje et al., 2014; van Gerwen et al., 2018). The effect of these processes on sand waves is discussed in detail in chapter 2 (section 2.2).

Further, past field observations also indicate the effect of wind and waves on sand waves. For example, in the Hinder Banks of the North Sea, Terwindt (1971) identified a correlation between the sand wave crests height and the frequency of heavy winds. The heavy winds eroded the crests, and intermediate calm weather built up the crests. The same work also showed the change in the direction of steep sides of sand waves while traversing from North to South of the Hinder Banks. The study postulated wind as one of the reasons for this change, but no confirmed explanation was given for this phenomenon. Furthermore, the migration rate varied for sand waves observed in the eastern Long Island Sound (USA) over different seasonal periods involving storms (Bokuniewicz et al., 1977; Fenster et al., 1990), and a study by Ferret et al. (2010) showed the local progradation of sand wave in a direction opposite to the residual currents. Another study showed that the temporal variation in the migration direction and asymmetry of sand waves were related to the monsoon-driven current in the Adolphus Channel, Australia (Harris, 1989). In addition to this, surface wave action may also influence sand waves, as Van Dijk & Kleinhans (2005) found that the dynamics of sand waves depend on a balance between the relative influence of surface waves and currents at a given depth. For instance, in wave-dominant areas (nearshore coastal sites), wave action resulted in asymmetrical and flattened sand waves. Whereas, in current dominant areas (offshore sites), sandwaves were comparatively more symmetrical. Ijzer (2010) found that sand waves height was lowered, and the asymmetry was changed during the pre-storm and post-storm studies due to change in magnitude or direction of near-bed residual velocity. The asymmetry translates into sand waves migration. These recorded observations demonstrated the physical effect of wind and waves on sand waves.

Following the above observations, Campmans et al. (2018) did a pioneer study to model the effects of wind and waves on sand waves bed patterns using a non-linear stability model. At present, two types of process-based models are used to analyse sand waves morphology: stability model and numerical geo-morphodynamics Delft3D model. The advantage of Delft3D models over stability models is that many complex non-linear physical processes such as the non-linear wave-current interaction, suspended transport, advanced turbulence models can be included in a sophisticated way. For instance, the advanced spatially and temporally

variable vertical eddy viscosity model (k - ϵ turbulence model) showed good agreement with field data on sand wave wavelength. In contrast, the constant vertical eddy viscosity model overestimated the wavelength of sand waves (Borsje et al., 2011). The estimation of actual vertical eddy viscosity, using the k - ϵ turbulence model, renders an accurate velocity or near-bed velocities as eddies contribute to the vertical exchange of horizontal momentum and mass between layers. Next to this, the recent model by Borsje et al. (2014) showed the importance of suspended load in sand wave field as it causes the suppression of long sand waves that keep the sand waves from tending towards very long wavelengths. The model by Van Gerwen et al. (2018) showed the dampening of sand wave height due to the suspended load. Also, the non-linearity in wave-current interaction enhances the bed shear stress due to a combination of waves and current (Deltares, 2014a). On the other hand, the linear wave-current interaction underestimates the bed shear stress and, thus, the bedload transport.

Table 1: Comparison of implementation of several physical processes in a model by Campmans et al. (2018) with the possible implementation of the same physical processes in the Delft3D and its advantage in modelling sand wave.

Physical Processes	Campmans et al. (2018)	Possible implementations in Delft3D	Advantages of using Delft3D in sand wave modelling
Vertical eddy viscosity	Constant coefficient	Spatially and temporally variable (k - ϵ turbulence model)	<ul style="list-style-type: none"> • Fair near-bed velocity • Provides good agreement on sand wave wavelength with field data
Suspended load transport	Excluded	Included in advanced form.	<ul style="list-style-type: none"> • Captures mechanism to suppress very long sand waves • Causes reduction in sand waves height
Wave-current interaction	Linear interaction	Non-linear interaction	<ul style="list-style-type: none"> • Proper estimation of bed shear stress and sediment transport

Table 2: Comparison of Campmans et al. (2018) model results with field observations of sand wave properties in the North Sea. (Note that parameters used in the model by Campmans et al. (2018) were similar to the North Sea conditions. That is why model results are compared with sand waves field observations made in the North Sea.)

Sand wave properties	Unit	Model results	Field observations (North Sea)		
		(Campmans et al., 2018)	(McCave, 1971)	(Besio et al., 2004)	(Dorst et al., 2011)
Wavelength	m	600 - 1000	200 - 500	120 - 500	400 - 700
Migration rate	m/year	34.3 (constant duration storm) 1.3 – 2.8 (intermittent storm)	-	1 - 8	0 – 7
Height	m	20 - 30	2 - 7	2 - 10	-

The study by Campmans et al. (2018) simplified the processes such as vertical eddy viscosity, wave-current interaction and excluded suspended load transport. A brief comparison of the implementation of physical processes used in the study by Campmans et al. (2018) and their possible implementations using Delft3D and its advantage is shown in Table 1. Nevertheless, the simplified Campman's model was able to obtain insight into physical mechanisms related to the effect of wind and waves on sand waves. They found that

waves alone do not induce migration, but it significantly affects sand wave growth and migration together with wind. However, the model still lacked a mechanism to keep sand waves from tending toward very long wavelengths. The dominant wavelength was roughly around 600-1000 m and still not in equilibrium. The migration rate obtained for the constant storm conditions was 34.3 m/year, which was larger than field observations. However, the migration rates obtained for intermittent storms were quite realistic. Additionally, sand waves reached up to 20-30 m in height within 20 years, which were quite high. A comparison of models results with recorded sand waves field observations in the North Sea is shown in Table 2. Overcoming the missing non-linearity of physical processes with state-of-the-art formulations using Delft3D will fill the existing gap. Further, it might improve the associated hydrodynamics, morphodynamics and thus, provide better insight into sand wave properties by producing more realistic results in the presence of wind and waves. In this regard, a research study is established to understand the effect of wind and waves on sand waves by including non-linear physical processes using Delft3D.

1.2. Research gap

The recent study by Campmans et al. (2018) involves constant viscosity coefficient instead of time and depth variant viscosity, which could affect the velocity profile accuracy through the vertical column. Similarly, the linear wave-current interaction can underestimate the bed shear stress and bedload transport. In addition, the exclusion of suspended load can affect the height and underestimate the damping effect of long-wavelength sand waves. These missing gaps in the form of non-linear processes could affect the hydrodynamics, sediment transport and produce an overall gap in understanding the effect of wind and waves on sand wave characteristics.

1.3. Research objective

This research study aims to analyse the effect of wind and waves on sand wave properties by including state-of-the-art formulations for several physical processes. It will add the missing non-linearity of these physical processes and further improve the hydrodynamic properties and related morphodynamics of sand waves. To achieve this, the advanced morphodynamic Delft 3D model is used. It includes evaluating vertical eddy viscosity coefficient using the advanced $k-\epsilon$ turbulence model, estimating non-linear wave-current interactions using several friction models available in Delft3D and applying

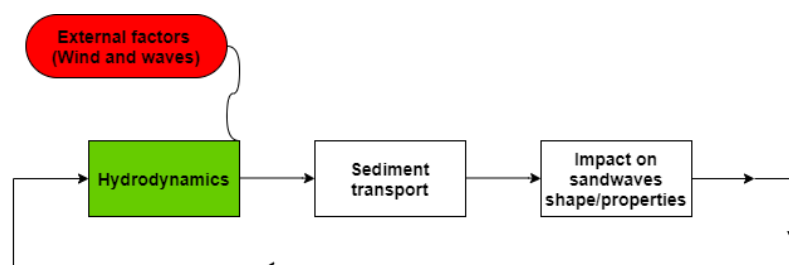


Figure 2: Morphodynamic loop

suspended load in its advanced form. Adding these processes will provide more insight related to the combined wind and waves effect on sand waves.

In general, the morphodynamic loop is the visualization of how these morphodynamic models work (Figure 2). It shows that any change in the hydrodynamics due to forced (or free) external factors affects the sediment transport, which successively changes the bed level. The present research relates to the external factors, wind and waves. Initially, this study focuses on the change in hydrodynamic properties when external factors such as wind and waves combine with the symmetrical tide flowing over sand waves. The model results include hydrodynamic properties such as absolute velocity, tidally average velocity, vertical eddy viscosity, turbulent energy, bed shear stress. Further, inferences are made on the possible sand wave migration and shape using the obtained hydrodynamic results. Finally, few test cases are established in synthetic storm conditions to see morphological development of small-amplitude sand waves or randomly perturbed seabed in 100 years. The model results include the mean sediment transport rate, shape, wavelength, height and migration rate of sand waves.

To summarize the research objective, our main research question is, **“How do wind and waves affect the hydrodynamics and morphodynamics of sand waves?”**

To outline the main question, it is breakdown into sub-questions,

- 1) What are the hydrodynamic properties in tide-only conditions over sand waves of different amplitudes?
- 2) How do the hydrodynamic properties change over sand waves when tide conditions combine with intermediate to severe wind and waves?
- 3) How do the morphodynamic properties of sand waves vary in the presence of wind and waves?

The first two sub-questions will discuss how hydrodynamic properties vary when wind and waves combine with tidal conditions over sand wave seabed. Then it will draw the inferences on sand waves morphology based on the change in hydrodynamic properties in wind and wave conditions. Finally, the last sub-question examines the change in morphodynamic properties of sand waves for 100 years in synthetic storm conditions. These changes in morphodynamic properties of sand waves will be related to the change in hydrodynamics over sand wave bed.

1.4.Approach

Delft3D is used in this study for setting up the numerical model with advanced non-linear processes. In particular, three modules of the Delft3D- Flow, Wave and Sediment, are implemented in different sub-questions of the research study. The Flow module is coupled

with the Wave module using a communication file. The tide current, wind conditions and sediment transport are established using the flow module, whereas the stationary wave conditions are set up using the third generation SWAN (Simulating Waves Nearshore) in the Wave module. Together the current and wave models are run in a quasi-nonstationary mode. It involves a two-way coupling of a nonstationary flow calculation combined with stationary wave model simulations. It is a 2DV model with a domain length running along the horizontal x-axis and the vertical depth along the z-axis. The in-depth model description is mentioned in chapter 3.

To answer the first sub-question, **“What are the hydrodynamic properties in tide-only conditions over sand waves of different amplitudes?”** the study domain is forced with only symmetrical S2 tide. Since this question deals with hydrodynamic properties, the sediment transport module is not activated. Thus, to check the change in hydrodynamic properties with the sand wave evolution, a set of four bed patterns of varying and increasing amplitude are used: a flat bed, 0.25 m finite-amplitude symmetrical sand wave, 0.25 m finite-amplitude asymmetrical sand wave and 3 m high asymmetrical sand wave. The wavelength of sand waves (FGM) is kept the same, 216 m, similar to the model by van Gerwen et al. (2018), for all the beds containing a wavy bed pattern. It might be slightly biased to show sand wave evolution in bed patterns of predefined shape and amplitude. However, it is computationally less intensive as each simulation run needs two tidal cycles, including one tidal cycle spin-up time. In addition to this, it would not affect the qualitative results and present a basic understanding of how hydrodynamic properties can be expected to vary over evolving sand waves in tide-only conditions. The details of the model parameters used in this sub-question are mentioned in section 4.1. The model results include vertical eddy viscosity, turbulent energy, tidally average velocity, bottom shear stress. It is a reference situation, and often it will be used to compare the hydrodynamic results obtained in the presence of wind and waves.

Subsequently, for the second sub-question, **“How do the hydrodynamic properties change over sand waves when tide conditions combine with intermediate to severe wind and waves?”** the study domain is forced with symmetrical S2 tide and combined wind and wave conditions. The wind and wave conditions are unidirectional (along the x-axis), and duration lies throughout the tidal cycle. In this study, two types of wind and wave conditions are used: intermediate and severe. The intermediate refers to the average occurrence value (50th percentile), whereas the severe is the extreme (95th percentile). The details of the wind velocity, wave height and wave period used in this study are mentioned in section 3.3. Since this question also deals with hydrodynamic properties, the sediment transport module is not activated. Like the previous question, four bed patterns of the same wavelength (FGM) are used to show the evolution of sand waves. The simulations run for two tidal cycles, including one tidal cycle spin-up time. The model results include vertical eddy viscosity, turbulent energy, tidally average velocity, bottom shear stress, and comparison with the reference situation of tide-only condition.

In the third sub-question, **“How do the morphodynamic properties of sand waves vary in the presence of wind and waves?”** the sediment transport module is activated as it deals with the changes in morphodynamic properties of sand waves. The morphological simulations are executed using a MORFAC value of 2000 (MORFAC is Morphological Acceleration Factor

used for morphological upscaling in the simulation of long term coastal evolution). All the simulations in this part will run for 100 years due to computational time constraints. The model results include sand wave shape and its asymmetry, wavelength, height, migration rate and migration direction after 100 years. In the first part, the results are compared for four weather conditions: the tide-only conditions, tide and severe wind conditions, tide and severe wave conditions and combined tide, severe wind and waves conditions. The wind and waves are constant duration and unidirectional in this part. Also, an initial bed of 0.25 m finite-amplitude symmetrical sand wave is used to analyse sand wave properties over 100 years in this part. In the second part, the effect of intermittent storms is analyzed on a randomly perturbed initial bed over 100 years. An intermittent storm is a synthetic storm set at a frequency of three months in a year using randomly distributed severe wind conditions. Since the intermittent storm generation is stochastic, two runs are made to analyze the effect of intermittent storms on the same initial perturbed bed. Further, sand wave morphology is compared with the 100 years of morphological development of sand waves in tide-only conditions on the same initial perturbed bed.

Most of the simulation runs are made at 25m as it is the point of interest near the Dutch coast in the North Sea. However, the depth effect is also being analysed for depth varying from 10m – 40m. Also, most simulations involve constant duration wind conditions; thus, extra runs are made to analyse the duration effect of wind. Overview of the value of common model parameters and forcings used in all the simulations are given in chapter 4. The complete schematic approach for the methodology is shown in Figure 3.

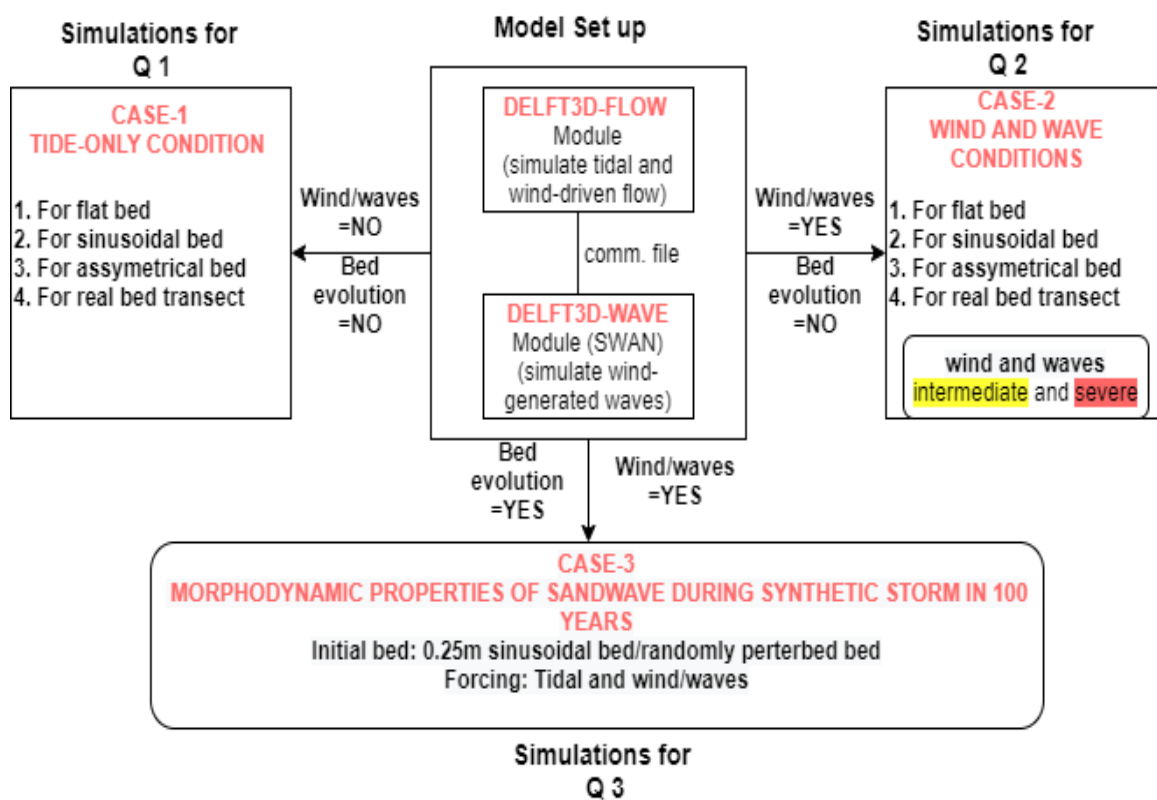


Figure 3: A schematic diagram for the approach used.

1.5.Outline

The outline of the master thesis is organized as follow. Chapter 2 discusses the background information related to physical mechanisms involving the sand wave formation and processes affecting the sand wave properties, including the past field observations. Further, it presents the prior research work related to the change in hydrodynamic properties on a flat bed and sand waves in the presence of combined wind and waves. Later it mentions sand wave model development that happened until now. Chapter 3 relates to the model description consisting of the formulations, computational grid, bathymetry and forces involved. Chapter 4 elaborates on the simulation runs to be executed and model parameters to be used. Finally, the successive chapter 5 to 8 describes the results followed by discussion, conclusion, and future recommendation.

2. Background

Bed patterns, one of the many inherent (free) instabilities of the morphodynamics system (Dodd et al., 2003), cover a large part of the sandy sea bottom. Their range varies from small-scale ripples to large-scale tidal banks. Several studies (Damveld et al., 2020; Dodd et al., 2003; Knaapen, 2005) documented the typical field characteristics of existing bedforms in the marine environment, summarized in Table 3. Among all intermediate to large rhythmic bed patterns in the marine environment, the most dynamic bed patterns are tidal sand waves. Sand waves are observed and studied worldwide to ensure safety in offshore activities. From the Atlantic and the Pacific coast of North and South America (Aliotta & Perillo, 1987; Perillo & Ludwick, 1984) to the Asian waters (Reeder et al., 2011), sand waves are observed and studied. In the North Sea, Veen (1935) pioneered to document the observed sand wave. Later it was elaborated by Stride (1982; 1963).

Table 3: The characteristic spacing, height, migration rate and evolution timescale of rhythmic bed patterns in the marine environment (Damveld et al., 2020; Dodd et al., 2003; Knaapen, 2005).

Bedforms	Spacing (m)	Height (m)	Migration rate (m/year)	Time scale
Ripples	$10^{-1} - 10^0$	$10^{-2} - 10^{-1}$	$10^2 - 10^3$	Hours
Mega ripples	$10^0 - 10^1$	$10^{-1} - 10^0$	$10^2 - 10^3$	Hours-days
Sand wave	$10^2 - 10^3$	$10^0 - 10^1$	$10^0 - 10^1$	Decades
Long bedwaves	~1500	~5	Unknown	Centuries
Shoreface-connected ridges	~ 10^3	$10^0 - 10^1$	10^0	Centuries
Tidal sandbanks	$10^3 - 10^4$	$10^0 - 10^1$	-	Centuries

Previous studies captured wandering mega-current ripples (height 0.2-2 m) on the flanks of sand waves (Figure 4). Sand waves are probably absent in areas covered with coarse sand ($D_{50} > 0.5$ mm) and areas where the bottom sediment contains more than 15% of mud ($D_{50} < 50$ μ m) (Terwindt, 1971; Van Dijk & Kleinhans, 2005). McCave (1971) studied environmental conditions, like tidal current strength to sand wave occurrence. Bokuniewicz et al. (1977) observed that as little as 10% of silt or coarse sand inhibits the sand wave formation. Field data from the southern North Sea reveal that sand waves are absent where suspended load transport is dominant. (Borsje et al., 2013, and references therein). Soundings made by Rijkswaterstaat during 1935-1938 and 1967-1969 by the Dutch Hydrographic Office reveal that the maximum height of sand waves along the Dutch coast was about 13 m. These highest sand waves were found just off the Dutch islands (Terwindt, 1971, and references therein). Knaapen (2005) used bathymetry data of 12 years derived from the echo soundings throughout the Southern Bight of the North Sea and the English Channel to predict sand wave migration based on shape. The extracted information from the collected data mainly showed asymmetric sand waves with spacing 164 m to 340 m, height ranging from 0.7 m to 3.4 m, migration from (-)0.2 m to 8.4 m/year (Knaapen, 2005). The collected data showed negative traces of migration even though the residual current was

positive, 0.1 m/s. Another study (Ferret et al., 2010) recorded dune movements in the direction of the residual tidal currents, with mean migration rates around 0.8 to 5 ± 0.25 m/year and up to 6.6 ± 0.7 m/year, respectively, at multi-decennial and decennial time scales. Remarkably, it also displayed locally opposite progradation to residual current.

Dorst (2009) developed deformation analysis using time series of bathymetric data and showed that the tidal sand wave in the Southern North Sea could have migration rates up to 7.5 m/year. Later, Santen et al. (2011) inferred wavelength ranging from 200 m – 800 m in the North Sea. A recent study by Damen et al. (2018) extracted sand wave properties by applying the 2-D Fourier transform of the bathymetry data near the Dutch coast in the North Sea. It illustrated that the wavelength varied non-linearly from 200 m – 300 m in the south to 500 m – 1000 m in the north. The lateral length varied from 100 m – 1000 m near the coast, and the height goes up to 10 m. The observed sand wave orientation was approximately

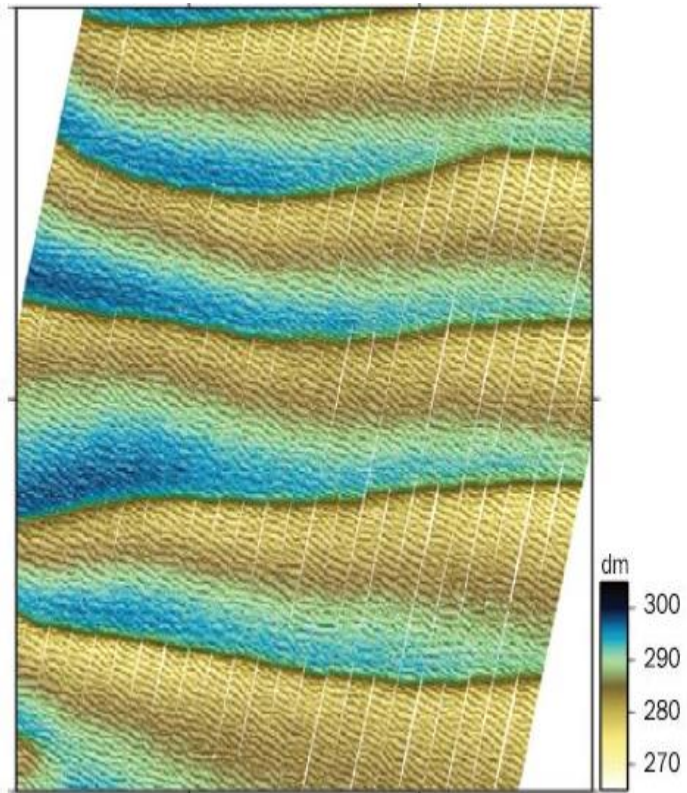


Figure 4: Interpolated survey images of 1 km² area, showing sand waves and megaripples near Egmond, Netherlands. Depths are given in decimeters to MSL. (Van Dijk et al., 2008)

perpendicular to the main tidal axis (Németh et al., 2002, and references therein). Stride (1982) observed symmetric and asymmetric sand waves in the Northern Hinder Banks. It presents low lee and stoss side slopes, on average 8° and 3°, respectively. Nearer to the Dutch coast, more north-west and south-east oriented sand wave crests were observed, almost orthogonal to the tide (Ferret et al., 2010; Terwindt, 1971).

Sand wave properties have such dynamic nature due to high local variability in environmental parameters (van Dijk et al., 2008; van Santen et al., 2011). They may grow comparable to shallow water depth and migrate at a speed of several meters per year. Also, the water depth over sand wave crest reduced by 10% - 30 % compared to depth over the troughs (Terwindt, 1971). This dynamic behaviour poses a hazard to offshore navigation channels as its growth risks the minimum shipping depth. Also, they can hamper the structural stability of offshore engineering structures such as offshore wind farms, pipelines, and telecommunication cables as sand waves migration could result in the buckling of pipelines or cables and form a risk for the stability of wind farms. Thus, extensive and frequent hydrographic survey programs are carried to monitor sand wave field and identify potential risks. However, this is a time-consuming and costly method based on the large spatial extent that needs to be covered (Damveld et al., 2020). Additionally, the offshore sand waves are

often dredged to fulfil the need for sand nourishment. These dredging activities can affect sand wave properties and overall bed topography. Thus, it is relevant to understand and model the major processes controlling their evolution and migration from an engineering perspective. In addition, it will help to understand and predict the behaviour of sand waves when subjected to human activities.

2.1. The physical mechanism behind sand wave formation

Sand waves form as a free instability of the sandy seabed perturbations when subject to tidal flow (Hulscher, 1996). The interaction of oscillatory tidal flow with the bottom waviness gives rise to tidally average residual flow in the form of vertical recirculating cells (Figure 5). Particularly, advective momentum generates both residual pressure gradients and residual current. These residual flow components cause residual

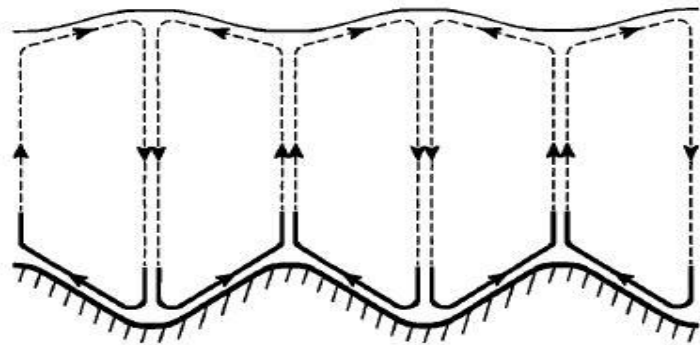


Figure 5: Strong near-bed circulation which supports the growth of the bottom perturbation. The backward circulation in the upper flow part uses a larger part of the water column and is weaker (Refer to figure 12, Hulscher, 1996)

circulating cells that leads to convergence of sediment transport towards the crest. If the movement is strong enough to overcome gravity effects that carry the sediment away from the crests toward the troughs, the perturbation grows and rises to wavy bottom patterns. Generally, the preferred wavelength also referred to as the fastest-growing mode (FGM), is used to understand and model sand wave growth dynamics, based on the fact that FGM has the highest growth rate and will be dominant. The growth and symmetry of sand waves depend on velocity, depth, eddy viscosity, tidal asymmetry, grain size and inclusion of suspended load (Németh et al., 2007; Németh et al., 2002). Later several studies (G. Besio et al., 2006; Borsje et al., 2011; Campmans et al., 2017; Németh et al., 2002) extended this theoretical approach in understanding the sand wave evolution and processes affecting them.

2.2. Physical processes affecting sand wave properties

The key properties of sand waves are sand wave height, wavelength, shape and migration rate (Figure 6). The migration rate is zero for symmetrical wavy seabed; combining tidal current and residual current should show sand wave migration due to distortion and loss of symmetry (Hulscher, 1996). The addition of residuals distort the circulation cells, shifts the point of convergence and changes the shape; lee-stoss asymmetry of bedforms is a sign for bedform migration in the steeper slope direction. (Németh et al., 2002). Tidal asymmetry can also cause sand waves to migrate in both flood and ebb directions, and it was concluded that the relative strength of the residual current with respect to the amplitude of the tidal constituent and the phase shift between the tide constituents control the direction of

migration (Besio et al., 2004). This study qualitatively verified the negative migration rate in the field (Knaapen, 2005). Borsje et al. (2013) mention that an increase in bed roughness can cause high migration rates. The migration rate increases linearly with residual current strength, and the change became more significant with the inclusion of both residual current and suspended load transport (van Gerwen et al., 2018). As sand wave evolves, sand wave migration rate reduces according to field data (Knaapen, 2005; Németh et al., 2007). Although sand wave migration speed decreases with increasing height, a study by Campmans et al. (2018) showed higher sand waves overtaking smaller sand waves, which is counterintuitive.

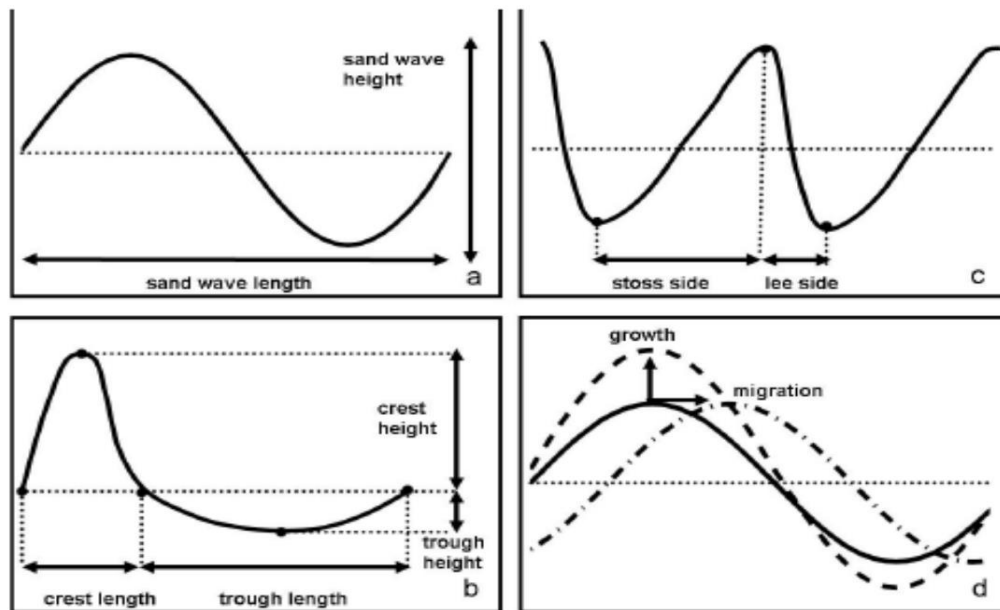


Figure 6: Schematic representation of (a) wavelength and height, (b) crest and trough length, crest and trough height, (c) lee and stoss asymmetry, (d) growth and migration of sand waves. Source: (Ijzer, 2010)

The stabilization mechanism defines sand wave height, and it is based on the balance between the shear stress at the seabed (flow effect) and the gravity effect that moves sediment downhill (Campmans et al., 2018; Németh et al., 2007). With an increase in the eddy viscosity, equilibrium wave height increases and the timescale to reach equilibrium height reduces (Németh et al., 2007). This increase in wave height is partly due to the longer fastest growing modes, which have relatively less inhibitions by the slope effect during their evolution. Later, Borsje et al. (2014) found that suspended sediment transport has a dampening effect on the growth of sand waves for varying grain sizes, resulting in the shift of sediment away from the crest region due to the phase lag between the suspended sediment concentrations and sand wave. Also, suspended sediment dynamics suppresses long-wavelength sand waves. Decreasing the grain size (say 0.20 mm), suspended load transport, and slope effect damps the bottom perturbations entirely. Overall, the decay effect is large for small grains (the suspended load regime) than large grains (the bed load regime). Similarly, high-velocity results in similar decay compared to low velocity (Borsje et al., 2014; van Gerwen et al., 2018). The decrease in grain size and increase in flow velocity generates critical conditions on sand waves growth due to the balance of damping effect by slope-induced flux and suspended transport load flux with bedload transport flux (Borsje et al., 2014). Tidal

asymmetry leads to lower sand wave heights, as tidal asymmetry also causes divergence from the crest region (van Gerwen et al., 2018).

The wavelength of sand waves increases with increasing water depth and tidal ellipticity while decreases with increasing tidal current amplitude (Németh et al., 2007; van Santen et al., 2011). The inclusion of suspended load increases the fastest-growing mode significantly (Campmans et al., 2017). However, several studies (Borsje et al., 2014; van Gerwen et al., 2018) suggest a slight influence of the suspended load on preferred wavelength. The possible reason could be a difference in the model processes as the Campmans et al. (2017) model involves the presence of severe wind effect in it, which results in wave-stirring effect responsible for the enhancement in suspended load movement and increase in the fastest growing mode, or exclusion of effects of higher order being a linear analysis. Past studies (Dodd et al., 2003; Németh et al., 2007) assumed the FGM mode to prevail until the equilibrium stage due to the weak non-linearity of the system, based on similarity of the results obtained by a linear model with field bathymetry data. Later, Van Gerwen et al. (2018) quantified this difference on a randomly perturbed bed using the Delft3D model and found a moderate difference (~100 m). Quantitative results in the presence of wind and waves conditions showed that the much longer wavelength dominates the fastest growing mode in the final stage in comparison to that was during the initial stage; however, the study involved the shortcoming of having no control over the suppression of longer wavelength (Campmans et al., 2018). The best resemblance of the modelled sand wavelength with field data is obtained when space and time-dependent vertical eddy viscosity is used along with the suspended load. The time-dependent eddy viscosity helps estimate the bed shear stress accurately, and the suspended load suppresses the longer wavelength (Borsje et al., 2013).

Relatively, large flow resistance leads to sand waves with their crest normal to the main tidal current direction. Less flow resistance leads to the rotation of sand wave crests due to the veering of the currents in the vertical direction (Hulscher, 1996). The field data usually find wave crests approximately transverse to the main tidal direction (Knaapen, 2005; van Dijk et al., 2005; Van Dijk et al., 2008). Further, the shape of sand waves changes when external factors such as tidal constituents or storm conditions add residual velocity, change the residual velocity's strength, or reverse its direction (G. Besio et al., 2006; Campmans, Roos, de Vriend, et al., 2018). It causes a shift in the point of convergence of deposition, changes shape, and introduces shape asymmetry.

2.3. Effect of wind and waves over various bathymetries

Since the external factor in this study is wind and waves. Its effect shall be discussed here separately. It is bifurcated into three parts; the first part includes the past studies for the effects of wind and waves over a flat bed. The second and third parts describe the field observations and previous model results related to the effect of wind and waves on sand wave properties, respectively.

Observations on a flat bed: The process wind effect includes wind-driven current and wind-generated waves. Wind can induce depth-averaged surge current up to 1 m/s in the North Sea (Flather, 1975). Davies et al. (1994) showed that tidal elevation amplitude and phases are

significantly changed in the shallow coastal regions in the presence of wind and waves. It happens due to enhanced frictional effects associated with the wind-driven flow and wind-wave turbulence on a flatbed. The study confirmed the importance of non-linearity produced by a surface wind-induced shear, non-linear wave-current interaction and a flow-dependent viscosity in influencing tidal current profiles. These non-linear terms, namely, the advective terms and quadratic bottom friction term in the hydrodynamic equations, can transfer the energy at the M2 frequency to higher harmonics and residual flow (Davies et al., 1994). The source of M4 tidal current was associated with wind-field and time variations of the eddy viscosity, which determines the rate at which wind's energy can diffuse to depth. Another study (Davies et al., 2000) related to the effect of wind forcing on the North Channel of the Irish Sea demonstrated depth mean flow in the direction of the wind in shallow water with a weak return flow opposite to wind direction at a depth in the deeper regions. This return flow is due to the gradients of the sea surface elevation set up by the wind. Ruessink et al. (2006) also displayed the non-linear effect of wind on rectilinear M2 tidal flow, excluding Coriolis effect, using a quadratic bottom stress formulation and time-dependent eddy viscosity derived from k- ϵ turbulence closure model at Terschelling, Netherlands. The study demonstrated wind-driven flow and energy transfer from M2 into the next overtide (M4, M6).

King et al. (1985) observed a drift opposite to wind in tidally averaged flow for the recorded observation near the Celtic Sea at 120 m. They speculated that this weak mean current through the water column near-bed might be caused by the wind flowing over the surface. Later Holmedal et al. (2013) modelled the observations recorded by King et al. (1985) and concluded that wind direction is essential for tidal drift through the water column; however, it remained open whether the non-zero mean velocities were caused by the wind alone or other non-linearities too. The presence of wind leads to an enhanced bottom shear stress, and its distribution becomes asymmetric through the tidal cycle (Holmedalet al., 2013). A qualitative study in the North Sea showed that the wind effect adds transport component apart from the already present tidal-based sediment transport, mainly when wind-driven flow and wind waves act together. The reason being, waves stir up the sand, and wind-driven currents facilitate the transport (Van Der Molen, 2002). For instance, the model results (Van Der Molen, 2002) showed an additional eastward sand transport component and suspended load towards the Dutch coast due to wind and waves, using ten years of wind data at the Texelhors meteorological station (Figure 7). At sites characterized by a relatively weak tide-induced flow (0.2 m/s), the moderate-speed wind (10 m/s) can reverse the tidal flow

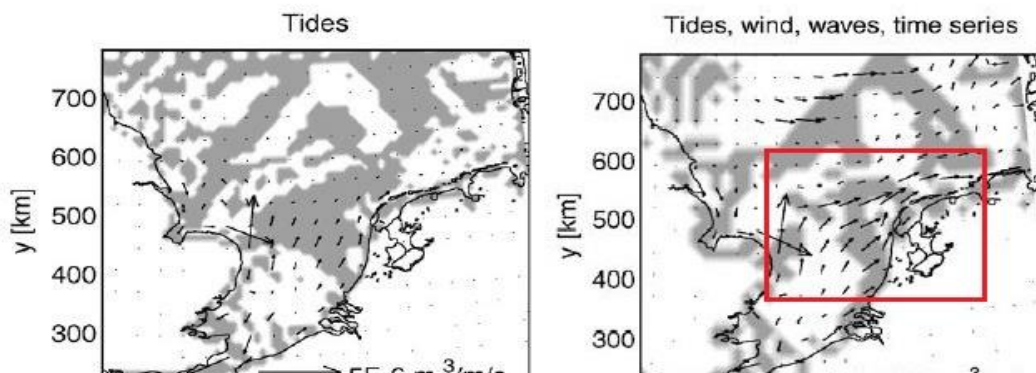


Figure 7: Eastward sand transport component and suspended load towards the Dutch coast using a model study (Van Der Molen, 2002) and ten years of wind data at the Texelhors meteorological station, due to (A) Tides, (B) Tides, wind and waves.

direction; these changes in hydrodynamic properties lead to change in morphodynamics due to bed shear stress variation (Colosimo et al., 2020).

Observations on sand wave seabed: Like flatbed, recorded observations show a significant effect of strong winds on wavy bed patterns such as sand waves. At one of the locations in the Hinder banks, it was observed that the height of sand wave crests depends on the frequency of occurrence of heavy gales (which erode the crests) and the length of the intermediate calm weather period (which build the crests). The maximum observed variation in the height of sand wave crests was about 2 m (Terwindt, 1971). The calculation was made for maximum orbital velocity ($\overline{u_{orb}}$) in the direction of wave propagation. It was found that about 95 percent of the time the value of $\overline{u_{orb}}$ is smaller than 0.275 m/sec, for which the effect was negligible. McCave (1971) correlated the variability in the position of sand wave field with wave activity. Fenster et al. (1990a) and Bokuniewicz et al. (1977) observed significantly different migration rates in the same area over different periods, suggesting strong seasonal winds (storms) as a crucial factor for this change.

Le Bot et al. (2000) attributed the sedimentary dynamics to the time scale. Over a long period (decades), it fits well with the residual tidal currents; over the medium period (several years), the frequency of meteorological forces either slow down the effect of tidal residual or reverse the effect of tidal currents leading to a reversal of dune asymmetry. Later, Ferret et al. (2010) hypothesized that submarine dune dynamics were controlled by tidal currents and wind forces, based on different field observations displaying local progradation opposite to the residual currents. Their postulations state that inconsistencies in sand wave profile in the eastern English Channel could result from the relative strength of tides and storm actions. Thus, strong winds can cause a change in sand wave shape and asymmetry. Van Dijk et al. (2005) studied the wave impact on sand waves and showed that storm waves of 3 m height could mobilize sediment of grain sizes up to 300 μm in water depths of 25 m.

Model Results on sand waves: Campmans et al. (2017) studied the spatially uniform and steady wind effect on sand wave formation, initially limited to small amplitude only, using linear stability analysis. They concluded that severe wind affects sand wave dynamics, decreases the growth rate, increases the preferred wavelength, and causes sand wave migration. The wind-driven current causes sand wave migration by adding asymmetry, whereas waves alone do not induce migration, but they enhance migration induced by the wind-driven current. Together, severe wind and waves can significantly oppose migration during fair weather and sometimes reverse the migration rate. Campmans et al. (2017) concluded the above observations for wind effect in the tidal direction with wind speed 20 m/s and wave height 5 m. This study also allowed variation in the wind speed and wind direction and included the Coriolis effect. The Coriolis effect causes a shift in the angle at which the maximum growth and migration rate occurs and reduces the magnitude of the migration rate. In particular, the wind effect depends very much on the wind duration, direction and not simply on magnitude (A. M. Davies & Lawrence, 1995). The extension of a linear model into a nonlinear model for finite-amplitude sand waves showed that their influence is still essential even if storm conditions occur for a short period (Campmans et al., 2018). For instance, the reduction in crest height varied from 9% to 60% for 1 month/year and a full-year duration storm compared to the equilibrium height in tide-only condition.

These observations and model results provide a firm indication about the effect of wind and waves on sand waves.

2.4. Sand wave model development overview

The general approach evaluates sand wave properties using data-driven models based on empirical laws (Dorst et al., 2009; Knaapen, 2005). These models work reasonably well for the data they were calibrated on but did not provide a complete understanding of the complex processes involved in sand wave evolution (Damveld et al., 2020). Next to this, the process-based models can help gain insights and understand the processes involved in sand wave evolution. Two types of process-based models are generally used to study the behaviour of large-scale bed features: stability model and morphodynamics Delft3D model. Physical processes are defined in simplified form in the stability model (Tonnon et al., 2007). The stability models can be further categorized into linear and nonlinear models; linear models are used to analyze the behaviour of small-amplitude sand waves, unlike nonlinear stability models that involve the interaction of unstable modes, thus obtaining information on the equilibrium height and shape of the bed wave patterns (van Gerwen et al., 2018). The advanced Delft3D model uses the Reynolds averaged Navier-Stokes equation by considering physical processes in a sophisticated way (e.g., wind-and wave-driven currents, density gradients, advanced turbulence models). However, they have a high temporal and spatial resolution, making them computationally expensive. Also, treatment of lateral boundary conditions requires care in numerical models (Borsje et al., 2013).

Hulscher (1996) developed a three-dimensional sand wave model that explicitly showed the importance of tidally averaged circulation cells in its formation using linear stability analysis. This model incorporated constant eddy viscosity and partial slip condition. Developing further, it was shown that sand wave migration could be caused by pressure gradient or wind-driven flow (Németh et al., 2002) and tidal asymmetry (Besio et al., 2004), for constant eddy viscosity. Later, Besio et al.(2006) added depth-dependent eddy viscosity and suspended load to it. The model reproduced sand wavelength at different locations on the Belgium Continental Shelf fairly well (Cherlet et al., 2007). The linear model was extended by adding the wind effect for variable wind direction and Coriolis effect; however, it calculated migration rate during the formation stage in hundreds of m/year (Campmans et al., 2017). For finitely large-amplitude sand waves, Nemeth et al. (2007) investigated sand wave dynamics in the presence of current induced by wind stress and pressure gradient using a non-linear stability model. This study was followed by Van den Berg et al. (2012) on a much longer domain. Campmans et al. (2018) analyzed sand wave properties in the presence of wind and waves. Shortcomings of these models include overprediction of sand wave height, and often the wavelength kept increasing for larger model domains (van Gerwen et al., 2018).

An early Delft3D based model was applied on an artificial sand wave at Hoek van Holland implementing a single representative wind and wave condition (Tonnon et al., 2007). Since their study focused on an artificially developed 3 m depth sand wave, it was difficult to understand the formation processes. Models by Borsje et al. (2011, 2013, 2014) are among the earliest to include the advanced turbulence model, suspended sediment dynamics, and

combination. Such an extensive model reasonably demonstrated sand wave properties close to field data of several studies (Dorst et al., 2009; van Santen et al., 2011). In addition to this, it gives a good result in the longer domain due to the suppression of longer wavelengths, which is at present impossible in the stability models. Recently, Van Gerwen et al. (2018) used the previous model developed by Borsje et al. (2014) to indicate the effect of tidal asymmetry and suspended load on equilibrium height and produced results similar to field data.

The stability models are favourable for the long-term qualitative and sensitivity analysis, and advanced Delft3D models are desirable for better quantitative results close to field observations. So far, the analysis in Delft3D is done for tide-only conditions. Thus, knowledge of the wind effect on sand wave dynamics can be further extended, improved and more insight can be gained by including the non-linear physical processes missing from the existing simplified model (Campmans et al., 2018). Inclusion of these non-linear effects might help to produce results compared to the field observations as already discussed in section 1.1 and shown in Table 2.

3. Sand wave model description

The growth of sand waves is modelled using the numerical shallow water model Delft3D (Lesser et al., 2004). As mentioned earlier, this research work in its initial stage simulates hydrodynamics for purely tidal conditions, later wind and wave conditions are added to tidal hydrodynamics. Advancing towards the end, morphodynamics features are also added. Thus, in its final form, the model requires coupling of the Delft3D modules, namely Flow, wave, and sediment transport. Therefore, a model description shall be given considering all the modules of Delft3D.

Flow module: Settings for tidal current and wind field, sediment transport is established in the flow interface, whereas a separate wave interface pops up to set up the conditions for the wave field. The connection between flow and wave interface is established through a communication file. The flow model description related to tidal current is similar to the model by van Gerwen et al. (2018).

Wave module: The wave module uses a third-generation SWAN model- SWAN is an acronym for Simulating Waves Nearshore, to simulate the evolution of short-crested waves. Further, wave-current dynamic interaction is executed through an online coupling of the wave with the flow. Through this coupling, both the effect of waves on current (via forcing, enhanced bed shear stress) and the effect of flow on waves (via set-up, current refraction and enhanced bottom friction) are accounted for (Deltares, 2014b).

Module integration: Each module can be executed independently or in combination with one or more other modules. The information exchange between modules is provided automatically using a so-called communication file; each module writes results required by another module to this communication file and reads from the same file regarding the information required from other modules.

SWAN: All information about the sea surface is contained in the wave variance spectrum or energy density E (σ' , Θ), distributing wave energy over frequencies σ' and propagation directions Θ . Θ shows the direction normal to the wave crest of each spectral component. The SWAN model evaluates the evolution of action density, $N = E/\sigma$, as it is conserved during wave propagation in the presence of ambient current, whereas energy density E is not (Deltares, 2014b). It is assumed that the ambient current is uniform with respect to the vertical coordinate and is denoted as \vec{U} . The rate of change of the action density at a single point in space (\vec{x} ; σ' , Θ) is governed by the action balance equation, which reads,

$$\frac{\partial N}{\partial t} + \nabla_{\vec{x}} \cdot [(\vec{c}_g + \vec{U})N] + \frac{\partial c_{\sigma'} N}{\partial \sigma'} + \frac{\partial c_{\Theta} N}{\partial \Theta} = \frac{S_{tot}}{\sigma'} \quad (1)$$

The left side of Equation 1 is the kinematic part of this equation. The first term is a temporal variation of action density that is zero in stationary waves. Its second term denotes the propagation of wave energy in geographical space \vec{x} including wave shoaling, with the group velocity \vec{c}_g , following the dispersion relationship. The third term represents the shifting of radian frequency due to variation in depth and mean currents, and the fourth term relates to depth induced and current-induced refraction. $c_{\sigma'}$ and c_{Θ} are propagation velocities in spectral space (σ' , Θ). Notice that the second, third and fourth terms are divergence terms

representing the amount of flux entering or leaving a point. Hence, they act as source (negative divergence, i.e., flux entering a point) or sink (positive divergence, i.e., flux leaving a point). The right-hand side contains, S_{tot} , a non-conservative source/sink that includes all physical processes which generate, dissipate, or redistribute wave energy at a point.

3.1. Hydrodynamics

The system of equations consists of the Navier-Stokes equations, flow and sediment continuity equations and sediment transport equations. The vertical momentum equation is reduced to the hydrostatic pressure relation as vertical accelerations are assumed to be small compared to gravitational acceleration. The model equations are solved by applying σ - layering in the vertical orientation. In this study, the model is run in the two-dimensional vertical (2DV) mode, i.e., considering flow and variation in the x- and z-direction only while assuming no flow and uniformity in the y-direction. Coriolis effects are assumed to have a negligible effect at the length scale of sand waves (Hulscher, 1996). For this study, sand wave is assumed to be perpendicular to the rectilinear tidal velocities.

Further, the wind is added to the existing 2DV flow model by van Gerwen et al. (2018), and the wave module based on SWAN 3rd generation model is integrated with it. The current and wave models are run in quasi-nonstationary mode. It involves a two-way coupling (6-min intervals) of a nonstationary flow calculation combined with stationary wave model simulations. Every 6 minutes during the hydrodynamic simulation time, SWAN is activated. It then performs a stationary simulation, using the wave spectra from given wave height, wave period, wave direction and range of frequency. Each wave simulation utilizes the corresponding water levels, mean current, and bed levels provided by the hydrodynamic model as boundary conditions from the flow module. Subsequently, the wave parameters calculated in the Delft3D-Wave module are used as input for the Delft3D-flow module to compute two-way wave-current interaction. This model considers the non-linear current-wave interaction, which shall be discussed later in this chapter.

In terms of σ -coordinates, the 2DV hydrostatic shallow water equations are described by,

$$\frac{\partial U}{\partial t} + U \frac{\partial U}{\partial x} + \frac{\omega}{(H+\zeta)} \frac{\partial U}{\partial \sigma} = -\frac{P_u}{\rho_w} + F_u + \frac{1}{(H+\zeta)^2} \frac{\partial}{\partial \sigma} \left(v_v \frac{\partial U}{\partial \sigma} \right) \quad (2)$$

$$\frac{\partial \omega}{\partial \sigma} = -\frac{\partial \zeta}{\partial t} - \frac{\partial [(H+\zeta)u]}{\partial x} \quad (3)$$

Here, U is the generalized Lagrangian horizontal velocity component for simulations including waves, $U=u+u_s$, where u is the horizontal Eulerian velocity and u_s is Stokes drift component due to wave propagation (Lesser et al., 2004). ω the vertical velocity relative to the moving vertical σ -plane, ρ_w the water density, H the water depth below reference datum, ζ the free surface elevation, P_u the hydrostatic pressure gradient and F_u describes the horizontal exchange of momentum due to turbulent fluctuations. The vertical eddy viscosity v_v is calculated by means of the k- ϵ turbulence closure model in which both the turbulent energy k and the dissipation ϵ are computed (Rodi, 1980). The resulting vertical eddy viscosity v_v is variable both in time and space. For details on the k- ϵ turbulence model formulations, see Burchard et al. (2008).

At the bed ($\sigma = -1$), a quadratic friction law is applied, and the vertical velocity ω is set to zero.

$$\tau_b = \rho_w \frac{v_v}{(H+\zeta)} \frac{\partial u}{\partial \sigma'} = \rho_w u_* |u_*|, \omega = 0. \quad (4)$$

in which τ_b is the bed shear stress due to wind-driven flow and tidal flow. u_* is the shear velocity that relates the velocity gradient at the bed to the velocity u in the lowest calculation grid point by assuming a logarithmic velocity profile. At the free surface, the wind is implemented as uniform shear stress (wind stress) due to wind speed. Wind stress magnitudes are computed by

$$|\overline{\tau_{wind}}| = \rho_a C_d U_{10}^2 \quad (5)$$

Wherein ρ_a is the density of air (kg/m^3), U_{10} the wind speed 10m above the free surface (m/s) and C_d the wind drag coefficients are defined using $C_d = (0.75 + 0.067 |U_{wind}|) 10^{-3}$ (Campmans et al., 2018). In Delft3D, the wind speed and their corresponding drag coefficients must be inserted manually for a definite range of wind speeds. For instance, several points 0 m/s, 10 m/s, 20 m/s and 100 m/s are selected for this study. Further, it uses linear interpolation or step function to calculate values at different wind speeds between 0 m/s and 100 m/s. If the intermediate wind speed is between 0 m/s and 10 m/s, it will use linear interpolation to calculate the drag coefficient at the intermediate wind speed. Similarly, if wind speed exceeds 100 m/s, it will simply assume the drag coefficient same as 100 m/s. On the surface, it satisfies

$$\frac{v_T}{(H+\zeta)} \frac{\partial u}{\partial \sigma'} = \frac{1}{\rho_w} |\overline{\tau_{wind}}| \cos \theta, \omega = 0. \quad (6)$$

Here $\theta = 90^\circ$ as wind is unidirectional coming from the positive x-axis (Figure 8).

Current and wave interaction: Unlike the previous study by Campmans et al. (2018), herein, non-linear wave-current interaction is considered. This non-linearity exists as the Reynolds averaged wave mean shear stress is non-zero and decay of waves induces mass-momentum transfer, also known as Stokes drift (Soulsby et al., 1993). Therefore, the bed shear stress due to combination of waves and current is enhanced beyond the value, which would result from the linear combination of bed stress due to waves ($\overline{\tau_w}$) and current ($\overline{\tau_c}$). In the non-linear formulation, it calculates maximum bed shear stress, ($\overline{\tau_{max}}$) for sediment transport modelling, while it calculates current velocity and the turbulent diffusion using mean bed shear stress, ($\overline{\tau_m}$). The schematic view of non-linear interaction of wave and current bed shear stresses is shown in Figure 9. This research study assumes current and wave propagation in the same direction (Figure 8). The parameterisation for the time-mean bed stress and maximum bed shear stress is of form:

$$|\overline{\tau_m}| = Y (|\overline{\tau_c}| + |\overline{\tau_w}|) \text{ and } |\overline{\tau_{max}}| = Z (|\overline{\tau_c}| + |\overline{\tau_w}|) \quad (7)$$

Y, Z are empirical parameters based on several friction models described in Soulsby et al. (1993). This study uses the friction model by Fredsoe et al. (1993). The magnitude of the wave-averaged bed shear-stress due to waves alone is related to the wave orbital velocity near the bottom $\overline{u_{orb}}$ and the friction coefficient f_w as, $|\overline{\tau_w}| = \frac{1}{2} \rho_w f_w u_{orb}^2$. The orbital velocity is

computed from the linear wave theory and is given by, $\vec{u}_{orb} = \frac{1}{4} \sqrt{\pi} \frac{H_{rms} \omega}{\sinh(kH)}$ where the root-mean-square wave height H_{rms} and the wave period $T(=2\pi/\omega)$ are read from the communication file (through which waves and current are connected). The wave friction factor varies with the relative orbital excursion at the bed under purely oscillatory flow (Deltares, 2014a).

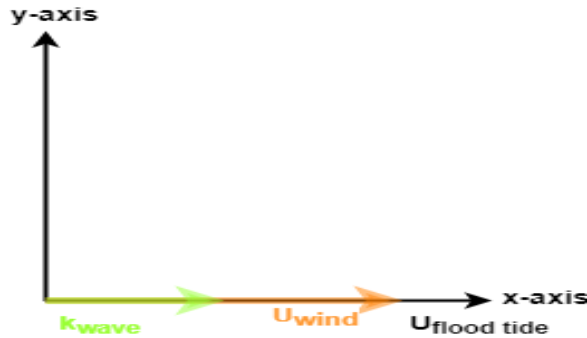


Figure 8: Definition sketch (top view) of the direction of tidal current (black), wind (orange) and wave vector (green).

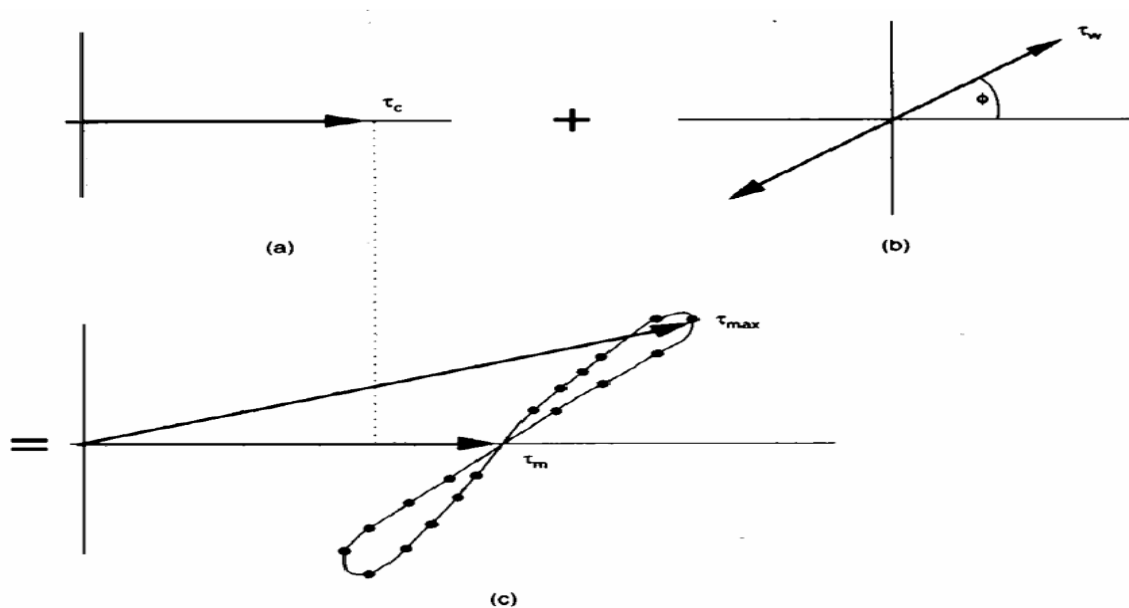


Figure 9: The schematic view of a non-linear interaction of wave and current produced bed shear stresses (Soulsby et al., 1993).

3.2. Sediment transport and bed evolution

The bedload transport, S_b is calculated by (van Rijn et al., 2004).s

$$S_b = 0.006 \alpha_s \rho_s w_s d_{50} M^{0.5} M_e^{0.7}, \quad (8)$$

where α_s is the correction parameter for the slope effects (see below), ρ_s the specific density of the sediment, w_s the settling velocity of the sediment, and d_{50} indicates the median

The effect of wind and waves on the hydrodynamic and morphodynamic properties of sand waves

sediment grain size. M and M_e are the sediment mobility number and excess sediment mobility number, respectively, that are given by

$$M = \frac{u_r^2}{(\rho_s/\rho_w - 1)gd_{50}}, M_e = \frac{(u_r - u_{cr})^2}{(\rho_s/\rho_w - 1)gd_{50}} \quad (9)$$

where u_r is the magnitude of the equivalent depth-averaged velocity computed from the velocity in the bottom computational layer assuming a logarithmic velocity profile, u_{cr} is the critical depth-averaged velocity for the initiation of motion of sediment based on the Shields curve. If $u_r < u_{cr}$, the bedload transport is set to zero. Bedload transport is affected by bed-level gradients, which causes sediment to move more difficult upslope than downslope. The correction parameter α_s for the slope effect depends upon tangent of the angle of repose of sand φ_s (van Gerwen et al., 2018). The angle of repose of sand φ_s is in the range between 15° and 30°. Whereas the suspended load is calculated by

$$S_s = \int_a^{(H+\zeta)} \left(uc - \epsilon_{s,x} \frac{\partial c}{\partial x} \right) \partial z, \quad (10)$$

where a is the reference height (see below) and c is the mass concentration, defined by

$$\frac{\partial c}{\partial t} + \frac{\partial(cu)}{\partial x} + \frac{\partial(\omega - w_s)c}{\partial z} = \frac{d}{dx} \left(\epsilon_{s,x} \frac{\partial c}{\partial x} \right) + \frac{d}{dz} \left(\epsilon_{s,z} \frac{\partial c}{\partial z} \right) \quad (11)$$

where $\epsilon_{s,x}$ and $\epsilon_{s,z}$ are the sediment diffusivity coefficients in the x- and z-direction, respectively. ω is vertical velocity relative to the moving vertical σ -plane. Sediment transported below the reference height $a=0.01H$ is regarded as bedload transport as it responds almost instantaneously to changing flow conditions (van Rijn et al., 2007). Transport above this height is assumed to be in suspension.

Finally, the bed evolution is governed by the sediment continuity equation (Exner equation), which reads

$$(1 - \epsilon_p)\rho_s \frac{\partial z_b}{\partial t} + \frac{\partial(S_b - S_s)}{\partial x} = 0 \quad (12)$$

In which $\epsilon_p = 0.4$ is the porosity, S_b the bedload transport (8), and S_s the suspended load transport (10). (12) simply states that convergence (or divergence) of the total transport rate must be accompanied by a rise (or fall) of the bed profile. Morphological changes occur on a much larger timescale than hydrodynamic changes. Therefore, a morphological acceleration factor (MORFAC) is introduced. It allows for faster computations by multiplying the bed evolution after each time step by this factor (Ranasinghe et al., 2011). The bottom roughness is described by the Chézy coefficient using the White-Colebrook equation, similar to the model by van Gerwen et al. (2018).

3.3. Model set up

The computational grid has a variable resolution in both x- and z- directions. In the centre of the domain, the horizontal grid resolution is fine such that the distance between grid nodes is 2 m. However, it is coarser up to 1500 m between the nodes towards the lateral boundaries.

The length of the domain in the x-direction is around 45 km (Figure 10a). The vertical resolution is divided into 60 sigma layers. Unlike the model by van Gerwen et al. (2018), these layers have high resolution towards the surface and bed, and it reduces while moving towards the centre of mean water depth (Figure 10b). The stability of few results for high vertical and horizontal resolutions of the computational grid is also checked and presented in Appendix 1.

The sediment transport module is not activated in the initial half of the study, where only hydrodynamic properties are investigated. Thus, four types of predefined bathymetry are used: a flat bed, 0.25 m finite-amplitude symmetrical bed, 0.25 m finite-amplitude asymmetrical bed and 3 m high asymmetrical bed to introduce the effect of evolving sand waves (Figure 11a). For wavy bed patterns, the centre of the domain (around 1km) comprises a sand wave field, which is then multiplied by an envelope function to ensure a gradual transition from a flat bed towards sand wave field. In the case of wavy patterns, the wavelength is set same for all predefined beds to the fastest-growing mode, 216 m. For simplicity, the FGM of 3 m high, wavy beds was also taken similar to 0.25 m sinusoidal bed, i.e., 216 m from van Gerwen et al. (2018). Considering predefined bed patterns might affect the hydrodynamic results quantitatively. However, the study aims at developing a qualitative understanding of how hydrodynamic properties vary over evolving sand waves in the presence of wind and waves. Also, it is computationally less intensive. The hydrodynamics related simulations are short term, i.e. run for two tidal cycles.

The sediment transport module is activated in the next half of the study, where only morphodynamic properties are investigated. The initial bathymetry is set as a 0.25 m sinusoidal bed for simulations involving complete duration wind and waves, whereas the initial bed is a randomly perturbed bed for simulations involving intermittent storm conditions. The MORFAC value is set at 2000 to speed up the geomorphological changes. Using a MORFAC of 2000, one tidal period corresponds to $12\text{h} * 2000 \approx 2.7$ years of geomorphological changes. The morphological simulations are run for 100 years.

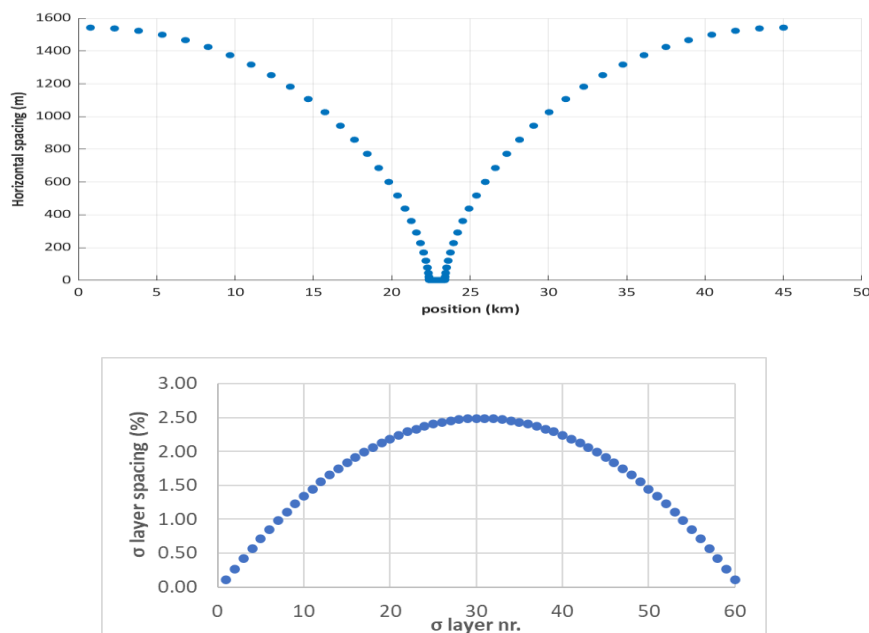
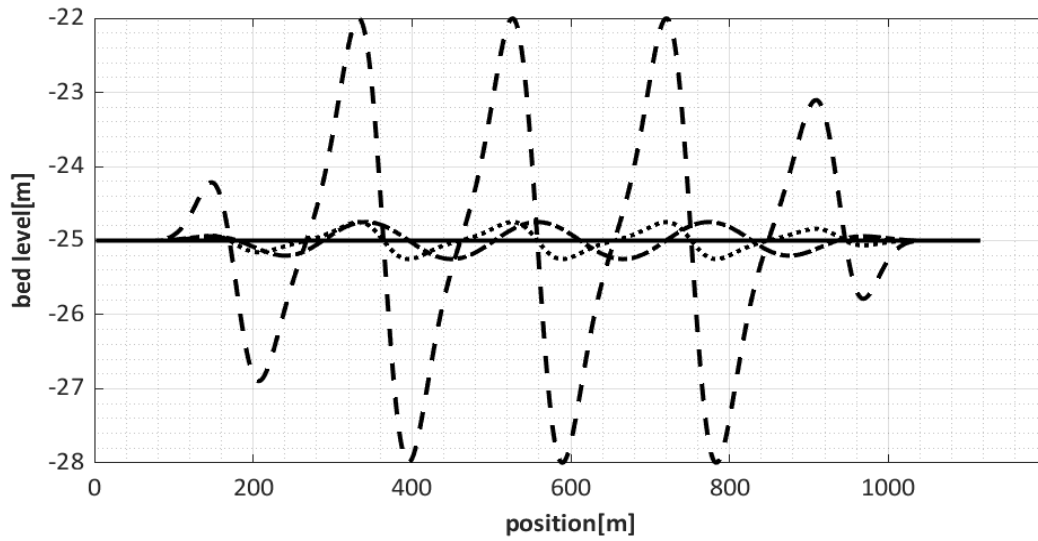
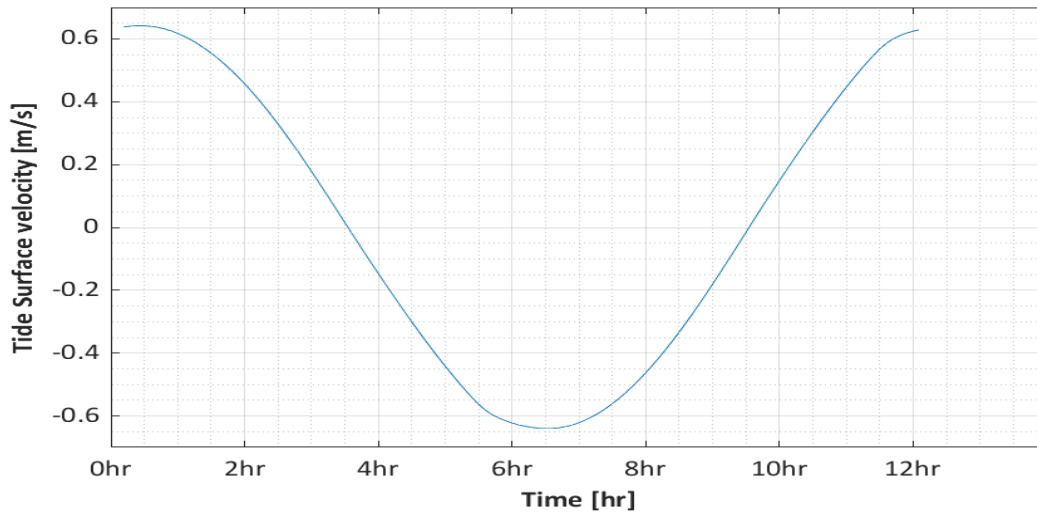


Figure 10: (a) Horizontal grid distribution for the model runs, using a fine grid in the centre where the sand waves are calculated and a coarser grid towards the lateral boundaries and (b) the vertical distribution of the σ -layers over the water column, showing the spacing of 60 σ -layers down the water column. The spacing between the layers is small near the bed and surface, resulting in 8 σ -layers at the lower 1 m and top 1 m.



(a)



(b)

Figure 11: (a) Types of initial bed used in this research study: a flat bed(solid black), 0.25 m finite-amplitude symmetrical bed (dotted red), 0.25 m finite-amplitude asymmetrical bed (dotted black), and 3 m developed bed (dashed black). Note that the wavelength of all the predefined wavy bed patterns is 216 m. (b) Symmetrical S2 Tidal cycle used in the model.

Riemann boundary conditions are imposed at the lateral boundaries. This boundary condition allows the tidal waves to cross the open boundary without being reflected back into the computational domain. The hydrodynamic time step is set to 12 s. The tidal amplitude of $U_{S2} = 0.65 \text{ m/s}$ is used with a tidal frequency of $\sigma_{S2} = 1.45 \cdot 10^{-4} \text{ rads}^{-1}$ (Figure 11b). The astronomical tide is symmetrical. The slope correction factor α_{bs} is set to 3 and Chézy roughness of $75 \text{ m}^{1/2} \text{ s}^{-1}$, chosen settings represent conditions in which sand waves are observed.

The meteorological conditions used in this study are similar to those observed near the Dutch coast. For better understanding, meteorological conditions are divided into intermediate and severe conditions. The Intermediate wind speed is taken as 7.5 m/s blowing in the positive x-direction. Previous studies by Campmans et al. (2018) and Molen et al. (2002)(Campmans et al., 2018; Van Der Molen, 2002) showed the dominance of moderate winds (5-10 m/s) from the southwest near the dutch coast (Figure 12). Thus, the intermediate wind speed of 7.5 m/s is taken as an average of 5 m/s and 10 m/s. Whereas, for severe conditions, wind speed is considered 20 m/s, similar to Campmans et al. (2017).

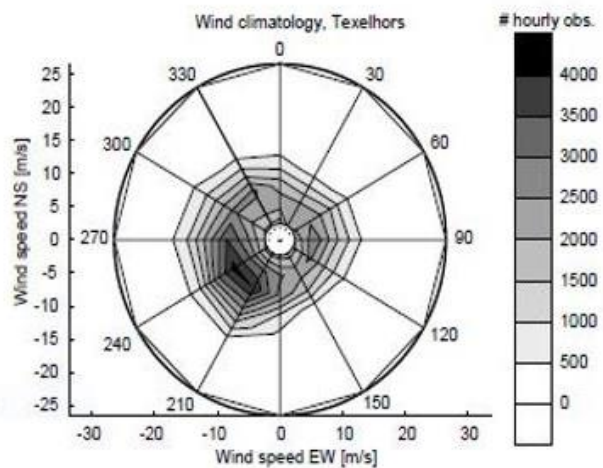


Figure 12: Wind climate derived from the 10-year time series of wind observations from Texelhors (KNMI, Verkaik, pers.comm.). Contours denote the observed number of hourly occurrences. Winds are from the direction (in compass degrees from north) indicated in the figure.

A hindcast database of 38 years for wave conditions in the North Sea, including the Dutch continental shelf, is used (Lavidas & Polinder, 2019). The configuration selected to build the database showed a good correlation for wave height and held minimal bias. The study showed that the spatial average of wave height near the Dutch coast was approximately 1.2 m with a standard deviation of 0.5 m, the 95th percentile value was around 2.5m. Whereas the mean wave period was 5s with a standard deviation of 1s, the 95th percentile value was around 7s. Thus, the 1.2 m wave height and 5 s wave period are used for intermediate conditions, whereas the 2.5 m wave height and 7 s wave period are used for severe conditions. Campmans et al. (2018) also concluded that wind and wave direction are highly correlated, suggesting that most measured waves were locally induced by wind conditions. Therefore, wave propagation is considered to be in the positive x-direction, similar to the wind direction. The wind is applied uniformly over the space, whereas wave conditions are coming from the x-axis.

4. Overview of model parameters for simulation runs

4.1. Reference situation: Hydrodynamic properties for sand waves in symmetrical tide-only forcing.

To answer the first part, RQ1, of the main question, symmetrical diurnal tide (S2) of 0.65 ms^{-1} will be forced on four types of sand wave bed patterns, initial amplitude ranging from 0-3 m. The model runs for two tidal cycles, including one tidal cycle as the spin-up time. The model results are analysed on hydrodynamic properties such as velocity vector, tidally average residuals, vertical eddy viscosity, turbulent energy, and bed shear stress. It is used as a reference situation to successive simulations where wind and waves are involved. Overview of common model parameters and tidal conditions used in this simulation are given in Table 4 and Table 5 (Case1).

Table 4: Overview of common model parameters used in simulations.

Description	Symbol	Value	Unit
Tidal frequency of S2 -tide	σ_{s2}	$1.45 \cdot 10^{-4}$	rads^{-1}
Chézy roughness parameter	C	75	$\text{m}^{1/2}\text{s}^{-1}$
Median sediment grain size	d_{50}	0.35	mm
Mean water depth	H_0	10-40	m
Initial bed (sand wave) amplitude	A_0	0, 0.25, 3	m
Timestep	dt	12	s

4.2. Hydrodynamic properties for sand waves in the presence of symmetrical tide, wind and waves

To answer the second part of the main question, RQ2, symmetrical diurnal tidal forcing of 0.65 ms^{-1} is combined with wind and waves on sand wave bed patterns (initial amplitude varying from 0-3 m). Two types of meteorological conditions are used to represent wind and waves: intermediate and severe. The intermediate conditions include the wind speed of 7.5 ms^{-1} , wave height of 1.2 m and wave period of 5 s. Whereas the severe conditions include wind speed of 20.0 ms^{-1} , wave height of 2.5 m and wave period of 7 s. The meteorological conditions persist for the whole tidal cycle coming from positive x-direction. Each bed type is analysed separately for tide+wave, tide+ wind, and tide + wind + wave for both intermediate and severe conditions. Overview of tidal and

Table 5: Overview of tidal and meteorological conditions used in different simulations.

Description	amplitude of horizontal S0 tidal velocity	Wind velocity	Wave height	Wave period
Symbol	U_{S2}	W	H_{rms}	T
Unit	ms^{-1}	ms^{-1}	m	s
Case 1 (Tide-only)	0.65	-	-	-
Case 2 (Intermediate wave)	0.65	-	1.2	5
Case 3 (Intermediate wind)	0.65	5	-	-
Case 4 (Combined wind and wave)	0.65	5	12	5
Case 5 (Severe wave)	0.65	-	2.5	7
Case 6 (Severe wind)	0.65	20	-	-
Case 7 (Severe wind and wave)	0.65	20	2.5	7

meteorological conditions used in this study are shown in Table 5 (Case 2-Case 7). The model results are analysed for hydrodynamic properties mentioned in section 4.1 without involving bed evolution. Further, they are compared with reference situation Case 1 for tide-only conditions.

Additionally, all the previous runs are made at the mean water depth of 25 m, and meteorological condition (if exist) are present throughout the complete tidal cycle. The simulations for severe wind or combined wind and waves are executed for different depths varying from 10-40 m to demonstrate the effect of depth. Similarly, different scenarios for wind duration are used to demonstrate the effect of wind duration: wind present only during an ebb time, wind present only during flood time, wind present only during half tidal cycle and complete tidal cycle.

4.3. Sand wave morphology in the presence of wind and waves

The simulations in this section are divided into three parts. In all parts, morphological development is analyzed for 100 years, considering computational time constraints. In the first part, sand waves evolution is checked for 100 years in four different weather conditions over initial bathymetry of 0.25 m symmetrical sand waves (FGM= 216m) at 25m mean water depth. The characteristics for the four weather conditions are same as for Case 1 (tide-only), Case 5 (severe wave), Case 6 (severe wind) and Case 7 (combined severe wind and wave), respectively (Refer Table 5). Wind and waves, if included, are uniform, steady and present for the complete duration. The model results analyse the mean bedload and suspended load transport, sand wave height, migration rate, change in wavelength, and sand wave profile.

In the second part, the sand wave properties are analyzed for 100 years at a mean water depth of 30m over initial bathymetry of 0.25m symmetrical sand wave (FGM= 216m). The weather conditions include severe wind present for the complete duration. Finally, the results are compared with results of same weather condition at 25m depth.

In reality, the wind conditions do not occur for complete duration, and initial bathymetry does not have a fixed wavelength or is not entirely symmetrical. Thus in the third part, the analysis is done for 100 years over a randomly perturbed bed in the presence of intermittent storms. A synthetic storm having a frequency of three months in a year is produced using severe wind conditions. Here one tidal period, 720 minutes, corresponds to approximately three morphological years. Thus, during the first 240 minutes of a tidal cycle, sand wave evolution roughly corresponds to its morphological development in one year. Likewise, storm with the frequency of three months in a year refers to $\left(\frac{3*2.7*30*24*60}{2000}\right) \approx 180$ minutes of storm conditions in one tidal cycle. Thus, 180 minutes of a storm is divided into three storms each of 60 minutes, and it is randomly distributed in three morphological years present in one tidal cycle. By random distribution, it means that a storm period of 60 minutes is evolved randomly and at once within one morphological year (or 240 minutes of a tidal cycle). Figure 13 shows storm distribution for one tidal cycle, in which the three intermittent storms each of 3 months evolved during the start of each morphological year. Later, the sandwave properties in intermittent storm conditions are compared with no storm conditions on the same initial randomly perturbed bed.

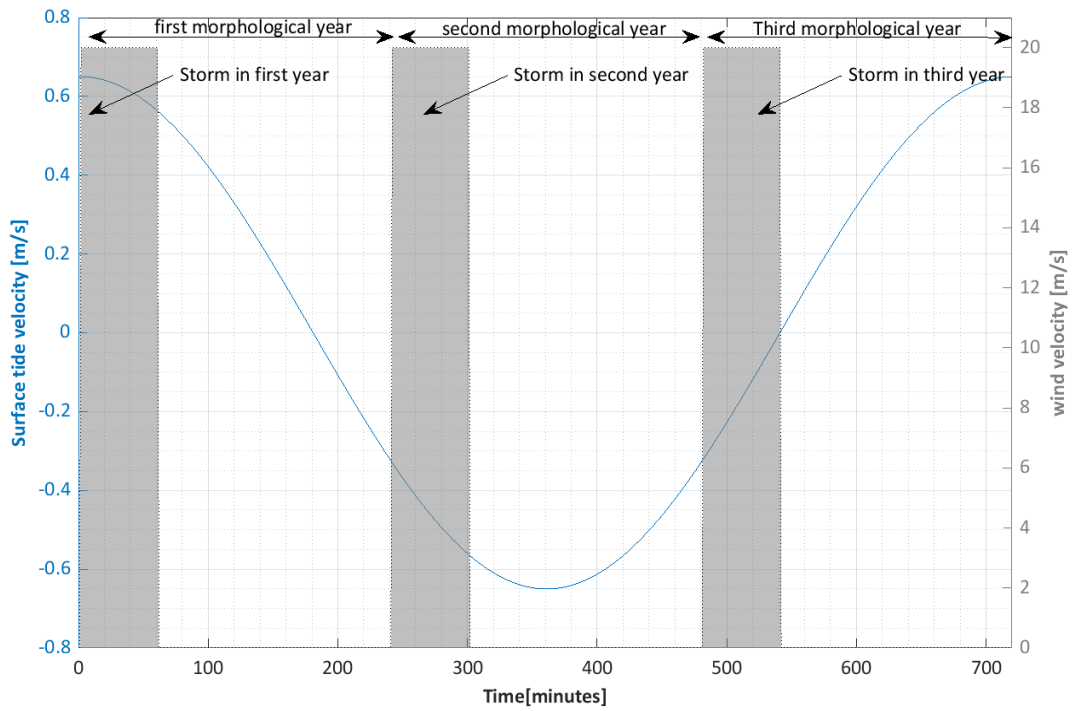


Figure 13: Distribution of intermittent storms, having a frequency of 3 months in a year, within one tidal cycle. It shows the distribution of three storms in three morphological years present in one tidal cycle based on the Morfac value of 2000. The left axis shows the surface tidal velocity, and the right axis shows the velocity of the wind. The grey shaded area shows the storm.

5. Results

5.1. Reference situation: Hydrodynamic properties for sand waves in a symmetrical tide

Initially, the model is forced with symmetrical tide conditions (Refer Case 1, Table 5). Bottom bed varied from being a flat bed to 0.25 m amplitude (a-)symmetrical bed and 3 m high asymmetrical bed at a mean water depth of 25 m. The absolute velocity profile is similar during flood and ebb periods. The maximum surface velocity goes to 0.65 m/s. The tidally averaged flow on a flat bed is zero due to symmetric forcing. As the bed transforms to a 0.25 m symmetrical bed, the tidally average water depth reduces over the sand wave crest and expands near the trough of the symmetrical sand wave. Thus, a circulation cell (Figure 14a) is

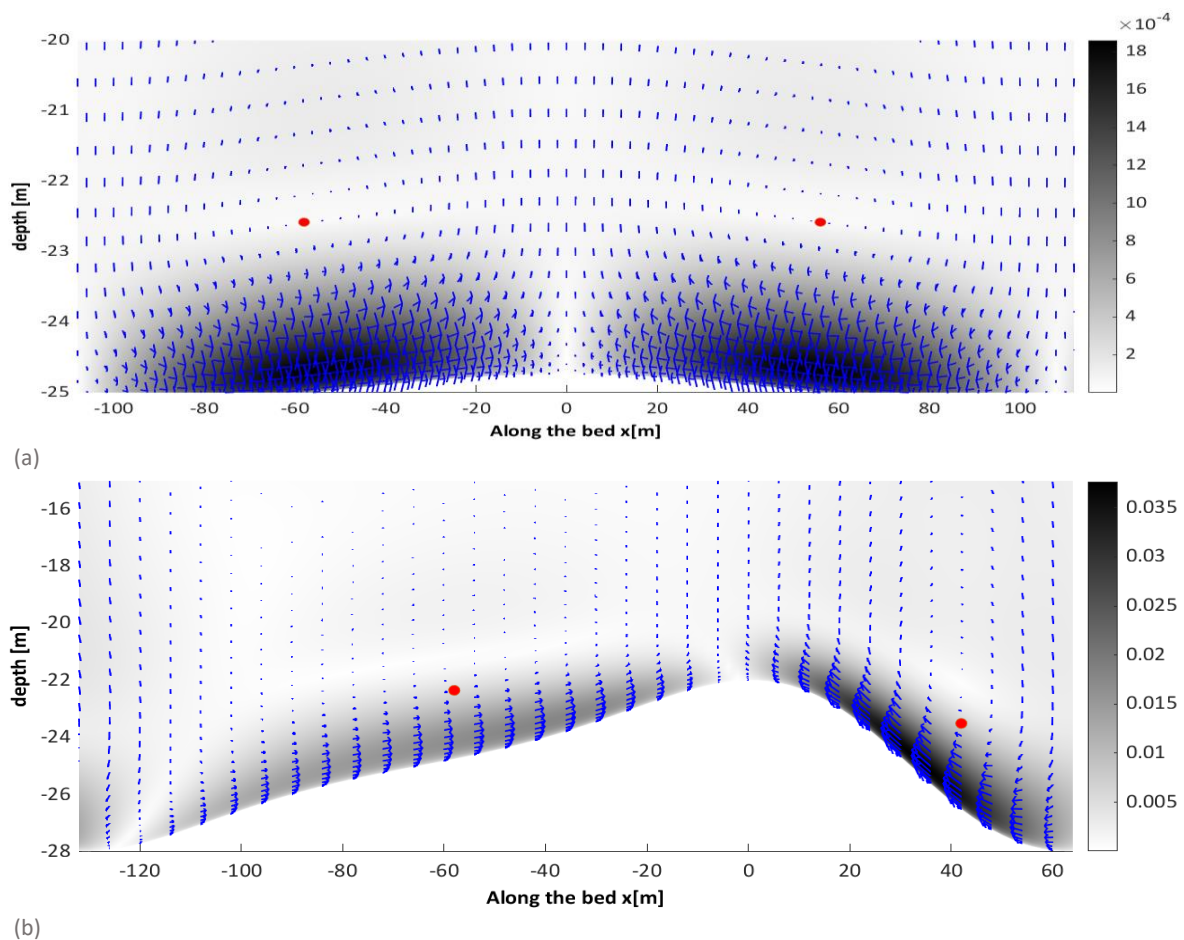


Figure 14: Tidally average velocity (in m/s) for 0.25 m symmetrical sand wave (a), for 3 m amplitude asymmetrical sand wave (b). Blue arrow shows the direction of mean velocity and red dots shows the centre of circulation cells. Note that wavelength of both the bed is 216 m.

established due to the interaction of symmetrical bottom perturbations with the tide that causes the growth of sand waves (Hulscher, 1996). Due to symmetrical forcing on the symmetrical bed, no horizontal tidal average flow is present at the crest ($x=0$ m in Figure 14a). On the other hand, as the bed becomes 0.25 m asymmetric, the strength of the circulation cell is stronger on the steeper side of sand waves due to the high tidal average velocity on the

steeper side. Also, small tidally average horizontal velocity is developed at the crest to attain symmetric shape as the tidal force is symmetric. Eventually, when the bed transforms to a large amplitude asymmetric bed (3 m), the strength of the circulation cell is magnified as the residual velocity on sand wave increases one order higher than the residual velocity on 0.25 m amplitude bed (Figure 14b).

A variation in the viscosity was observed during the tidal cycle (Figure 15a, top). It is significantly less during slack tide (4hr and 10hr). A similar observation was made by Borsje et al. (2013). During the slack tide, the tidal velocity is nearly zero. Thus, the exchange of horizontal momentum between vertical layers reduces, and hence the value of eddy viscosity also drops. The eddy viscosity is almost bi-linear with a maximum value almost at the centre (0.05 m²/s) and it reduces towards the surface and bottom. The mean value of vertical eddy viscosity is 0.035 m²/s. The magnitude and distribution of vertical eddy viscosity are almost similar while sand wave amplitude changes from 0.25m to 3m. Similarly, turbulence is larger near the bed due to bottom roughness and friction, i.e., 2. 10⁻³ m²/s² (Figure 15a, bottom). The turbulent energy increases near the crest and reduces near the trough of sand waves as amplitude changes from 0.25 m to 3 m. It happens due to depth reduction near the crest and an increase in depth near the trough. Overall mean turbulent energy increases with increase in sand wave amplitude.

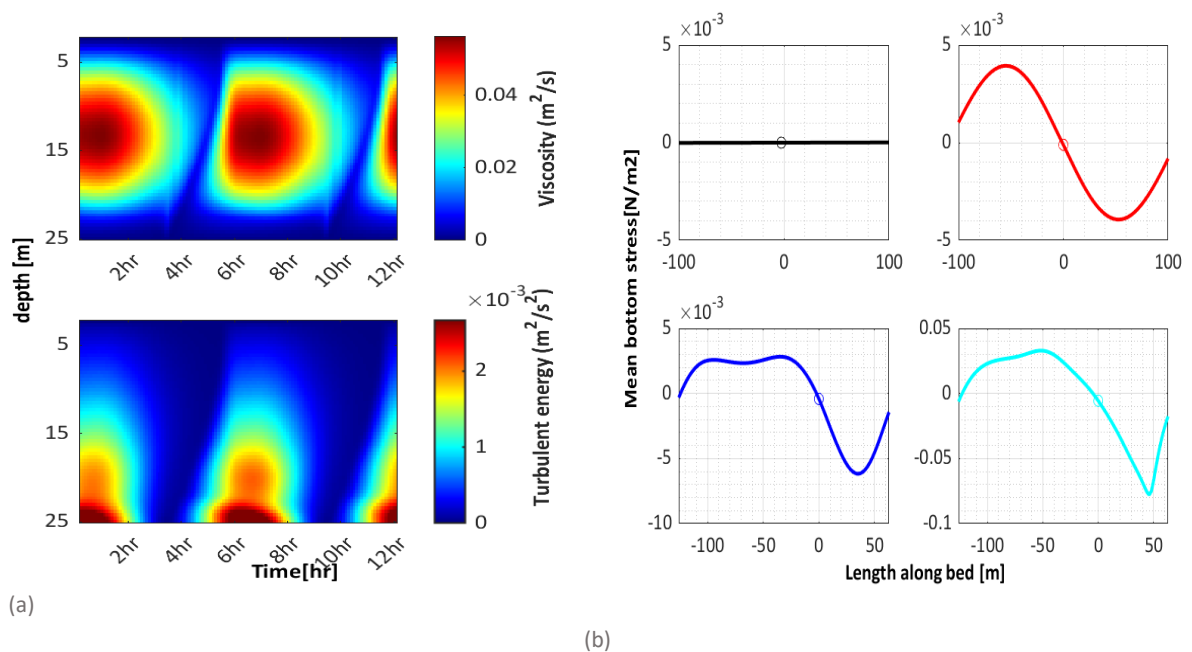


Figure 15: (a) Variation of vertical eddy viscosity (top) and turbulent energy (bottom) at crest position with tide duration. (b)Variation of tidally averaged bottom stress with sand wave evolution: a flat bed (black), 0.25m symmetrical sand wave (red), 0.25m asymmetrical sand wave (blue), real bed (cyan). The circle shows the stress at the crest position of sand waves (x=0m). It is in the presence of tide-only conditions.

Further, mean bottom stress is analysed with sand wave evolution. It is in line with the direction of tidally averaged velocity described earlier. As the bed grows higher and becomes asymmetric, mean bottom stress increases on the steeper side because the residual velocity is higher on the steeper side. Also, minor bottom stress at the crest position is developed pointed towards the less steep side. It indicates the possible sediment movement in

asymmetric beds to regain symmetric shape when the forcing is symmetric (Figure 15b). The circles in Figure 15b shows the bottom shear stress at the crest position of sand waves. The results of sand evolution in the presence of tide-only condition acts as a reference situation for further analysis.

5.2. Hydrodynamic properties for sand waves in the presence of symmetrical tide, wind and waves

5.2.1. Physical effects of wind and waves on the finite-amplitude sand wave

As discussed in section 4.2, this model run involves integrating wind, waves, combined wind and waves with symmetrical tide using the model parameters described for Case 2 to Case 7 (Table 5). The wind and wave propagation is in the flood tide direction (positive x-axis).

(i)Physical effect of combined tide and wind: When symmetrical diurnal tide and unidirectional wind (in flood direction) is combined, it causes the surface water to drift in the wind direction. The maximum surface velocity reaches 0.75 m/s and 1.2 m/s during intermediate and severe wind conditions, respectively. The drift at the surface in wind direction is due to stress generated by wind at the free surface defined by expression (6) under section 3.1. The wind drag at the surface cause increase in the roughness at the surface water, and this surface roughness increases with wind speed (Deltares, 2014a). This increase in roughness causes dissipation of energy at the surface, which was zero in tide-only conditions. It leads to an increase in turbulence at the surface. Similarly, it affects the formation of vertical eddies and the transfer of horizontal momentum down the surface. In intermediate wind conditions, vertical eddy viscosity reaches a maximum value of $0.065 \text{ m}^2/\text{s}$ and the tidally average value of $0.04 \text{ m}^2/\text{s}$. In severe wind conditions, it reaches a maximum value of $0.09 \text{ m}^2/\text{s}$ and the tidally average value of $0.075 \text{ m}^2/\text{s}$. Also, the maxima shift slightly towards the surface from the centre; it is at the centre of mean depth in tide-only conditions.

Contrary to their average values, absolute vertical eddy viscosity increases during the flood period and decreases during the ebb period due to the directional effect of wind (constantly flowing in the flood direction). Refer to Figure 16 (left) that shows the viscosity increases to $0.09 \text{ m}^2/\text{s}$ during flood time (1hr-3hr and 9hr-12hr), and the viscosity decreases to $0.03 \text{ m}^2/\text{s}$ during an ebb time (3hr-9hr) in comparison to tide-only condition. This difference in viscosity profile during flood and ebb time will affect the transfer of horizontal momentum between vertical layers and horizontal velocity. It will be discussed later in this section only. Similarly, the surface roughness due to wind shear increases surface turbulence which was zero in tide-only conditions. The flow is turbulent over the entire water depth in severe wind conditions (Figure 16, right), but it is only significant near the bed in tide-only conditions (Figure 15a, bottom).

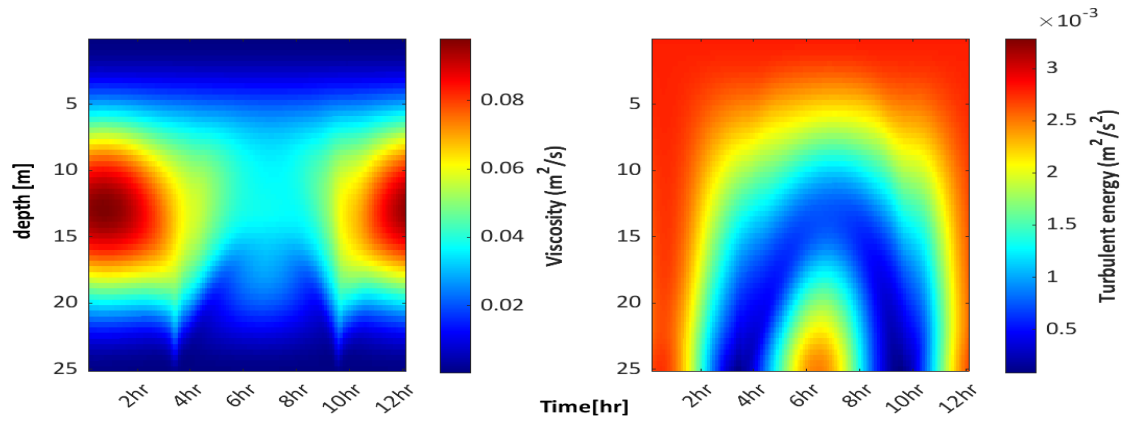


Figure 16: Variation of vertical eddy viscosity (left) and turbulent energy (right) at crest position over 0.25 m symmetrical sand wave in the presence of severe wind speed of 20 m/s.

Further, in the presence of intermediate wind conditions, the tidally average horizontal velocity profile is two-layered, of which the top layer is in wind direction (surface drift), and the bottom layer is in the direction opposite to wind (reverse drift). However, in the presence of severe wind conditions, the tidally average flow profile is three-layered, of which the top first layer is in wind direction (surface drift), the middle second layer is drift in the direction opposite to wind (reverse drift), and the thin bottom third layer near the bed exists in the wind direction (bottom drift) (Refer Figure 17). For simplicity, the terms surface drift, reverse drift, and bottom drift will refer to the above-explained description, wherever used. The tidally average surface drift in wind direction is due to wind-generated surface shear. Contrary to this, a reverse drift opposite to wind direction is observed close to the bottom half depth. Earlier it was seen that viscosity decreases during the ebb phase and viscosity increases during the flood phase in the presence of wind when compared to tide-only conditions (Figure 16, left). In other words, the average depth viscosity during an ebb period in wind+tide conditions is less than that during the tide-only conditions. The profile of vertical eddy viscosity changes completely during an ebb period (4hr-10hr). This temporal variation in viscosity profile causes variation in the transfer of horizontal momentum from surface to bottom. It indicates that the wind affects the velocity profile differently during flood and ebb periods. This difference in velocity profile can cause a possible reverse drift when tidally averaged.

To verify whether the reverse drift is actually caused due to decrease in vertical eddy viscosity during the ebb period, an additional run was made combining vertical eddy viscosity from $k-\epsilon$ turbulence model and small background vertical eddy viscosity, $0.005 \text{ m}^2/\text{s}$, together. The value of background vertical eddy viscosity is taken so that the average depth viscosity during an ebb period in wind+tide conditions is more than during tide-only conditions. It is found that the reverse drift was removed (results shown in Appendix 2). This verification proves that the decrease of absolute viscosity, compared to tide-only conditions, during the ebb period in flood directed wind conditions is one reason behind this reverse drift.

Additionally, a phase lag exists between the top and bottom layers due to wind. Fourier analysis is executed on the resultant horizontal velocity profile, S , using the expression (13) to check the phase lag between the top and bottom layer at 25m. A similar Fourier expression was used by Borsje et al. (2013). The lag difference between the top and bottom

layers is 1.5 degrees (around 36 minutes). Thus, this change in frequency of oscillation in water depth introduces phase lag between the top and bottom layers so that the flood period is not equal to the ebb period at each layer down the water depth in the presence of wind. Therefore, it can cause possible distortion in the tidally-average horizontal velocity profile.

$$S = \underbrace{A0(z) \cos\phi_0}_{S0} + \underbrace{A2(z) \cos(\sigma t - \phi_2(z))}_{S2} + \underbrace{A4 \cos(2\sigma t - \phi_4(z))}_{S4} \quad (13)$$

In addition to this, a bottom drift is observed in severe wind conditions, showing residual flow in wind direction near the bed. Fourier analysis shows that this bottom residual in tidally average flow results from wind-driven residual flow $S0$ and higher tide $S4$ that generates due to wind. The unidirectional wind increases the bottom friction drag when tidal current is in same direction and reduces the bottom friction drag when tidal current is in the opposite direction. Thus, the addition of unidirectional wind (in flood direction) causes the asymmetrical behaviour of bottom drag during wind-current interaction. It causes the difference in which bottom bed affects the principal profile $S2$ during flood and ebb period. Therefore, the asymmetrical mean bottom stress due to wind results in energy loss and decreased amplitude of the current profile. It causes transfer of the lost energy to higher overtide $S4$ and residual $S0$. This energy transfer to $S4$ and $S0$ translates in positive wind-driven flow (bottom drift) observed during tidally average flow.

The residual components due to wind-driven flow result in distortion of residual circulation cells formed due to symmetric tides. The intermediate wind conditions introduce small distortion in circulation cells, and severe wind conditions strongly affect circulation cells. The horizontal residual at the crest is non-zero, and the point of convergence shifts from the crest in 0.25m symmetric sand waves. It indicates the possibility of asymmetrical behaviour in sand waves due to wind. Similarly, the mean bottom stress is following the tidally average residuals near the bottom. It is asymmetrical throughout the tidal cycle in the presence of wind. In severe wind conditions, mean bottom stress at the crest is 0.05 Nm^2 . It indicates the possibility of asymmetric behaviour to the initial symmetrical bed that will translate to migration.

(ii) Physical effect of tide and wave: When symmetrical diurnal tide and unidirectional wave propagation (in flood direction) are combined, minor surface drift is observed in intermediate and severe wave conditions. The maximum surface velocity reaches 0.75m/s in case of severe wave conditions. The viscosity profile is almost similar to the tide-only conditions. The maximum vertical eddy viscosity reaches $0.06 \text{ m}^2/\text{s}$, which was $0.05 \text{ m}^2/\text{s}$ during the tide-only condition (Figure 18, left). Thus, viscosity is not affected much due to the addition of waves. However, surface turbulence is intensified due to the breaking or decaying of waves at the surface in severe wave conditions (Figure 18, right). The turbulent surface energy increased to $4.10^{-3} \text{ m}^2/\text{s}^2$, which was $3.10^{-3} \text{ m}^2/\text{s}^2$ in severe wind conditions. In severe wave conditions, the effect of additional turbulence remains only 5 m depth from the surface, compared to the severe wind conditions where the effect was transferred throughout the depth.

This study accounts for two-way non-linear wave-current interaction (Soulsby et al., 1993). This wave-current interaction enhances bottom friction felt by current due to wave boundary layer and enhancement of bed stress due to interaction with the current boundary

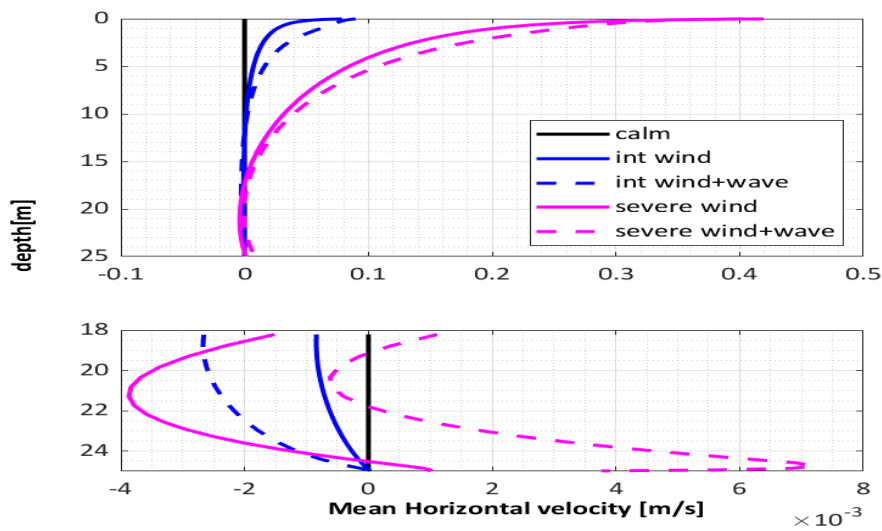


Figure 17: Effect of intermediate wind (solid blue), severe wind (solid purple), combined intermediate wind and wave (dashed blue), combined severe wind and wave (dashed purple) in the presence of symmetrical tide at crest position of 0.25 m symmetrical sand wave in 25 m mean water depth.

layer. By inspection, it was found that mean bottom stress varies by approximately 10% by including non-linear wave-current interaction. A small drift in the ebb direction is found near the bottom half for intermediate conditions, resulting from comparatively high-water depth during flood than during ebb. It is known that the effect of the wave is more significant in smaller depths. However, in severe wave conditions, strong drift in flood direction can be seen because of large mass-momentum transfer in the direction of wave propagation (Stokes drift) for a given wave period. The Stokes drift occurs because the velocity of particles above the crest is higher than particles below the trough. The Stokes drift could be least expected during intermediate wave conditions due to small wave height and wave period.

Like wind conditions, bottom residuals from waves also distort the circulation cell formed by symmetric tide over 0.25 m symmetrical sand wave resulting in non-zero horizontal residual at the crest and indicating the possibility of migration of sand waves in wave conditions. Similarly, the mean bottom stress is asymmetric in the presence of waves; however, the extent of asymmetric behaviour is less than wind. In severe wave conditions, mean bottom stress at the crest is 0.03 Nm^2 due to the wave stirring effect.

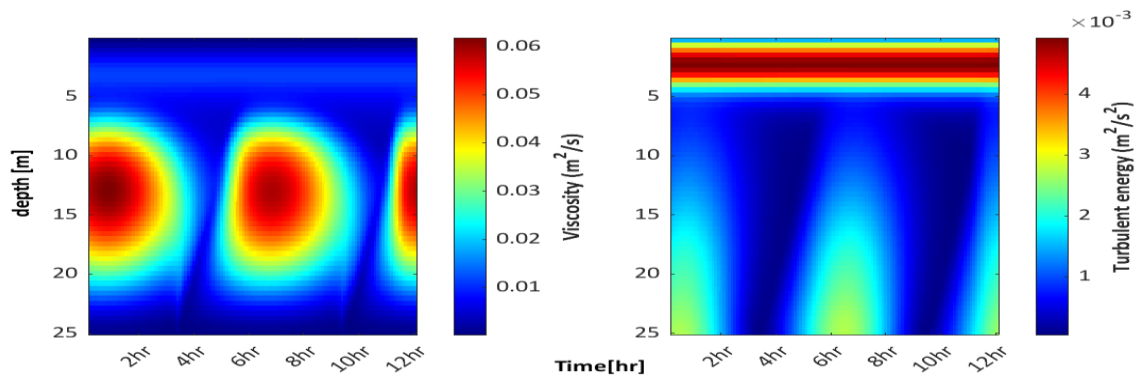


Figure 18: Variation of vertical eddy viscosity (left) and turbulent energy (right) at crest position in the presence of severe wave height of 2.5m over 0.25m symmetrical sand wave.

(iii) Physical effect of combined wind and wave with the tide: Combined effect of wind and waves are similar to the combination of physical effects obtained when wind and waves are combined separately with the tide in previous sections. The combined effect of wind and wave increases the surface velocity and viscosity slightly more than that observed in combined tide and wind conditions (Figure 19). However, surface turbulence intensifies due to surface roughness added by wind shear and wave breaking. In this case also, viscosity during the ebb period decreases due to the directional effect of wind compared to tide-only conditions. Further, it leads to similar two-layer (surface drift, reverse drift) and three-layer vertical distribution (surface drift, reverse drift and bottom drift) of mean velocity during intermediate and severe conditions, respectively. The reason for surface drift, reverse drift and bottom drift is similar to what is explained in the case of only wind and tide conditions (Figure 17). The bottom drift or near bed residual increases non-linearly in severe wind conditions due to a combination of wind-driven flow, higher tidal component and Stokes drift.

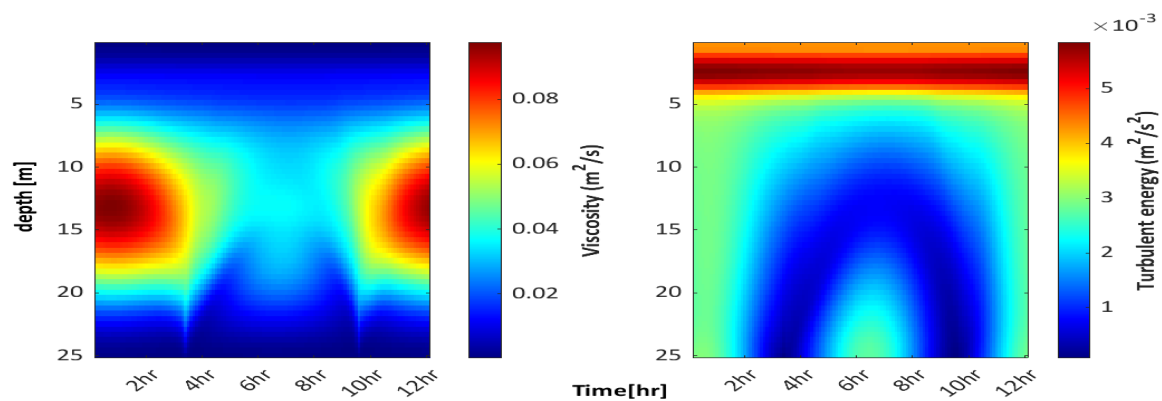


Figure 19: Variation of vertical eddy viscosity (left) and turbulent energy (right) at crest position in the presence of severe wind of 20m/s and severe wave height of 2.5m over 0.25m symmetrical sand wave.

In case of severe wind and wave condition mean bottom stress at the crest is 0.1 Nm^2 due to both wind bottom stress and wave stirring effect. The bottom stress is asymmetric, suggesting possible migration. A comparison of the hydrodynamic properties in tide-only, wind, wave, combined wind and wave conditions is shown in Table 6. Further, the Fourier analysis of velocity for combined severe wind and wave conditions is illustrated in Figure 20. It shows the distortion (decrease) in fundamental S2 current amplitude (Figure 20b), lag in phase between top part (0-10 m) and the bottom part (10-25 m) of the water depth by more than 1.5 degrees (Figure 20e), wind-driven residual flow S0 (Figure 20g), generation of higher harmonics S4 (Figure 20i). Reconstruction of horizontal velocity profile using S0 and S4 demonstrates the importance of S4 in increasing positive residual near the bottom (bottom drift) during severe conditions obtained in tidally average flow. Such redistribution of energy from fundamental harmonics to residual flow or higher harmonics plays a vital role in shaping profiles down the vertical depth.

Table 6: Comparison of hydrodynamic properties in tide-only, tide+wave, tide+wind and tide+wind+wave conditions over 0.25 m symmetric sand wave at a mean depth of 25 m. Only severe wind and wave conditions are shown here. The shades of colour weigh the property impact, where blue shows the low impact, yellow shows medium impact and red shows the highest value.

Property Description	Unit	Tide	Tide + severe wave	Tide + severe wind	Tide + severe wind and wave
Surface velocity	m/s	0.65	0.75	1.2	1.4
Maximum viscosity (flood period)	m ² /s	0.05	0.06	0.09	0.09
Maximum viscosity (ebb period)	m ² /s	0.05	0.06	0.035	0.035
Surface turbulence	m ² /s ²	0.00E+00	3.00E-03	4.00E-03	5.00E-03
Near bed turbulence	m ² /s ²	2.00E-03	2.50E-03	2.50E-03	3.00E-03
Mean bottom stress at crest	N/m ²	0	0.03	0.05	0.1

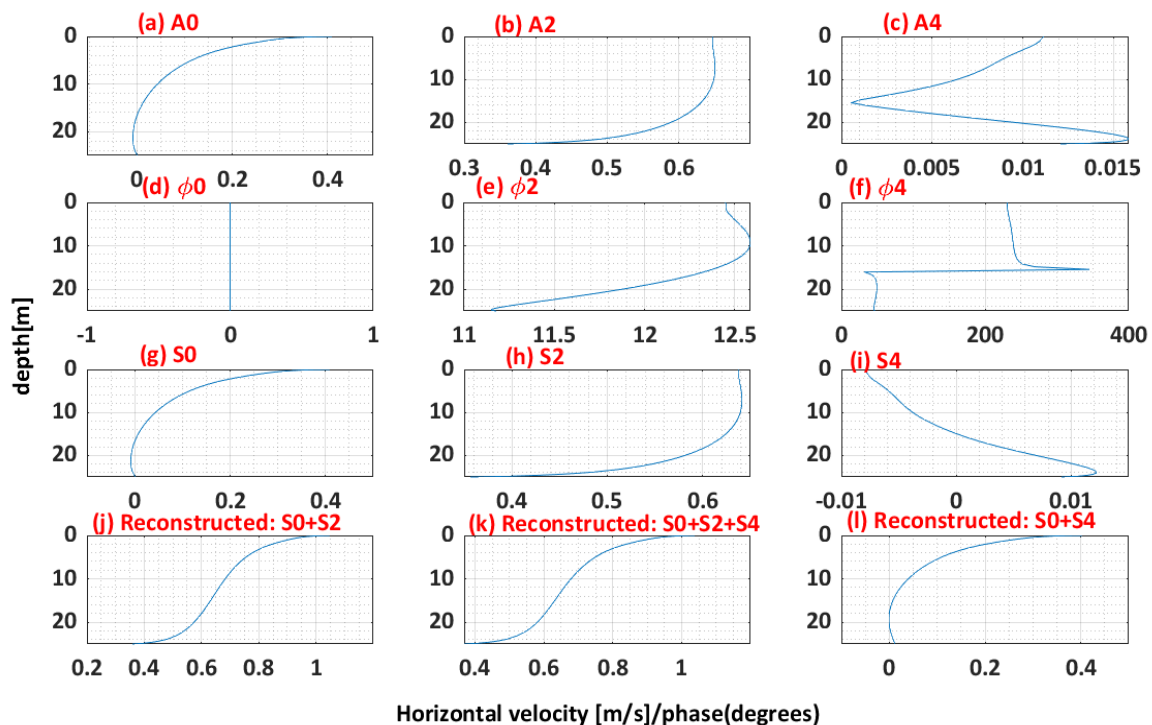


Figure 20: Vertical distribution of the amplitude (a, b, c) and phase (d, e, f) of zero frequency component (A_0 and ϕ_0), first harmonics (A_2 and ϕ_2) and second harmonics (A_4 and ϕ_4) of horizontal velocity in the presence of combined severe wind and severe wave at a mean depth of 25m. Respective amplitudes and phases are combined to get components S_0 , S_2 and S_4 (g, h, i). Horizontal velocity is reconstructed using S_0+S_2 (j), $S_0+S_2+S_4$ (k), S_0+S_4 (l).

Overall the results demonstrate that the physical effect of complete duration severe wind and waves is more significant than intermediate conditions on hydrodynamics over sand waves. In particular, severe wind conditions has more physical effects than severe wave conditions on hydrodynamic properties. Severe wind conditions affect viscosity due to its directional effect relative to the tidal current direction. It reduces the amplitude of principal current S2 and transfers lost energy to S0 and higher harmonics S4. Consequently, It distorts the tidally average horizontal velocity resulting in surface, reverse, and bottom drift. The reverse drift occurs due to decreased viscosity when current flows opposite to wind and phase lags between the top and bottom layers in the water column. The bottom drift occurs due to a combination of wind-driven residual (S0) and higher tide (S4). Alone waves cause surface turbulence and bottom stress. Together with wind, waves intensify the turbulence, bottom drift and mean bottom stress. The combined effect increases the velocity residual over the crest and enhances the distortion of circulation cells. Further, it shifts the point of convergence, makes mean bottom stress distribution over sand waves asymmetrical, indicating possible migration and asymmetrical sand waves. Also, the reverse drift can potentially affect the direction or magnitude of mean bedload and suspended load transport. The morphodynamic behaviour based on mean velocity is just an indication or a possibility. It is discussed in detail under section 5.3.

5.2.2. Effect of combined severe wind and wave at different mean water depth and wind duration on finite-amplitude sand waves

So far, the mean depth was kept constant, 25 m, for all the cases, and wind/waves were present for complete duration throughout the tidal cycle. In this section, the effect of depth and duration of wind is discussed for severe conditions.

(i) Depth effect: For a mean water depth of 10 m, the tidally average horizontal velocity profile is single-layered in wind direction for severe wind conditions (Figure 21, left). Similar results were obtained by Ruessink et al. (2006) at 9m. Using Fourier analysis, it was found that in 10 m depth, the phase lag between the top and bottom part is less than 0.1 degrees compared to 1.5 degrees in 25 m depth (Figure 20e). However, as depth increases to 25m, the profile becomes three-layered (as discussed in 5.2.1). In severe wind conditions, the depth of frictional influence corresponding to the severe wind speed dominates the water depth 10m. Here the depth of influence is a fictitious depth in which the distribution of viscous effect or roughness occurs throughout the water column. It could be realized by evaluating the Stokes number, ϵ_v , for different mean water depths.

Table 7: Variation of Stokes number with water depth

Water depth (H)	Mean Eddy viscosity	$S_d = \sqrt{\frac{\epsilon_v}{2}}$
10	0.02	1.17
25	0.08	0.94
30	0.09	0.83
40	0.1	0.66

The square root of half the Stokes number $\sqrt{\frac{\epsilon_v}{2}}$, say S_d , quantifies the part of the water column (the Stokes depth) in which viscous effects significantly influence the oscillatory tidal motion. Here $\epsilon_v = \frac{2A_v}{\sigma H^2}$ in which A_v is mean eddy viscosity under given tide+wind conditions, σ is the frequency of tidal oscillation, and H is mean water depth (Hulscher, 1996). In other

words, $\sqrt{\frac{\epsilon_v}{2}}$ is a ratio of the depth of frictional influence ($\frac{A_v}{\sigma H}$) to mean water depth (H). At a depth of 10 m, the depth of frictional influence is 1.17 times bigger than mean water depth (Table 7). Thus, when this frictional depth dominates the entire water column, the residual flow is one-layered in wind direction, and phase lag between the top and bottom layer is negligible. However, when the frictional depth of influence is some portion of mean water depth, it is more than one layer, and phase lag exists between the top and bottom layer.

Further, at 30 m and 40 m mean water depth, an increase in reverse drift was observed that nullifies the effect of bottom drift (third layer), leading to two-layered flow (Figure 21, left). The addition of severe waves adds a residual in wave propagation direction. However, the effect of waves decreases with increase in mean water depth (results not shown here). So far, depth 25 m was our area of interest. However, Figure 21 (left) shows the transition of mean horizontal velocity at 30 m from positive to negative near the bottom in severe wind conditions.

(ii) Duration effect: This section discusses the change in mean horizontal velocity with the variation in wind duration at 30 m. The wind is unidirectional in flood direction. It is found that when severe winds are only present during the flood period, the viscosity increases during the flood period in comparison to tide-only conditions. At the same time, the viscosity during an ebb period is same as in tide-only conditions. Thus, the tidally average velocity profile is single-layered. Contrary to this, when severe winds are only present during the ebb phase, the viscosity decreases during the ebb period compared to tide-only conditions. At the same time, the viscosity during the flood period is same as in tide-only conditions. Thus, the tidally average velocity profile is two-layered. It re-confirms that a decrease in viscosity during the ebb period is one reason for reverse drift in the presence of wind conditions (as discussed in 5.2.1). Remarkably, the impact on mean velocity when the wind is present only during the flood period is less than when the wind is present only during the ebb phase. It could be due to the non-linear effect of wind-current interaction. In addition, it has less reverse drift when the wind is present during half of the tidal cycle than when it is present throughout the tidal cycle.

The depth effect shows that the phase lag between the top and bottom layers is a function of Stokes depth. The phase lag exists when the frictional depth of influence does not dominate the mean water depth, resulting in the reverse drift. Also, the reverse drift increases with depth and reverses the near-bed mean horizontal velocity at 30m or greater water depth. On the other hand, the duration effect illustrates that increased wind duration has a non-linear effect on near-bed residual velocity.

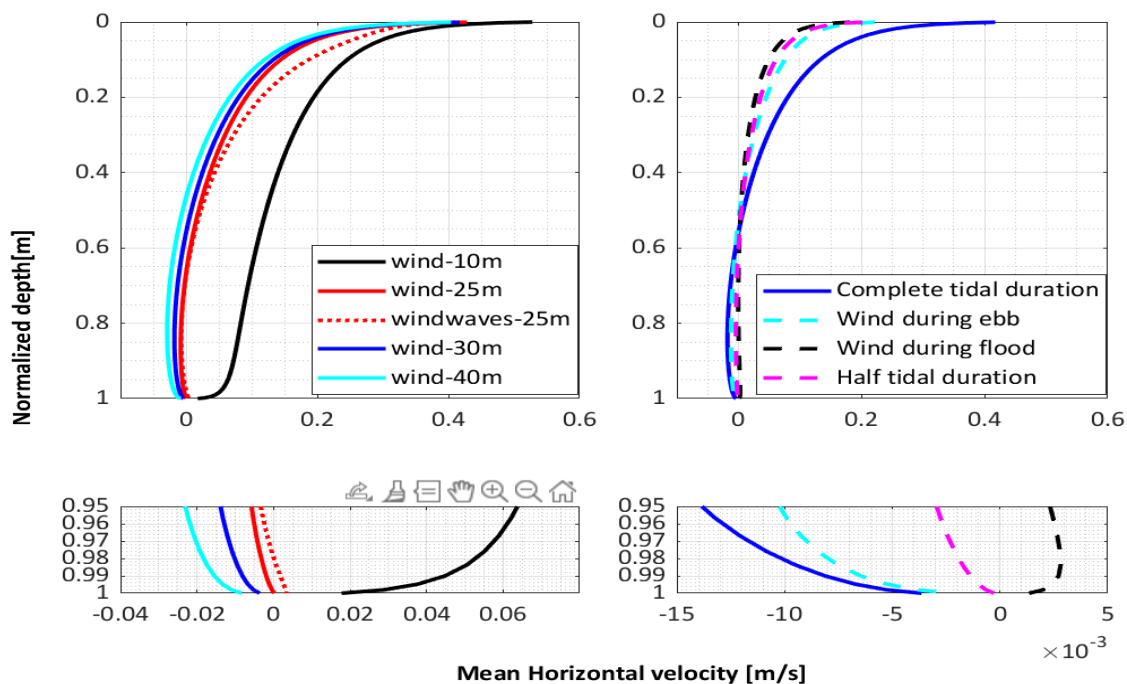


Figure 21: Effect of severe wind on 0.25 m symmetrical sand wave crest at different water depth: 10 m (solid black), 25 m (solid red), 30 m (solid blue), 40 m (solid cyan); and effect of severe wind and wave at 25 m (dotted red) (left figure). Effect of several duration of severe wind on 0.25 m symmetrical sand wave crest at 30 m water depth: wind during the complete tidal cycle (solid blue), wind during ebb phase only (dashed cyan), wind during flood phase only (dashed black), wind during half tidal cycle (dashed magenta) (right figure). Note that the graph is plotted on normalized depth, and the bottom figure gives a zoomed view of velocity near 5% bottom depth.

5.2.3. Variation in the effect of severe wind and wave with sand wave evolution

So far, the results were analysed at the crest position of 0.25 m amplitude sand wave pattern for wind and wave conditions. It is found that transition of near-bed mean horizontal velocity occurs at 30 m water depth due to the increase in the reverse drift at higher depth, as discussed in section 0. For smaller amplitude sand waves, say 0.25 m, the depth at the crest is almost equal to the depth at the trough. Thus, the near-bed mean horizontal velocity direction is in the same direction at the crest and trough for the given mean depth. For instance, near-bed mean horizontal velocity at 25 m mean water depth is in flood direction at both crest and trough in the presence

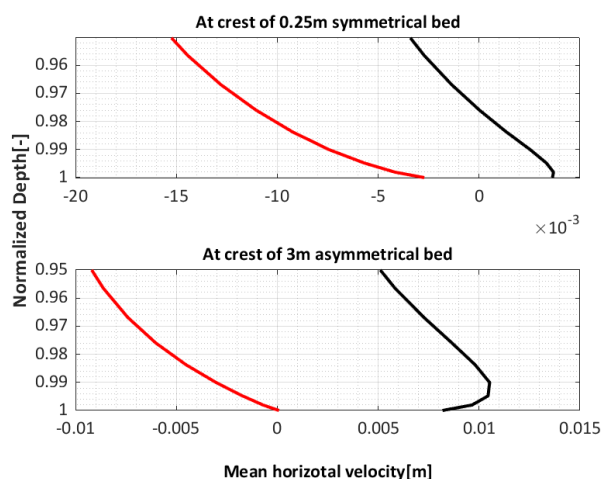


Figure 22: Mean horizontal velocity at the crest position of 0.25 m symmetrical sand wave (top) and 3 m asymmetrical sand wave (bottom) at mean water depth of 25 m depth (solid black line) and 30 m depth (solid red line). The graph is plotted for the bottom 5% normalized depth.

of combined wind and waves, and it is in ebb direction at 30 m mean depth (Figure 22, top).

However, this situation differs when sand wave amplitude increases to 3m, where the depth at the crest is 22 m and at the trough is 28 m for 25 m mean water depth. Similarly, the depth at the crest is 27 m and at the trough is 33 m for 30 m mean water depth. Also, there is an additional contraction in depth at crest and expansion at trough near the water surface due to sand wave shape. Thus, as sand wave amplitude increases, the mean velocity near the crest increases, whereas the mean velocity reduces and might change direction opposite to wind (and waves) at the trough. For instance, at 25 m mean water depth, the mean velocity will be in flood direction at the crest, whereas it will be comparatively slower in flood direction or even reverse in ebb direction at the trough. On the other hand, at 30 m mean water depth, it will be small in flood or ebb direction at the crest, and it will be ebb directed at the trough (Figure 22, bottom).

If morphological changes go in line with the mean velocity residual, it could change the shape, degree of asymmetry of sand wave or cause a change in migration direction. However, not always morphological changes go in line with the mean residual velocity as sediment transport only occurs when velocity near-bed is greater than the critical velocity required for initiation of motion as shown in expression (9). Also, sediment transport is proportional to the fourth power of velocity. The morphological behaviour will be discussed in the next section.

5.3. Morphodynamic properties of sand waves in the presence of severe wind and waves

5.3.1. Physical effects of wind and waves on sand wave growth and migration

The near-bed residuals are higher in severe wind and wave conditions than intermediate wind and wave conditions. Thus, severe wind and wave conditions are chosen for analysis of the morphodynamic changes. The initial bathymetry considered is 0.25m amplitude sand wave of wavelength 216m. It is forced separately with the tide-only (Case I), tide+wind (Case II), tide+wave (Case III), tide+wind+wave (Case IV) at 25m water depth. In Case II, III and IV, wind and waves are present in the complete duration of the tidal cycle. Here the morphological development of 100 years is analysed.

Case I: In case I of purely symmetrical tide conditions, no migration is observed, and sand waves develop a maximum height of more than 10 m due to convergence of symmetrical circulation cells formed on either side of sand waves crest. Thus, sand waves are almost symmetrical, with a steepness value of 0.10 on either side of the crest. The steepness value is calculated using the ratio of height and length of sand waves. The initial sand wave wavelength is 216m at $t=0$, and it did not change much after 100 years. Since there is no migration, the crest and trough position after 100 years is similar to the initial crest position on the x-axis (Figure 23). In addition to this, the mean bedload transport reaches a maximum of $5 \cdot 10^{-8} \text{ m}^3 \text{ s}^{-1} \text{ m}^{-1}$. The mean suspended load reaches a maximum of $2 \cdot 10^{-8} \text{ m}^3 \text{ s}^{-1} \text{ m}^{-1}$. There is a spatial lag in the convergence of the mean bedload and mean suspended load

profile, which affects the shape slightly at the crest position. Moreover, a study by Van Gerwen et al. shows that suspended load results in a dampening effect. Therefore, it was not analysed to what extent it caused the reduction in sand waves growth if the suspended load is included. Refer to Figure 23 that shows sand waves morphological development in 100 years. The growth rate of sand waves is significantly reduced after $t=75$ years. Precisely after $t=60$ years, equilibrium height is attained (Figure 28).

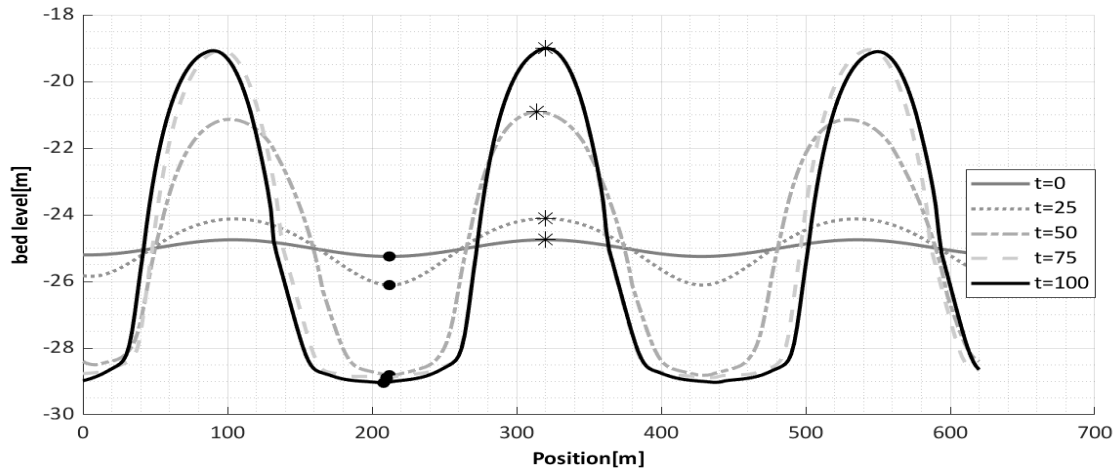


Figure 23: Bed evolution in time (years) of 0.25 m symmetrical sand wave in the presence of symmetrical tide. The growth of the crest and trough is tracked with an asterisk and dot, respectively.

Case II: When waves of 2.5 m height are added to the symmetrical tide in case II, it causes wave stirring near the bed and small migration. The wave stirring effect enhances the near-bed stress due to wave-current interaction and increases mean transport in the form of the suspended load. The small migration is caused due to Stokes drift in the wave propagation direction. The Stokes drift adds a residual near-bed and causes disturbance of the circulation cells such that convergence of sediment is no longer observed exactly at the crest. Instead, a tide-averaged flow is observed over the crest in the wave propagation direction. Tide-averaged flow velocities on the stoss side are larger than on the lee side. It causes a transport in the wave propagation direction. This transport translates into migration and asymmetry. However, the difference in tide-averaged velocities on the stoss and lee sides are small. Thus, the magnitude of migration and extent of asymmetric behaviour is small in the bedform. It inhibits sand wave growth rate compared to tide-only conditions resulting in lower sand wave height. Consequently, the sand wave height after 100 years is 9m, which was more than 10m in case I (Figure 24). The crest is flattened in shape when compared to tide-only conditions. The additional stress and transport due to severe wave conditions flatten the crest but do not break the symmetry of sand waves. The steepness value on either side of the sand wave crest is in the range of 0.08-0.1. The mean bedload transport reaches a maximum value of $5 \cdot 10^{-8} \text{ m}^3 \text{ s}^{-1} \text{ m}^{-1}$, and the mean suspended load reaches a maximum of $5 \cdot 10^{-8} \text{ m}^3 \text{ s}^{-1} \text{ m}^{-1}$. This sudden increase in mean suspended load occurs due to the wave stirring effect that causes resuspension of sediments. Remarkably, the initial formation rate is relatively higher than in Case I till $t=50$ years. However, as the height increases to a significant amount, the growth

rate reduces and equilibrium is obtained after 50 years (Figure 28). One possible reason is that as the crest height increases with time, the net water depth at the crest position reduces, and the wave effect increases with a reduction in depth. The final wavelength did not change much compared to the initial wavelength of 216m at t=0.

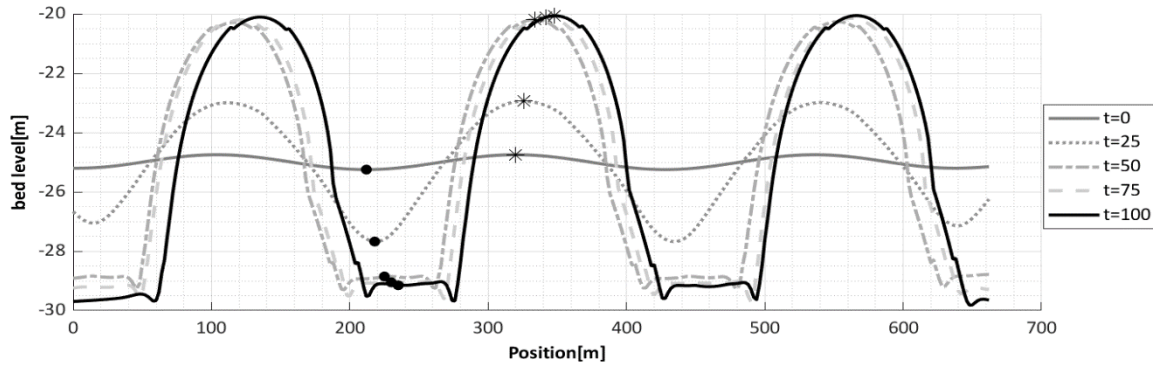


Figure 24: Bed evolution in time (years) of 0.25 m symmetrical sand wave in the presence of symmetrical tide and severe wave. The growth of the crest and trough is tracked with an asterisk and dot, respectively.

Case III: When the severe wind of 20 m/s is added to the symmetrical tide in Case III, it causes strong migration in the wind direction (Figure 27c). The severe wind conditions add residual near the bed (bottom drift) in the wind direction. The residual causes disturbance in the circulation cells such that convergence of sediment is no longer observed exactly at the crest. Instead, a tide-averaged flow is observed over the crest in the wind direction. Tide-averaged flow velocities on the stoss side are larger than on the lee side. It causes transport in the wind direction. This transport translates into migration and asymmetry with time. However, the difference in tide-averaged velocities on the stoss and lee sides are comparatively larger than observed in case II. Thus, the magnitude of migration and extent of asymmetric behaviour is large in the bedform. It translates to an average migration rate of 4 m/year (average migration rate considers an average of crest and trough movement). The strong migration consistently causes the shift in point of convergence from the initial crest position at t=0 to the position ahead of it in the wind direction (Figure 25). It inhibits sand wave growth rate compared to tide-only conditions resulting in lower sand wave height. Thus, the equilibrium sand wave height is more than 7 m, compared to 10m in case I and 9m in case II. The severe wind condition causes 33% reduction in height compared to tide-only conditions. The bottom stress due to wind increases the mean bedload and suspended load transport. It reaches a maximum value of $8 \cdot 10^{-8} \text{ m}^3\text{s}^{-1}\text{m}^{-1}$ and $7 \cdot 10^{-8} \text{ m}^3\text{s}^{-1}\text{m}^{-1}$, respectively. The intense increase in suspended load contributes to the dampening of sand wave height. Sand wave is asymmetric, with a steepness value of 0.04 and 0.07 on the stoss and lee sides, respectively. The initial sand wave wavelength is 216m at t=0, and it increases to 250-270 m after 100 years with an increase in the length of the stoss side and a decrease in the lee side length.

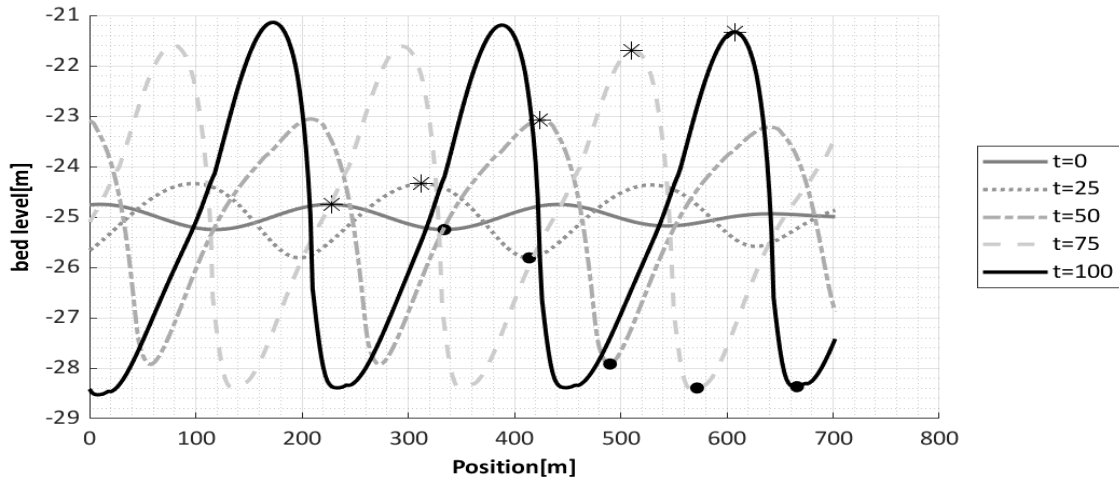


Figure 25: Bed evolution in time (years) of 0.25 m symmetrical sand wave in the presence of symmetrical tide and severe wind. The growth of the crest and trough is tracked with an asterisk and dot, respectively.

Case IV: When wave and wind are combined in Case IV, the effect intensifies as the average migration rate increases to 6-8 m/year due to the increased bottom residual (Figure 27, bottom right). The enhanced bottom stress increases sediment mobility and an overall mean transport. Sand wave height is reduced to 6.5 m due to the consistent shift of convergence from the crest position with time (Figure 26). Sand wave shape is asymmetric and flattened at the top. The strong asymmetry and flattening at the top is mainly due to wind and waves, respectively. The initial sand wave wavelength is 216m at $t=0$, and it increases to 250-270 m after 100 years. The mean bedload transport reaches a maximum value of $13 \cdot 10^{-8} \text{ m}^3 \text{ s}^{-1} \text{ m}^{-1}$, and the mean suspended load reaches a maximum of $7 \cdot 10^{-8} \text{ m}^3 \text{ s}^{-1} \text{ m}^{-1}$. A significant increase in mean bedload is observed. Remarkably, the mean suspended load did not increase much in comparison to Case III. The phase difference between suspended load due to wind and wave over sand wave field could be one possible reason for this behaviour.

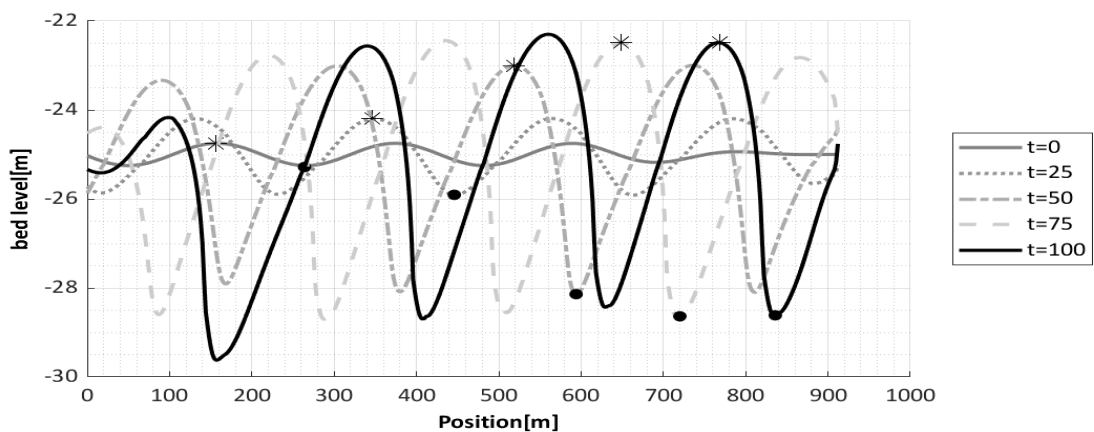


Figure 26: Bed evolution in time (years) of 0.25m symmetrical sand wave in the presence of symmetrical tide, severe wind and wave. The growth of the crest and trough is tracked with an asterisk and dot, respectively.

To summarize the main physical effect of wind and waves on sand waves, a set of comparisons are made for the respective four cases. Sand waves evolution for the four cases is shown in Figure 27. It demonstrates that overall sand wave height damps or growth decreases in the presence of wind and waves. It occurs due to the shift of convergence point with time and increase in suspended load. The morphological change in crest and trough vertical position of a particular sand wave is illustrated with time in Figure 28. It shows that the sand wave attains equilibrium height after 60 years in tide-only conditions. Remarkably, the initial growth rate is much higher, and equilibrium is achieved early after 50 years in the presence of severe waves (Case II). However, in other cases involving wind, the equilibrium is not attained even after 100 years. Thus, wind and waves play a significant role in deciding the equilibrium time scale. Figure 29 compares sand wave field shape at $t=100$ years in four cases. It is evident that the addition of wind make sand waves asymmetrical while waves alone do not break the symmetry. In Case III and Case IV, the simulated front slope of the sand wave seems to be steep. Similarly, the wavelength does not vary much after 100 years in Case I and Case II. However, it increases to 250-270 m in case III and case IV. Figure 30 compares the average migration rate in four cases. It shows that waves alone do not cause migration; however, the migration rate intensifies when wind combines with waves. The average migration rate is around 4 m/year in wind conditions. However, it is between 6 m/year to 8 m/year in combined wind and waves. The migration rate in Case III and Case IV decreases as equilibrium is not reached yet.

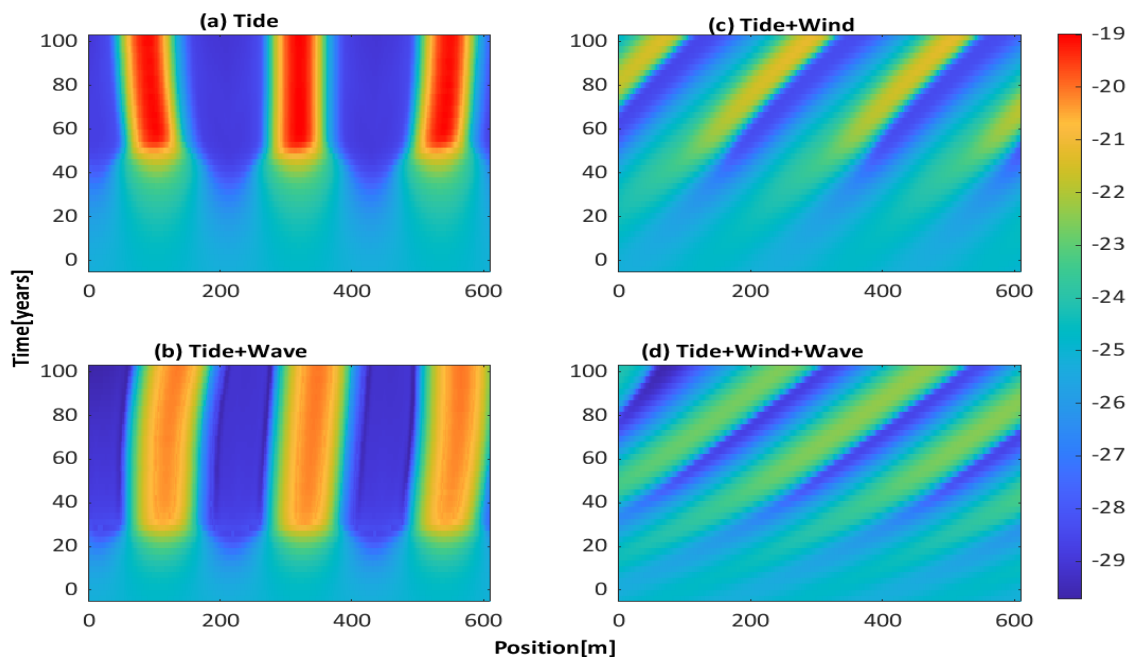


Figure 27: Sand wave profile development in the presence of tide (a), tide +wave (b), tide+ wind (c) and tide+ wind + wave (d) over 0.25 m symmetrical initial bed for 100 years. The vertical colour bar shows the bed level (m).

Overall, wind has a significant effect on morphodynamics than waves. It causes an increase in asymmetric behaviour, migration, wavelength, bedload, suspended load and a decrease in sand waves height. On the other hand, wave causes sand wave flattening,

comparatively small decrease in sand wave height and increase in suspended load. Together, they intensify most of the physical effects. A quantitative comparison of the morphodynamic properties in four cases is shown in Table 8.

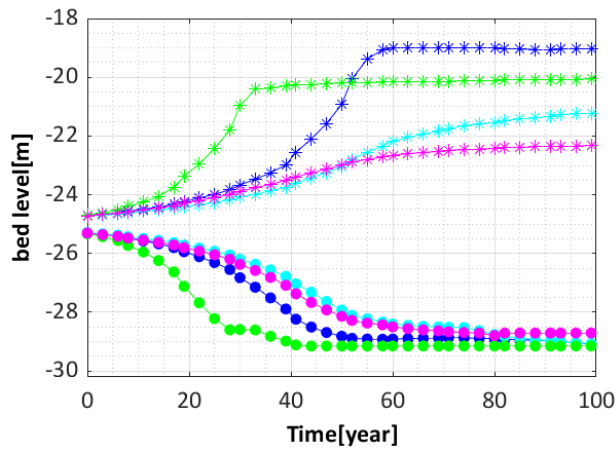


Figure 28: Position of crest and trough of sand wave profile in the presence of tide (blue), tide +wave (green), tide+ wind (cyan) and tide+ wind + wave (purple).

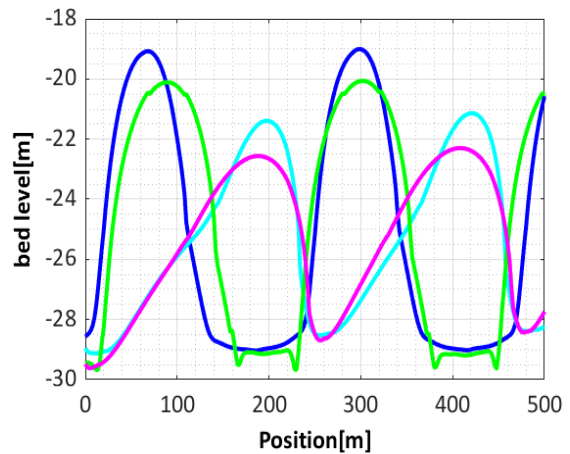


Figure 29: Sand wave profile in the presence of tide (blue), tide +wave (green), tide+ wind (cyan) and tide+ wind + wave (purple). The final sand wave profile is generated from 0.25 m initial amplitude sand wave (FGM=216 m) after the morphological development of 100 years.

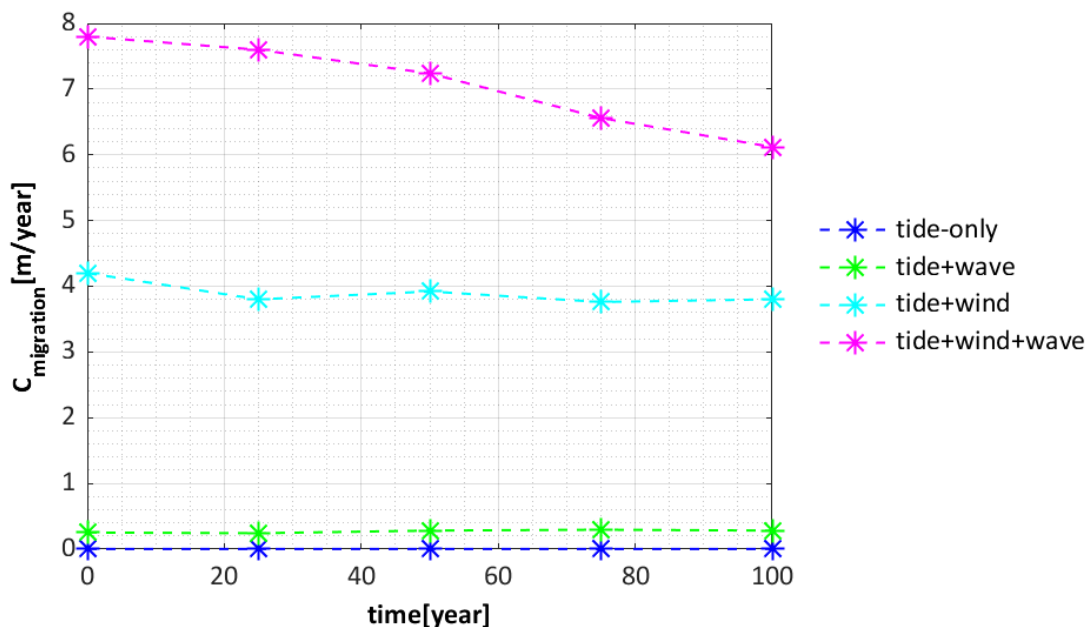


Figure 30: The average migration rate, obtained through the average horizontal movement of crest and trough, in the presence of tide (blue), tide +wave (green), tide+ wind (cyan) and tide+ wind + wave (purple).

Table 8: Comparison of morphodynamic properties in tide-only, tide+wave, tide+wind and tide+wind+wave conditions over 0.25 m symmetric sand wave at a mean depth of 25 m. Only severe wind and wave conditions are shown here. The shades of colour weigh the property impact, where blue shows the low impact, yellow shows medium impact and red shows the highest impact.

Property Description	Unit	Tide	Tide + severe wave	Tide + severe wind	Tide + severe wind and wave
Wavelength after 100 years	m	216	222	250-270	250-270
Equilibrium sand wave height	m	10	9	7	6.5
Steepness stoss side	-	0.1	0.08	0.04	0.04
Steepness lee side	-	0.1	0.09	0.07	0.07
Migration speed	m/year	0	≈0	4	6-8
Maximum Mean bedload	$m^3s^{-1}m^{-1}$	5.00E-08	5.00E-08	8.00E-08	1.30E-07
Maximum Mean suspended load	$m^3s^{-1}m^{-1}$	2.00E-08	5.00E-08	7.00E-08	7.00E-08

5.3.2. Sand wave shape and migration at 25 m and 30 m depth

As discussed in sections 5.2.2 and 5.2.3, there is a transition (reversal) in mean flow velocity at 30 m or greater depth. Thus, to analyse sand wave morphodynamic properties at 25 m and 30 m mean depth, a 0.25 m amplitude sand wave is developed for 100 years in severe wind conditions. Figure 31 shows the comparison of sand wave field after 100 years at 25 m and 30 m mean water depth. The developed sand wave height after 100 years is 6.5m at 30m depth. It is of almost similar height but different shape, when compared to sand wave in 25m, mean water depth (Figure 31).

Further, the difference in shape happens due to the increase in the reverse drift at a depth greater than 30 m. In 30 m mean water depth, the maximum depth near the trough is around 33 m, while at the crest, it is 27 m deep after 100 years. Thus, the migration rate significantly reduces near trough due to the reverse drift explained in section 5.2. Figure 32 shows the sand wave evolution in 100 years. To demonstrate this change in migration rate, the crest and trough movement is traced separately at 30 m mean water depth (Figure 33, right). At the crest, the increase in migration rate is comparatively smaller after 50 years. However, the migration rate decreases steeply after 50 years with an increase in depth at trough due to an increase in the reverse drift at higher depth. Contrary to this, the change in migration rate both at the crest and trough is small after 62 years at 25m mean water depth (Figure 33, left). This relative difference in the crest and trough movement causes a change in sand waves shape or asymmetrical behaviour at 25 m and 30 m. Additionally, the average

migration rate is approximately 2 m/year in 30 m water depth and 4 m/year in 25 m water depth.

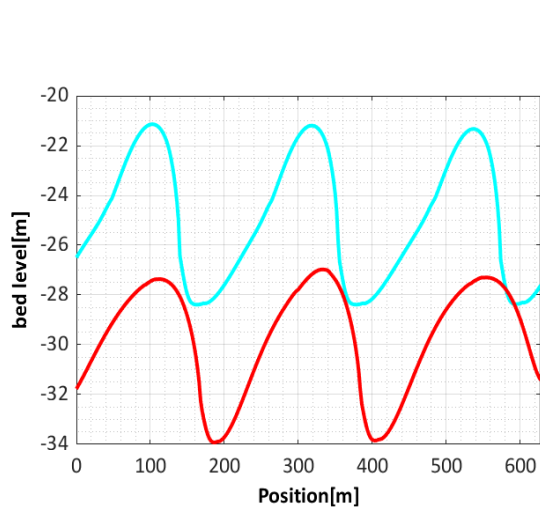


Figure 31: The sand wave field at 25m (cyan) and 30m (red) water depth in tide and severe wind after t=100 years.

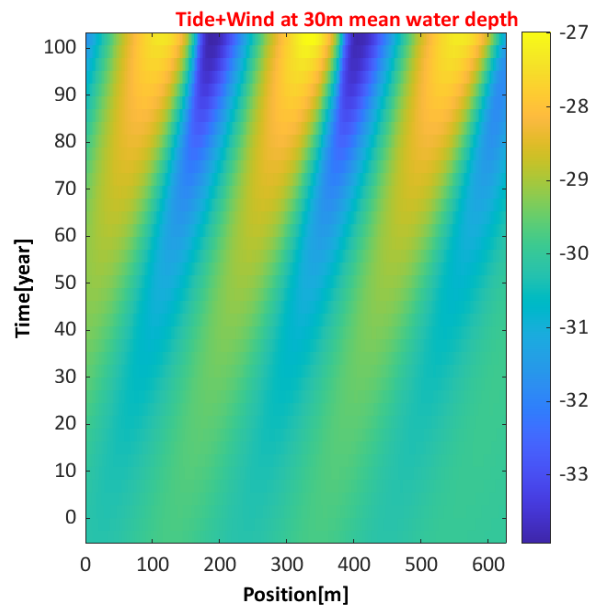


Figure 32: Sand wave evolution in the presence of tidal and severe wind conditions for 100 years at 30m mean depth. The vertical colour bar shows the bed level (m).

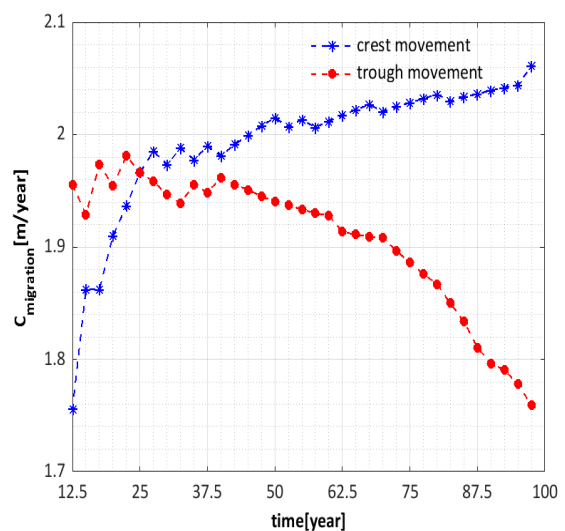
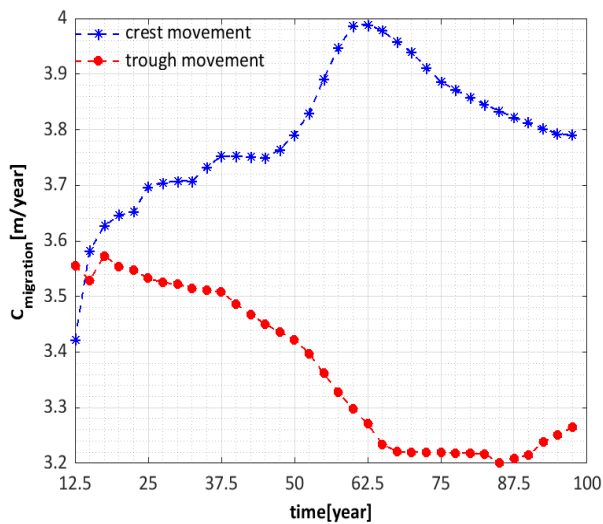


Figure 33: Migration of crest and trough at 25m (left) and 30m (right) water depth. The growth of the crest and trough is tracked with a blue asterisk and red dot, respectively.

Further, a steep decrease in migration rate near the trough was observed at a mean depth of 30 m, but no reverse migration is observed. It is because mean bedload and suspended load are in opposite directions, mostly near the trough (for instance, near $x=400$ m in Figure 34), but the absolute value of mean suspended load is higher than mean bed load. Thus, no reversal in migration is observed. Instead, a decrease in migration rate near the trough is observed. Thus, mean residual flow gives a better indication of mean bedload transport but not of mean suspended load transport. In general, suspended load distribution along sand waves depends on several other factors apart from velocity, such as sand wave wavelength, grain size (Borsje et al., 2014). Moreover, mean bedload and suspended sediment transport reduces at 30m compared to 25m depth.

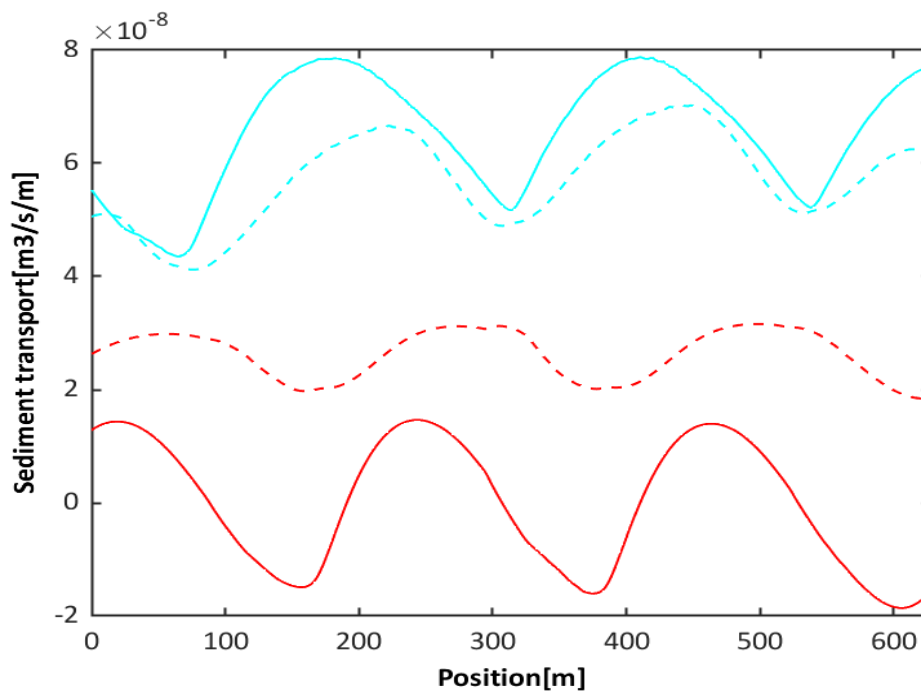


Figure 34: Comparison of mean bedload transport (solid line) and mean suspended load transport (dashed line) at a mean depth of 25m (cyan) and 30m (red).

5.3.3. Effect of an intermittent storm on sand wave morphology

In previous sections, the effect of constant wind and wave conditions on sand wave morphology is investigated. In reality, storms occur intermittently. In this section, a randomly perturbed bed is subjected to 3 months of an intermittent storm in a year at 25m depth. Also, the storm is randomly distributed throughout the tidal cycle. Therefore, the bed is subjected to severe wind conditions for three months and calm conditions for nine months in a year. The storm conditions consist of 20 m/s wind conditions. The wave conditions are not included in this simulation as it requires a time-varying wave condition. Therefore, it was not set up based on a definite time constraint in the research study. The intermittent storm sequence of 3 months in a year shows a migration rate within a range of 0.5-1.0 m/year for two random

runs of storms (Figure 35). It is comparable to those reported in the literature under section 2.1. Figure 36 shows the sand wave profile in the intermittent storm after 100 years. Sand wave height ranges from 4.1-9.2m in no storm conditions, while 3.5-8.8 m in intermittent storm conditions. The average reduction in height is 5%-8% due to intermittent storms compared to 33% reduction in height in complete duration storms. For this study, the height of sand wave fields depends on the phase of tidal current at which storm conditions occur as it will affect the near-bed velocity, sediment transport and further shift of point of convergence. The extent of height reduction also depends upon the frequency of storms and calm conditions. The storm erodes by shifting the point of convergence, and the calm condition builds by restoring the symmetric behaviour similar to Terwindt (1971) field observations.

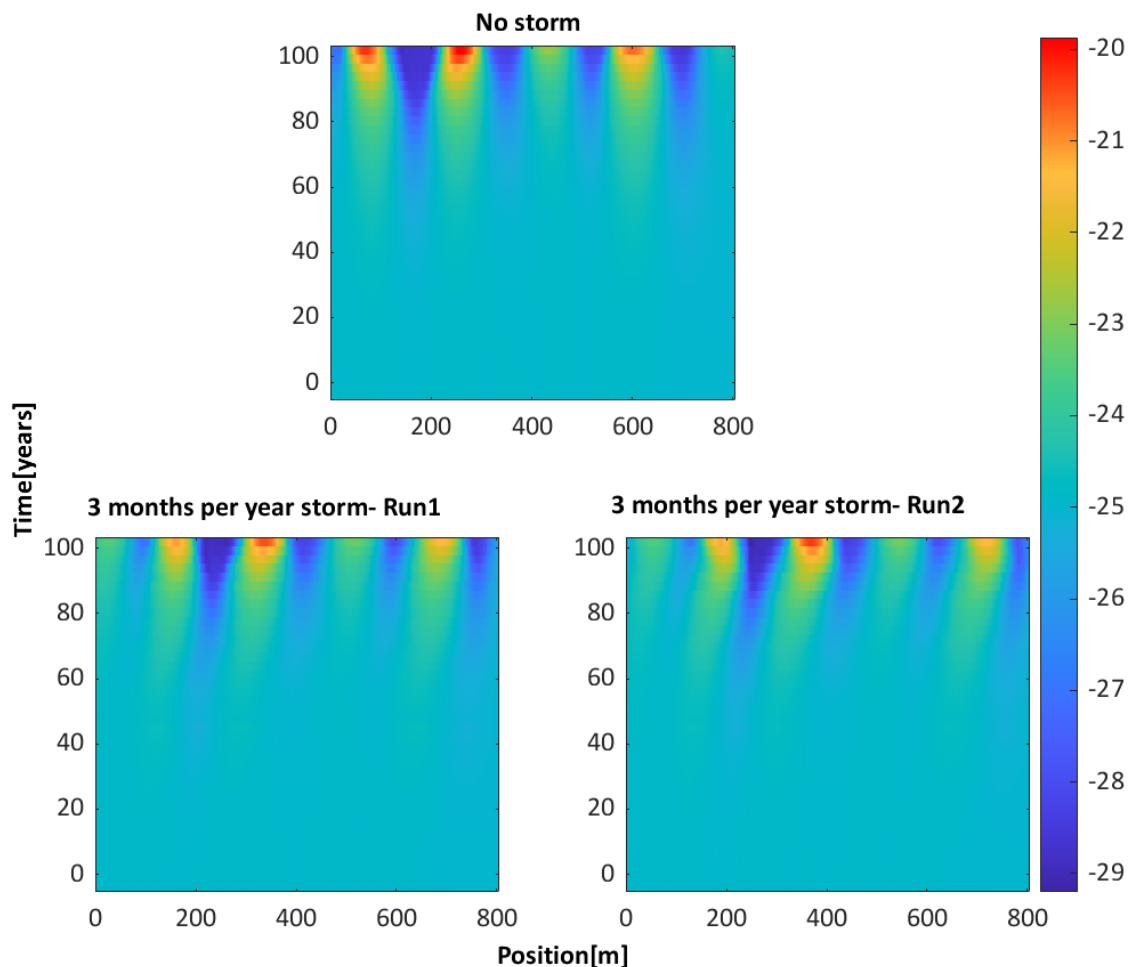


Figure 35: Sand wave evolution in the no storm (left) and intermittent storm conditions of 3 months/year (right) for 100 years at 25 m depth. The vertical colour bar shows the bed level (m).

Sand wave is symmetric in no storm condition. However, the symmetric shape of sand waves is not affected much in intermittent storms. The possible reason is that severe wind conditions are only present for three months. In the remaining nine months, forcing is symmetrical tide. Thus the asymmetric behaviour introduced during three months of the storm will be reduced by the symmetric forcing during calm conditions for nine months.

Section 5.1 discussed this behaviour where an additional residual is formed at the crest when the bed is asymmetric, and forcing is symmetric to restore the symmetric behaviour. In reality, the tidal conditions are not symmetric. However, including residual current will make the study hard to differentiate between the effect of wind and residual current. The wavelength of sand waves is in the range of 180 -220m for both cases, comparable to field observations.

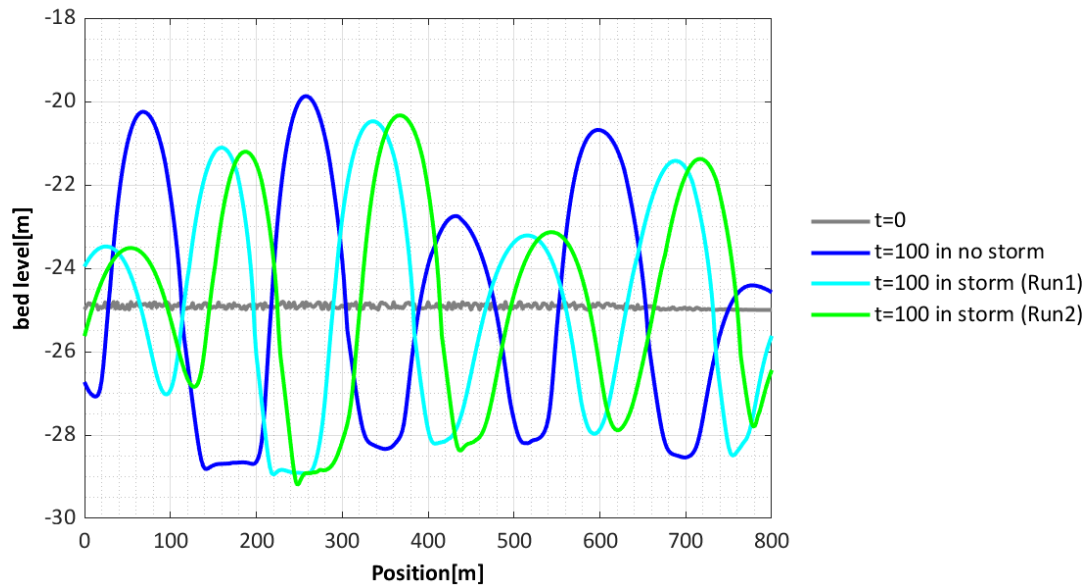


Figure 36: Sand wave profile in the no storm (blue) and two random intermittent storm conditions of 3 months/year (cyan and green) after 100 years at 25 m mean depth. The same randomly perturbed bed is used at t=0 (grey) for the simulations presented here.

6. Discussion

In this research study, the physical effects of wind and waves are studied on sand waves by extending the work of Campmans et al. (2018). The focus of the study was to determine the influence of the wind and waves on sandwave properties, particularly hydrodynamic and morphodynamic properties. This study presented relevant results comparable to field observations and past studies with several limitations and assumptions regarding the magnitude and direction of the forces involved.

6.1. Relevance of the study

Interestingly, the present study produces reverse drift in tidally average flow in wind conditions over flat and wavy bed patterns, similar to Holmedal (2013), which used the field data by Kings et al. (1985) to produce the reverse drift. However, they concluded that wind plays an essential role in the tidal drift direction but to what extent it causes the drift was kept an open question. This model domain used the $k-\epsilon$ turbulence model similar to the present study, but it involved only flatbed, non-linear interaction of the Moon and Sun and Coriolis force. Another study by Ruessink et al. (2006) showed the non-linear effect of wind on rectilinear tidal flow at 9 m depth. Therefore, a check was made using the present model at 10m, and findings such as viscosity, turbulence, velocity and mean velocity profile were similar to those obtained by Ruessink et al. (2006). Thus, it helped to understand that depth is vital in deciding the wind effect on the mean velocity profile. In our study, the Fourier analysis of velocity profile under severe wind and wave conditions showed the phase change, a reduction in amplitude of principal profile S2, and lost energy is transferred to residual S0 and higher tides S4. Similar findings were displayed by Ruessink et al. (2006). Furthermore, the amplitude profile of S4 (Figure 20c) matches the findings of Davies et al. (1994), which showed that the advective terms and quadratic bottom friction term in the hydrodynamic equations could transfer the energy at the M2 frequency to higher harmonics and residual flow.

The model calculates a maximum of 6 m/year migration rate and equilibrium height of 6.5 m after 100 years when severe conditions prevail for the complete duration of the tidal cycle. The results are predicted fairly well compared to Campmans et al. (2018) study that overestimated the equilibrium height of 20 m after 20 years and the 34 m/year migration rate. Also, the study by Campmans excluded the suspended load. In contrast, our study showed an increase in mean suspended load almost equal to the mean bedload in the storm conditions. The suspended load helps in an additional reduction in sand wave equilibrium height (van Gerwen et al., 2018). Similar to Campmans et al. (2018) study, our work also shows that waves alone do not contribute much to migration, but together with the wind, it intensifies the migration and reduction in sand wave height. The model results estimated sand wave migration of 0.5 m/year and an average reduction in sand wave height of 5%-8% in three-months per year intermittent storm conditions, compared to tide-only conditions. These values are comparable to those reported in the literature (Fenster et al., 1990b; Van Dijk & Kleinans, 2005). This study showed the effect of relative frequency of calm and

intermittent storm conditions on sand wave asymmetric behaviour similar to Terwindt (1971) field observations. However, in our study, no residual current is considered. In reality, there is residual current, but it would have created difficulty in differentiating the wind effect on sand waves if considered. Van Gerwen et al. (2018) showed that a residual current of 0.05 m/s could add a 5 m/year migration rate. Thus, combined effect intermittent storm conditions and residual current will make the study more realistic.

The reverse drift resulted in the reversal of mean velocity near the bottom at 30m depth opposite to wind direction. Thus, it resulted in the migration of mean bedload transport opposite to wind at a depth greater than 30 m. Surprisingly, Campmans et al. (2018) also found the migration rate of some small sand waves in a direction opposite to wind for tide+wind simulation at some instances. However, they subjected this reversal in migration direction to pattern interactions. The study by Campmans et al. (2018) did not explicitly examine hydrodynamic properties, so the links of negative migration in their study with the change in hydrodynamics remain unclear. Another simulation result on a randomly perturbed bed under severe wind conditions at 25 m mean depth (not presented in results) showed that higher sand waves overtook smaller sand waves. One of the possible reasons is explained in section 5.2.3, which states that as the crest grows, water depth reduces and thus mean wind-driven residual increases, translating into faster crest movement for higher sand waves than smaller sand waves. However, no field observations exist that support this mechanism as the conditions considered in the case, such as complete duration wind of 20 m/s and 2.5 m high waves in one direction, zero residual current or symmetric tide hardly exists. Campmans et al. (2018) also found high sand waves overtaking the smaller sand waves and consider them counterintuitive.

Part of the Netherlands Continental Shelf is covered with sandwaves. This study found that wind and waves add new dynamics based on the water depth, wind magnitude, direction, and duration. It will cause depth reduction at crest and depth dilation near troughs, and accordingly, the wind effect will vary with depth. Also, depending on the water depth, its residual direction might add, reduce, or reverse the residual current. Based on the present model results, storm conditions can increase migration from 0.5 m/year to a maximum of 6 m/year in a depth range of 25-30 m. An enhancement in migration rate could make navigation channels susceptible to sand waves. Furthermore, it might affect the frequency of the dredging operations and increase the area to be dredged to meet the minimum depth criteria. Furthermore, the non-linearity induced due to wind will affect the recovery process of sand waves. Also, the construction of wind farms is increasing, and if the seabed contains sandwave patterns, its migration can affect the structural stability of cables, pipelines and foundations of wind farms and turbines. Thus, from the engineering perspective, it is relevant to account for design safety factors by including wind conditions while designing offshore structures if the magnitude is high and the duration of storms conditions is comparable to calm conditions.

6.2. Model limitations

(i) Biasness due to predefined bed patterns: The hydrodynamic properties were checked on predefined bed patterns of amplitude varying from 0-3 m. The predefined wavelength of 216m was obtained from Van Gerwen et al. (2018) model. These predefined assumptions affect the quantitative results, but our study aims at producing qualitative results that would

be comparatively less affected. A check on mean horizontal velocity was made in which the bed was allowed to evolve to 3 m and become asymmetric in the presence of severe wind conditions using the MORFAC value of 2000. The qualitative profile was similar to that obtained in this study. However, the quantitative value was different as the bed slope and wavelength differed at an amplitude of 3 m. To reach the amplitude of 3m, it took 18 tidal runs, which is equivalent to the computational time of 15 hours. The simulations made in this study to examine hydrodynamic properties took only 2 tidal runs, i.e., 1 hour. Thus, it was a trade-off between the quality of results and computational time. If more accurate hydrodynamic results are needed under given conditions, it is preferable to let the bed patterns evolve independently. On the other hand, a predefined bed can be considered to develop a basic understanding of hydrodynamic properties with sand wave evolution when accuracy is not of prime importance.

(ii) Sensitive model parameters: The model results of the velocity were sensitive to the number of vertical sigma layers, horizontal spacing and Chézy constant; however, qualitative results were the same as obtained in this study. The other half involved studying morphodynamic properties. It was found that the model prediction, such as sand wave height, was sensitive to the MORFAC value. It influences sand wave height in order of meters. Ranasinghe et al. (2011) indicated that complex real-life situations might require significantly smaller MORFAC values. The study by Tonnon et al. (2007) involved a MORFAC value of 182. Similarly, in simulations involving waves, the model predictions were sensitive to the longitudinal slope parameter α_s .

(iii) Suitability of lateral boundary conditions: Treatment of lateral boundary conditions requires care in numerical models. Riemann boundary conditions being less reflexive are implemented at the boundaries to avoid numerical waves in the domain (Borsje et al., 2013). These numerical waves affect the formation of the circulation cells. It was observed that mean vertical velocity at the end boundaries was increased in wind and wave conditions. They were in the order of 10^{-4} m/s in wind conditions compared to 10^{-5} m/s in the tide-only conditions. In addition to this, there was a phase lag between both ends in the presence of wind and waves. The phase lag was prevailing in tide-only conditions also. Thus, it was challenging to understand whether these sudden changes in vertical velocities and phase lag at the boundaries affected the area of interest or not, as they were also present in tide-only conditions but of comparatively lower order. Figure 37 shows the mean vertical velocity near the lateral boundaries for wind conditions. However, a closer look outside the centre-domain containing sand waves did not show any phase difference in mean vertical velocity. No relevant results were produced on the tidal average of the velocity vector in the complete domain length of 45km. The reason being, grid size in the outside domain was changing consistently and was as large as 1500m.

In ideal conditions, the properties at the lateral boundaries should be similar. Thus, it might affect the suitability of Riemann boundary conditions in presence of wind as phase lags were observed at the boundaries. Therefore, the periodic boundaries can be used to keep all the boundary conditions equal and in phase with each other. However, its implementation is not available in the present version of Delft3D. Thus, it was not possible to reckon whether these phase lags due to differences in boundary conditions were making any impact on the area of interest or not. The model by Campmans et al. (2018) implemented the periodic

boundaries, and the study was done at 30m depth with a constant coefficient viscosity. The model does not indicate any reverse drift. However, our present study showed that viscosity decreases when the current is directed opposite to the wind, and it causes reverse drift (Refer section 5.2.1).

In the domain of interest, the strength of the circulation cells are of the order 10^{-3} m/s for small amplitude sand waves and of the order 10^{-2} m/s for high amplitude sand waves. Thus, if these numerical waves exist, it might affect the domain when they are of order comparable to these circulation cells. If any numerical wave exists in wind and wave conditions, the vertical velocity of the numerical wave is of order 10^{-4} m/s. Also, this sudden change in average vertical velocity might confine the mass in the given domain length and affect the average horizontal velocity due to conservation of mass. Assuming it confines the water within the domain, the numerical wave is distributed uniformly throughout the depth of 25 m. Since the mean vertical velocity phase difference is found only at the end grid nodes of length 1500 m, the rough mean horizontal velocity of the numerical wave could be $(1500 \text{ m} * 10^{-4} \text{ m/s}) / 25 \text{ m} \approx 10^{-3} \text{ m/s}$. Thus, the strength of numerical wave could be of the order 10^{-3} m/s subjected to the condition that the mass confines near the boundaries due to the existing phase difference. Then, they are likely to affect the simulations involving small sand waves than large sand waves. However, it is just a rough estimation with several assumptions. A better estimate of their existence could be found by checking the same model setting with periodic lateral boundaries instead of Riemann boundary conditions.

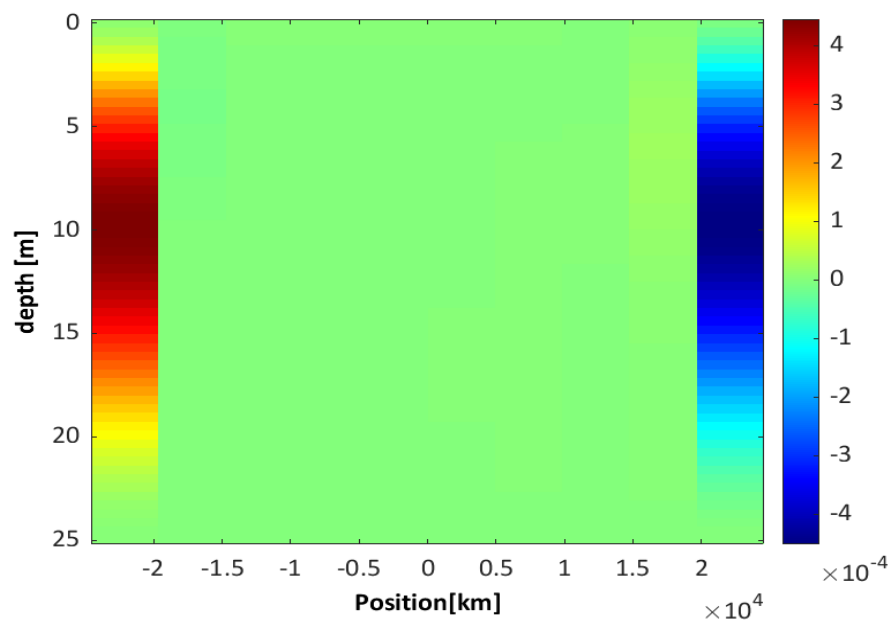


Figure 37: The tidal average vertical velocity (m/s) at the grid nodes near the lateral boundaries for wind conditions.

6.3. Improvements in model

It is a 2DV model study that restricted the inclusion of the Coriolis effect (Ekman's layer), elliptical tidal profile. The Coriolis effect strongly influences sand waves behaviour due to Ekman's layer in the presence of wind effects. It causes the water column to rotate at a varying angle to the wind, clockwise or anticlockwise, depending on the hemisphere (Campmans et al., 2017). Thus its rotational effect can have a significant effect on wind-driven flow and sediment transport. Similarly, tides are taken rectilinear in this study, but it is elliptical in reality. Besides this, wind direction controls reverse drift direction, and this study assumes wind as unidirectional. However, wind is multidirectional on the field, and thus their residuals could either add, reduce or reverse the tidal current residual. Thus, extending the model to 3D will help in including additional spectrums to the existing model to make it more realistic. Also, field observations show that ripples and megaripples are present on sand waves (Van Dijk & Kleinhans, 2005); thus, including a roughness predictor will give a spatially accurate velocity profile.

As mentioned earlier, these boundary conditions are not entirely suitable to study sand waves. However, the model can be tested for studying estuarine sand waves in storm conditions. It can be done by making a semi-enclosed basin for similar Riemann conditions at the lateral boundaries and keeping land enclosed side boundaries.

6.4. Calibration

The authenticity of the model is based on whether the model is calibrated and validated with field observations. It is challenging and complicated to collect field observations such as near-bed velocity, bedload transport or suspended load transport. In the case of sediment transport, the longitudinal slope parameter α_s can be calibrated. Also, Van Rijn (2004) formula distinguishes the bed load due to currents, bedload due to waves, suspended load due to waves separately. Therefore, these three transport components can be calibrated independently in Delft3D using Bed, BedW and SusW in the morphology input file, respectively. Similarly, suspended sediment reference concentration can be calibrated using the factor Sus if the suspended concentration profile is available (Deltares, 2014a). Similarly, if a velocity profile for vertical depth is available, it can be used to model the optimum settings that generate the particular velocity profile. However, in reality, such calibration is site-specific and requires accurate and long time interval data.

7. Conclusion

To summarize the research objective, “**How do wind and waves affect the hydrodynamics and morphodynamics of sand waves?**” all the sub-questions are answered sequentially.

1) **What are the hydrodynamic properties in tide-only conditions over sand waves of different amplitudes?**

Circulation cells are formed on either side of sand waves crest due to tidally average residual flow as the bed transforms to a 0.25 m symmetrical sand wave. These circulation cells help in the growth of sand waves. However, circulation cells are asymmetric over 0.25 m asymmetrical sand wave with comparatively strong circulation cells on the steeper side. The strength of circulation cells is intensified with an increase in sand wave amplitude. The mean horizontal residual is zero at the crest position on the symmetrical bed. However, a residual is developed over the crest pointed towards a less steep side over the asymmetric bed. It happens to regain symmetrical shape as the forcing is symmetrical. The maximum vertical eddy viscosity is same during flood and ebb periods. The turbulence at the surface is zero and higher near the bed due to bed roughness. The bottom stress is in line with the mean residual velocity and is asymmetric in nature for asymmetrical sand waves. With bed evolution, vertical eddy viscosity has not changed much; however, near-bed turbulence and maximum bed shear stress increase with evolution. These properties in tide-only conditions act as a reference for analysis in wind and waves conditions.

2) **How do the hydrodynamic properties change over sand waves when tide conditions combine with intermediate to severe wind and waves?**

The effect of wind and waves on the hydrodynamic properties when compared to tide-only conditions over 0.25 m symmetrical sand wave are as follows,

- **Near Surface velocity:** Wind increases the near-surface velocity depending on its wind intensity and shear at the surface. Waves do not add much to surface drift.
- **Vertical eddy viscosity:** Wind, unidirectional in flood direction, increases the viscosity during the flood period and decreases the viscosity during the ebb period. Thus, it affects how velocity is transferred from the surface to the bottom. The viscosity during the ebb period falls below compared to tide-only conditions. Waves do not affect it much.
- **Turbulence:** Wind shear and wave breaking or decaying increases surface turbulence. At the same time, bottom roughness or friction increases near-bed turbulence. Moreover, turbulence due to wind reaches down the depth, whereas turbulence due to waves remains few metres within the surface.
- **Mean horizontal velocity profile:** First and foremost, if the depth of influence (Stokes depth) corresponding to wind conditions dominates the actual water depth, then the mean horizontal velocity profile is single-layered in wind direction. It happens as the frequency of oscillation of the surface and bottom is almost identical. Secondly, if the depth of influence is comparable or less than the actual water depth, a phase difference exists between the top and bottom layers. In addition to this, the flood directed wind reduces the viscosity during the ebb period, compared to tide-only conditions. Therefore,

a reverse drift in a direction opposite to wind could be expected. The bottom drift (near-bed residuals) are present due to a combination of wind-driven residual S_0 , high tides (S_4) and Stokes drift in waves. Consequently, a two-layered or three-layered mean horizontal velocity profile occurs. Comparatively, bottom residuals are more in severe conditions than in intermediate conditions. Thus, severe conditions will affect morphodynamics more as bottom residuals indicate the possibility of sediment transport near-bed.

- **Mean bottom stress:** In the case of a 0.25 m symmetrical sand wave, the stress distribution is symmetrical on sand wave due to identical circulation cells, and the crest is the point of convergence where the mean bottom stress is zero. However, in wind and waves presence, the mean bottom stress is distributed asymmetrically over sand wave with non-zero mean residual and mean bottom stress over the crest. Therefore, it indicated the possibility of asymmetric bed and migration of bed.
- **Effect with sand wave evolution:** The mean residual profile changes with sand wave evolution as the depth near crest reduces and depth near trough increases. Following this, a transition (reversal) in mean velocity is observed at 30m, or greater mean depth due to increase in reverse drift with depth.

Overall the physical effect of wind is more significant than waves on hydrodynamic properties over sand waves. Alone waves cause surface turbulence and bottom stress. With wind, waves intensify the turbulence, bottom drift and mean bottom stress. The combined effect increases the velocity residual over the crest and makes mean bottom stress distribution over sand waves asymmetrical, indicating possible migration and asymmetrical sand waves.

3) How do the morphodynamic properties of sand waves vary in the presence of wind and waves?

The presence of wind and waves shifts the point of convergence from the crest position distorting the symmetry of circulation cells produced due to symmetrical diurnal tide and causes residual velocity over the crest position. This shift translates into asymmetric shape, migration and reduces the final sand wave height after 100 years. Wind introduces asymmetry and increases wavelength whereas, waves cause flattening of sand wave crest. The addition of waves and wind increases the suspended load substantially, increasing the reduction in sand wave height. To summarize, waves alone do not cause much migration; together with the wind, it intensifies the migration. Lastly, the simulations involving wind did not attain equilibrium even after 100 years, and the simulation involving only tide+waves attained an early equilibrium compared to tide-only conditions.

Comparing sand wave morphology in 100 years at a mean depth of 25 m and 30 m shows that the migration behaviour is different at the crest and trough. It happens because depth reduces at the crest and increases at the trough with sand wave evolution. Since a reversal in near-bed mean velocity was observed at 30m or greater depth, the steeply reducing migration rate was also observed near trough position at a depth greater than 30 m. However, the migration direction was not reduced due to high mean suspended load than the bedload transport. Thus, mean residual flow gives a better indication of mean bedload transport but not of mean suspended load transport as suspended load distribution along sand waves depends on several other factors apart from velocity.

Lastly, morphological development of 100 years on a randomly perturbed bed in an intermittent storm of three months per year showed migration of 0.5-1.0 m/year and 5%-8% height reduction compared to tide-only conditions. The results are comparable to field observations. However, it did not affect much the symmetrical behaviour of sandwaves. It happens because the nine months of calm conditions reduced the asymmetric behaviour developed during three months of the storm. It indicates that even small-moderate duration storms could cause a substantial migration rate of 1 m/year. Thus, it is essential to account for the safety factor while designing long-life offshore structures such as the foundation of wind farms, submarine pipelines and cable. It will also affect the operational frequency of dredging work maintenance.

8. Future recommendation

The future study can be the effect of storms in the presence of residual current. During simulation for the effect of intermittent storm conditions on sand waves, the shape did not change much. The calm condition in symmetrical tide was producing the residual to regain the lost symmetrical behaviour of bed. In reality, the tides are not symmetrical. Thus, residual current should be involved in the simulation along with the intermittent storm conditions. Later, the 2D Fourier decomposition of the sand wave bed level can demonstrate the effect of residual current and storms separately. This study shows that three months of intermittent storm per year can cause a 0.5 m/year migration. Similarly, a study by van Gerwen et al. (2018) showed a residual current of 0.05 m/s causes migration of 5 m/year. Thus, their non-linear effect on migration rate can be checked by comparing the combination with the individual migration rate due to residual current and storms.

As discussed in section 6.2, the Riemann boundary conditions are not entirely suitable for this study due to the phase difference between certain properties at the boundaries. Such phase differences can create a possibility of numerical waves within the simulation. It can potentially affect the model results, especially during the initial phase of sand waves evolution. Thus, the ideal case will be conducting a similar research study with periodic boundary conditions to ensure that all the properties at the lateral boundaries are in phase with each other and avoid any numerical wave. Also, the study with periodic boundaries can check the extent to which the Riemann boundaries are suitable for such a study.

Another extended research can be the wind effects on sand waves in a domain comparable to tidal length. The domain length in this study is 45km. However, the length of tides is hundreds of kilometres. Thus, a future study related to the wind effect can be done on domain length equivalent to the order of tidal length. Since wind results in the generation of higher tides and residuals, the effect of tidal length available in the domain can vary the wind effect on sandwaves.

Also, in this study, the vertical momentum equation is reduced to the hydrostatic pressure relation as vertical accelerations are assumed to be small compared to gravitational acceleration. However, there are situations where the vertical acceleration, and thereby the non-hydrostatic pressure component, cannot be neglected (Deltares, 2014b). Thus, when flows over abruptly changing bottom topography, such as orbital movements in short wave motions or intensive vertical circulations, are considered. In order to capture non-hydrostatic flow phenomena, the non-hydrostatic version of the Delft3D modelling suite can be used.

References

- Aliotta, S., & Perillo, G. M. E. (1987). A sand wave field in the entrance to Bahia Blanca Estuary, Argentina. *Marine Geology*. [https://doi.org/10.1016/0025-3227\(87\)90013-2](https://doi.org/10.1016/0025-3227(87)90013-2)
- Barnard, P. L., Hanes, D. M., Rubin, D. M., & Kvitek, R. G. (2006). Giant sand waves at the mouth of San Francisco Bay. *Eos*, 87(29), 285–289. <https://doi.org/10.1029/2006EO290003>
- Besio, G., Blondeaux, P., & Vittori, G. (2006). On the formation of sand waves and sand banks. *Journal of Fluid Mechanics*. <https://doi.org/10.1017/S0022112006009256>
- Besio, Giovanni, Blondeaux, P., Brocchini, M., & Vittori, G. (2004). On the modeling of sand wave migration. *Journal of Geophysical Research C: Oceans*. <https://doi.org/10.1029/2002JC001622>
- Bokuniewicz, H. J., Gordon, R. B., & Kastens, K. A. (1977). From and migration of sand waves in a large estuary, Long Island Sound. *Marine Geology*. [https://doi.org/10.1016/0025-3227\(77\)90027-5](https://doi.org/10.1016/0025-3227(77)90027-5)
- Borsje, B. W., Kranenburg, W. M., Roos, P. C., Matthieu, J., & Hulscher, S. J. M. H. (2014). The role of suspended load transport in the occurrence of tidal sand waves. *Journal of Geophysical Research: Earth Surface*. <https://doi.org/10.1002/2013JF002828>
- Borsje, B. W., Roos, P. C., Kranenburg, W. M., & Hulscher, S. J. M. H. (2013). Modeling tidal sand wave formation in a numerical shallow water model: The role of turbulence formulation. *Continental Shelf Research*. <https://doi.org/10.1016/j.csr.2013.04.023>
- Borsje, Roos, P. C., Kranenburg, W. M., & Hulscher, S. J. M. H. (2011). Modeling sandwave formation in a numerical shallow water model. *7th IAHR Symposium on River, Coastal and Estuarine Morphodynamics*.
- Burchard, H., Craig, P. D., Gemmrich, J. R., van Haren, H., Mathieu, P. P., Meier, H. E. M., Smith, W. A. M. N., Prandke, H., Rippeth, T. P., Skillingstad, E. D., Smyth, W. D., Welsh, D. J. S., & Wijesekera, H. W. (2008). Observational and numerical modeling methods for quantifying coastal ocean turbulence and mixing. In *Progress in Oceanography*. <https://doi.org/10.1016/j.pocean.2007.09.005>
- Campmans, G. H. P., Roos, P. C., de Vriend, H. J., & Hulscher, S. J. M. H. (2017). Modeling the influence of storms on sand wave formation: A linear stability approach. *Continental Shelf Research*. <https://doi.org/10.1016/j.csr.2017.02.002>
- Campmans, G. H. P., Roos, P. C., de Vriend, H. J., & Hulscher, S. J. M. H. (2018). The Influence of Storms on Sand Wave Evolution: A Nonlinear Idealized Modeling Approach. *Journal of Geophysical Research: Earth Surface*. <https://doi.org/10.1029/2018JF004616>
- Campmans, G. H. P., Roos, P. C., Schrijen, E. P. W. J., & Hulscher, S. J. M. H. (2018). Modeling wave and wind climate effects on tidal sand wave dynamics: A North Sea case study. *Estuarine, Coastal and Shelf Science*, 213, 137–147. <https://doi.org/10.1016/j.ecss.2018.08.015>
- Cherlet, J., Besio, G., Blondeaux, P., van Lancker, V., Verfaillie, E., & Vittori, G. (2007). Modeling sand wave characteristics on the Belgian Continental Shelf and in the Calais-Dover Strait. *Journal of Geophysical Research: Oceans*. <https://doi.org/10.1029/2007JC004089>
- Colosimo, I., de Vet, P. L. M., van Maren, D. S., Reniers, A. J. H. M., Winterwerp, J. C., & van Prooijen, B. C. (2020). The impact of wind on flow and sediment transport over intertidal flats. *Journal of Marine Science and Engineering*. <https://doi.org/10.3390/jmse8110910>

- Damen, J. M., van Dijk, T. A. G. P., & Hulscher, S. J. M. H. (2018). Spatially Varying Environmental Properties Controlling Observed Sand Wave Morphology. *Journal of Geophysical Research: Earth Surface*. <https://doi.org/10.1002/2017JF004322>
- Damveld, J. H., Borsje, B. W., Roos, P. C., & Hulscher, S. J. M. H. (2020). Biogeomorphology in the marine landscape: Modelling the feedbacks between patches of the polychaete worm *Lanice conchilega* and tidal sand waves. *Earth Surface Processes and Landforms*. <https://doi.org/10.1002/esp.4914>
- Davies, A. M., & Lawrence, J. (1994). Examining the influence of wind and wind wave turbulence on tidal currents, using a three-dimensional hydrodynamic model including wave-current interaction. *Journal of Physical Oceanography*, 24(12), 2441–2460. [https://doi.org/10.1175/1520-0485\(1994\)024<2441:ETIOWA>2.0.CO;2](https://doi.org/10.1175/1520-0485(1994)024<2441:ETIOWA>2.0.CO;2)
- Davies, A. M., & Lawrence, J. (1995). Modeling the effect of wave-current interaction on the three-dimensional wind-driven circulation of the eastern Irish Sea. *Journal of Physical Oceanography*. [https://doi.org/10.1175/1520-0485\(1995\)025<0029:MTEOWI>2.0.CO;2](https://doi.org/10.1175/1520-0485(1995)025<0029:MTEOWI>2.0.CO;2)
- Davies, Alan M., & Hall, P. (2000). The response of the North Channel of the Irish Sea and Clyde Sea to wind forcing. *Continental Shelf Research*, 20(8), 897–940. [https://doi.org/10.1016/S0278-4343\(00\)00009-1](https://doi.org/10.1016/S0278-4343(00)00009-1)
- Deltares. (2014a). *3D/2D modelling suite for integral water solutions: Hydro-Morphodynamics (Delft3D Flow)*. 710.
- Deltares. (2014b). *3D/2D modelling suite for integral water solutions: Hydro-Morphodynamics (Delft3D Wave)*. 710.
- Dodd, N., Blondeaux, P., Calvete, D., De Swart, H. E., Falqués, A., Hulscher, S. J. M. H., Rózyński, G., & Vittori, G. (2003). Understanding Coastal Morphodynamics Using Stability Methods. *Journal of Coastal Research*.
- Dorst, L. L., Roos, P. C., & Hulscher, S. J. M. H. (2011). Spatial differences in sand wave dynamics between the Amsterdam and the Rotterdam region in the Southern North Sea. *Continental Shelf Research*, 31(10), 1096–1105. <https://doi.org/10.1016/j.csr.2011.03.015>
- Dorst, L. L., Roos, P. C., Hulscher, S. J. M. H., & Lindenbergh, R. C. (2009). The estimation of sea floor dynamics from bathymetric surveys of a sand wave area. *Journal of Applied Geodesy*. <https://doi.org/10.1515/JAG.2009.011>
- Fenster, M. S., Fitzgerald, D. M., Bohlen, W. F., Lewis, R. S., & Baldwin, C. T. (1990a). Stability of giant sand waves in eastern Long Island Sound, U.S.A. *Marine Geology*. [https://doi.org/10.1016/0025-3227\(90\)90037-K](https://doi.org/10.1016/0025-3227(90)90037-K)
- Fenster, M. S., Fitzgerald, D. M., Bohlen, W. F., Lewis, R. S., & Baldwin, C. T. (1990b). Stability of giant sand waves in eastern Long Island Sound, U.S.A. *Marine Geology*, 91(3), 207–225. [https://doi.org/10.1016/0025-3227\(90\)90037-K](https://doi.org/10.1016/0025-3227(90)90037-K)
- Ferret, Y., Le Bot, S., Tessier, B., Garlan, T., & Lafite, R. (2010). Migration and internal architecture of marine dunes in the eastern English Channel over 14 and 56 year intervals: The influence of tides and decennial storms. *Earth Surface Processes and Landforms*, 35(12), 1480–1493. <https://doi.org/10.1002/esp.2051>
- Flather, R. A. (1975). A tidal model of the north-west European continental shelf. *MEM. SOC. ROYALE SCI. DE LIEGE, SER.6*.

- Fredsoe, J., Diegaard, R. (1993). Mechanics of Coastal Sediment Transport. *Journal of Coastal Research*, 9(4).
- Harris, P. T. (1989). Sandwave movement under tidal and wind-driven currents in a shallow marine environment: Adolphus Channel, northeastern Australia. *Continental Shelf Research*, 9(11), 981–1002. [https://doi.org/10.1016/0278-4343\(89\)90003-4](https://doi.org/10.1016/0278-4343(89)90003-4)
- Holmedal, L. E., & Myrhaug, D. (2013). Combined tidal and wind driven flows and bedload transport over a flat bottom. *Ocean Modelling*, 68, 37–56. <https://doi.org/10.1016/j.ocemod.2013.04.005>
- Hulscher, S. J. M. H. (1996). Tidal-induced large-scale regular bed form patterns in a three-dimensional shallow water model. *Journal of Geophysical Research C: Oceans*. <https://doi.org/10.1029/96JC01662>
- Ijzer, S. (2010). *Influence of surface waves on sand wave migration and asymmetry*. June.
- King, H. L., Davies, A. G., & Soulsby, R. L. (1985). *A numerical model of the turbulent boundary layer beneath surface waves and tides*.
- Knaapen, M. A. F. (2005). Sandwave migration predictor based on shape information. *Journal of Geophysical Research: Earth Surface*. <https://doi.org/10.1029/2004JF000195>
- Lavidas, G., & Polinder, H. (2019). North sea wave database (NSWD) and the need for reliable resource data: A 38 year database for metocean and wave energy assessments. *Atmosphere*. <https://doi.org/10.3390/atmos10090551>
- Le Bot, S., Trentesaux, A., Garlan, T., Berne, S., & Chamley, H. (2000). Influence des tempêtes sur la mobilité des dunes tidales dans le détroit du Pas-de-Calais. *Oceanologica Acta*. [https://doi.org/10.1016/S0399-1784\(00\)00115-8](https://doi.org/10.1016/S0399-1784(00)00115-8)
- Lesser, G. R., Roelvink, J. A., van Kester, J. A. T. M., & Stelling, G. S. (2004). Development and validation of a three-dimensional morphological model. *Coastal Engineering*, 51(8–9), 883–915. <https://doi.org/10.1016/j.coastaleng.2004.07.014>
- McCave, I. N. (1971). Sand waves in the North Sea off the coast of Holland. *Marine Geology*. [https://doi.org/10.1016/0025-3227\(71\)90063-6](https://doi.org/10.1016/0025-3227(71)90063-6)
- Németh, A. A., Hulscher, S. J. M. H., & Van Damme, R. M. J. (2007). Modelling offshore sand wave evolution. *Continental Shelf Research*. <https://doi.org/10.1016/j.csr.2006.11.010>
- Németh, Attila A., Hulscher, S. J. M. H., & De Vriend, H. J. (2002). Modelling sand wave migration in shallow shelf seas. *Continental Shelf Research*, 22(18–19), 2795–2806. [https://doi.org/10.1016/S0278-4343\(02\)00127-9](https://doi.org/10.1016/S0278-4343(02)00127-9)
- Perillo, G. M. E., & Ludwick, J. C. (1984). Geomorphology of a sand wave in lower Chesapeake Bay, Virginia, U.S.A. *Geo-Marine Letters*. <https://doi.org/10.1007/BF02277080>
- Ranasinghe, R., Swinkels, C., Luijendijk, A., Roelvink, D., Bosboom, J., Stive, M., & Walstra, D. J. (2011). Morphodynamic upscaling with the MORFAC approach: Dependencies and sensitivities. *Coastal Engineering*. <https://doi.org/10.1016/j.coastaleng.2011.03.010>
- Rijn, L.C. van, Walstra, D. J. R., & Ormond, M. van. (2004). WL | delft hydraulics Description of TRANSPOR2004 and Implementation in Delft3D-ONLINE. In Z3748. Deltares (WL). <https://repository.tudelft.nl/islandora/object/uuid%3Aea12eb20-ae3-4f58-99fb-ebc216e98879>
- Rodi, W. (1984). *Turbulence models and their application in hydraulics*. <https://doi.org/10.1016/0045->

The effect of wind and waves on the hydrodynamic and morphodynamic properties of sand waves

Author: Singh,A.

Page 70

- Ruessink, B. G., Houwman, K. T., & Grasmeijer, B. T. (2006). Modeling the nonlinear effect of wind on rectilinear tidal flow. *Journal of Geophysical Research: Oceans*, 111(10), 1–11. <https://doi.org/10.1029/2006JC003570>
- Soulsby, R. L., Hamm, L., Klopman, G., Myrhaug, D., Simons, R. R., & Thomas, G. P. (1993). Wave-current interaction within and outside the bottom boundary layer. *Coastal Engineering*, 21(1–3), 41–69. [https://doi.org/10.1016/0378-3839\(93\)90045-A](https://doi.org/10.1016/0378-3839(93)90045-A)
- Stride, A. H. (1982). *Offshore tidal sands. Processes and deposits*. <https://doi.org/10.2307/1352150>
- STRIDE, A. H. (1963). Current-swept sea floors near the southern half of Great Britain. *Quarterly Journal of the Geological Society*, 119(1–4), 175–197. <https://doi.org/10.1144/GSJGS.119.1.0175>
- Terwindt, J. H. J. (1971). Sand waves in the southern bight of the North Sea. *Marine Geology*. [https://doi.org/10.1016/0025-3227\(71\)90076-4](https://doi.org/10.1016/0025-3227(71)90076-4)
- Tonnon, P. K., van Rijn, L. C., & Walstra, D. J. R. (2007). The morphodynamic modelling of tidal sand waves on the shoreface. *Coastal Engineering*. <https://doi.org/10.1016/j.coastaleng.2006.08.005>
- van den Berg, J., Sterlini, F., Hulscher, S. J. M. H., & van Damme, R. (2012). Non-linear process based modelling of offshore sand waves. *Continental Shelf Research*. <https://doi.org/10.1016/j.csr.2012.01.012>
- Van Der Molen, J. (2002). The influence of tides, wind and waves on the net sand transport in the North Sea. *Continental Shelf Research*. [https://doi.org/10.1016/S0278-4343\(02\)00124-3](https://doi.org/10.1016/S0278-4343(02)00124-3)
- Van Dijk, T. A. G. P., & Kleinhans, M. G. (2005). Processes controlling the dynamics of compound sand waves in the North Sea, Netherlands. *Journal of Geophysical Research: Earth Surface*. <https://doi.org/10.1029/2004JF000173>
- van Dijk, T. A. G. P., Lindenbergh, R. C., & Egberts, P. J. P. (2008). Separating bathymetric data representing multiscale rhythmic bed forms: A geostatistical and spectral method compared. *Journal of Geophysical Research: Earth Surface*. <https://doi.org/10.1029/2007JF000950>
- van Gerwen, W., Borsje, B. W., Damveld, J. H., & Hulscher, S. J. M. H. (2018). Modelling the effect of suspended load transport and tidal asymmetry on the equilibrium tidal sand wave height. *Coastal Engineering*. <https://doi.org/10.1016/j.coastaleng.2018.01.006>
- van Rijn, Leo C., Walstra, D.-J. R., & van Ormondt, M. (2007). Unified View of Sediment Transport by Currents and Waves. IV: Application of Morphodynamic Model. *Journal of Hydraulic Engineering*, 133(7), 776–793. [https://doi.org/10.1061/\(asce\)0733-9429\(2007\)133:7\(776\)](https://doi.org/10.1061/(asce)0733-9429(2007)133:7(776))
- van Santen, R. B., de Swart, H. E., & van Dijk, T. A. G. P. (2011). Sensitivity of tidal sand wavelength to environmental parameters: A combined data analysis and modelling approach. *Continental Shelf Research*. <https://doi.org/10.1016/j.csr.2011.03.003>
- Van Veen, J. (1935). Sand waves in the North Sea. *Hydrogr. Rev*, 12(1), 21. <https://repository.tudelft.nl/islandora/object/uuid%3Abe27faa7-c09c-4e98-a1b5-1ddcaaea23e1>

Appendices

Appendix-1: Model Sensitivity to vertical, horizontal, and temporal resolution

The sensitivity of the model is checked for horizontal and temporal resolution along with vertical sigma layers. For the demo run, horizontal resolution is increased from 2m to 1m in sand wave area, temporal resolution is increased from 0.2 minutes to 0.1 minutes, and vertical layers were increased to 90. Figure 38 shows the mean horizontal velocity profile for comparatively finer resolution and large number of vertical layers at 60 m depth. The difference is minimal.

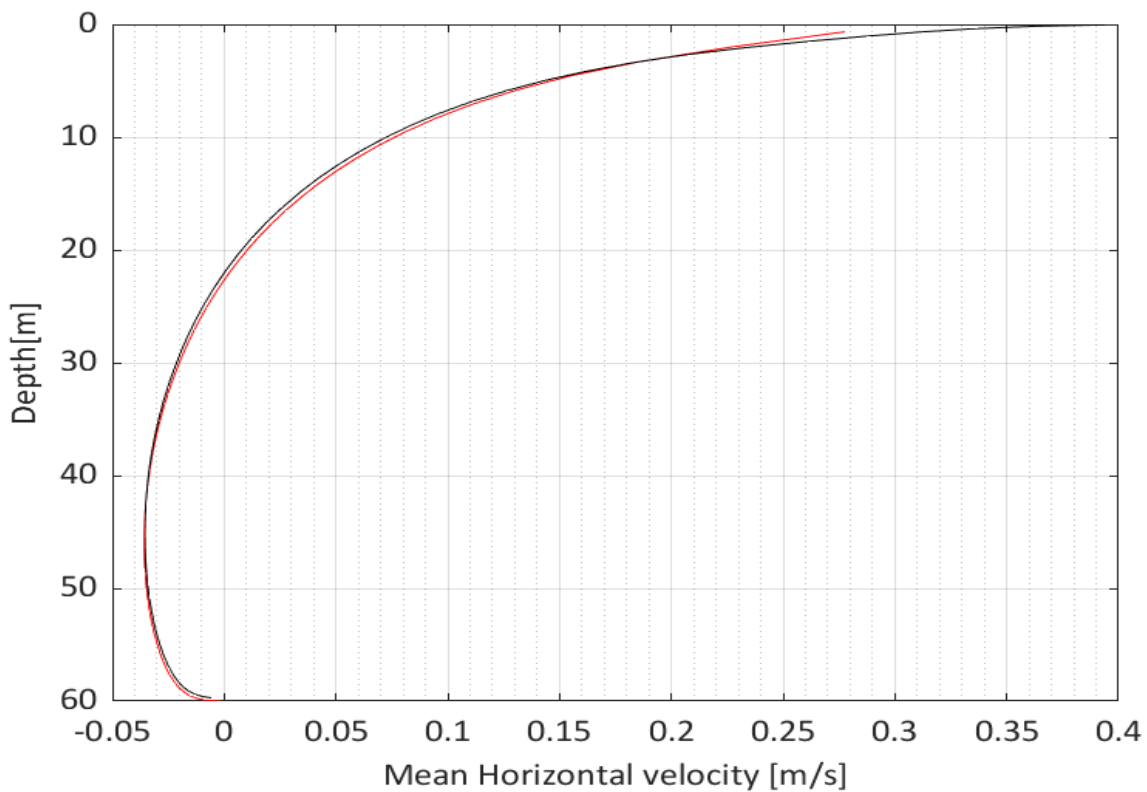


Figure 38: Mean Horizontal velocity at depth 60 for numerical settings- number of sigma layers (90 layers), horizontal distribution near the centre of the grid (1m) and hydrodynamic time step (0.1 minutes) (red) and - number of sigma layers (60 layers), horizontal distribution near the centre of the grid (2m) and hydrodynamic time step (0.2 minutes) (black)

Appendix-2: Effect of adding background viscosity

A demo run is made for a background viscosity from $0.005 \text{ m}^2/\text{s}$ along with the viscosity from the $k-\epsilon$ turbulence model. It resulted in the removal of reverse drift, which happened due to decreased viscosity during the ebb period (when current is opposite to wind). The additional background viscosity provides the net viscosity lost during the ebb period. Quantitative results are shown for the addition of $0.005 \text{ m}^2\text{s}^{-1}$ viscosity in Figure 39. It confirms that a decrease in viscosity opposite to wind direction or during ebb period is one of the reasons responsible for reverse drift.

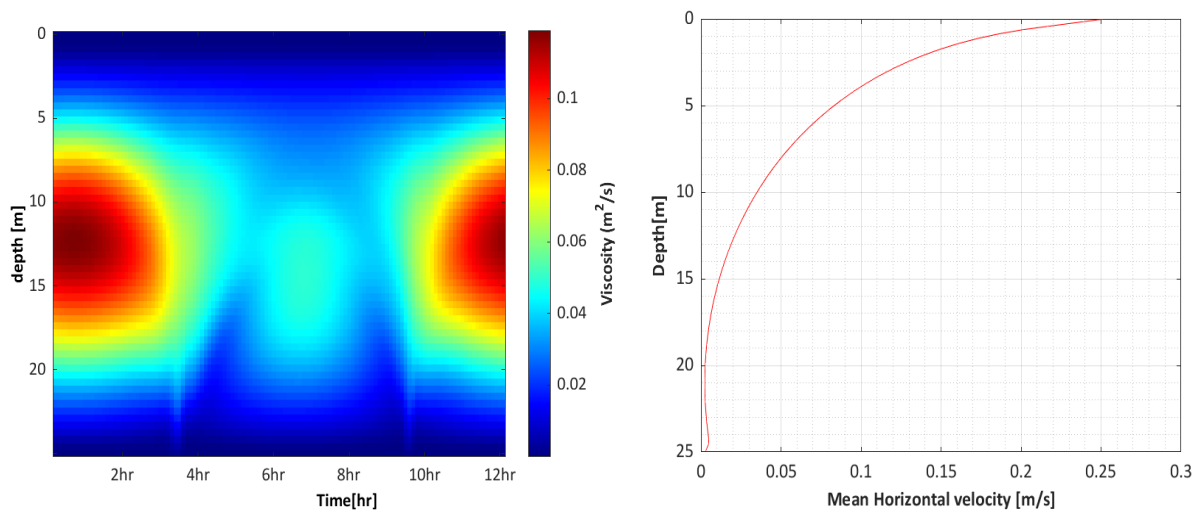


Figure 39: The effect of adding background viscosity $0.005 \text{ m}^2/\text{s}$ to $k-\epsilon$ turbulence model on final vertical viscosity profile (left) and mean horizontal velocity (right).